

University of Alberta

Decision Support System for Crane Selection and Location Optimization
on Construction Sites

by

Md. Shafiul Hasan

A thesis submitted to the Faculty of Graduate Studies and Research
in partial fulfillment of the requirements for the degree of

Doctor of Philosophy

in

Construction Engineering and Management

Department of Civil and Environmental Engineering

© Md. Shafiul Hasan

Fall 2013

Edmonton, Alberta

Permission is hereby granted to the University of Alberta Libraries to reproduce single copies of this thesis and to lend or sell such copies for private, scholarly or scientific research purposes only. Where the thesis is converted to, or otherwise made available in digital form, the University of Alberta will advise potential users of the thesis of these terms.

The author reserves all other publication and other rights in association with the copyright in the thesis and, except as herein before provided, neither the thesis nor any substantial portion thereof may be printed or otherwise reproduced in any material form whatsoever without the author's prior written permission.

*This thesis is dedicated with love and respect to my grandparents and
to my son “Raheel Hasan”*

Abstract

Selecting the most appropriate cranes and identifying ideal crane locations on site can improve the productivity and safety of large-scale construction projects. A significant proportion of crane accidents have been caused by improper crane selection, lack of a proper crane support system, or a failure to calculate actual support reactions. This research presents a methodology to select feasible crane and optimize crane locations by evaluating the crane support reactions. This research seeks to provide practitioners with a methodology for successful crane operations through the utilization of decision support system. The developed system assists in proper crane selection, and also calculates the crane support reactions in order to design the support system. The proposed methodology optimizes the load moments for all lifted loads in order to identify the ideal crane location, which can in turn assist in selecting the most appropriate crane. Three case studies are described in order to demonstrate the use of the presented methodology for improving crane operations. This research aims to establish crane operational standardization for large projects involving multiple heavy lifts, such as modular building construction and Alberta Oil-Sands projects.

ACKNOWLEDGEMENTS

There have been a great number of exceptional people who have contributed to my research.

First and foremost, I wish to express my deepest gratitude to my supervisor, Dr. Mohamed Al-Hussein, for his continuous encouragement, support and valuable advice throughout all stages of this research. I would also like to extend my gratitude to my co-supervisor, Dr. Ahmed Bouferguène, for his valuable advice and support and assistance in developing different mathematical equations.

I also appreciate the assistance from NCSG Crane & Heavy Haul Services, Edmonton, Canada and Wilbert Kranservice GmbH, Germany. I would like to thank my wife, Mrs. Wahida Zaman, and my parents for their encouragement and support, which made all this work possible.

Finally, I am grateful to the Natural Sciences and Engineering Research Council of Canada (NSERC) for their financial support throughout this research.

TABLE OF CONTENTS

Chapter 1: Introduction	1
1.1 Motivation and Background.....	1
1.2 Research Objective.....	3
1.3 Organization of the Thesis	4
Chapter 2: Literature Review	5
2.1 Introduction	5
2.2 Past Research on Crane Selection Process	5
2.3 Past Research on Simulation and Visualization of Crane Operations	8
2.4 Past Research on Crane Safety.....	10
2.5 Past Research on Crane Stability	12
2.6 Past Research on Wind Effects on Crane Operations	14
2.7 Past Research on Site Layout Optimization.....	16
2.8 Past Research on Building Information Model for Crane Operations ...	18
2.9 Past Research on Complex Industrial Lifts	21
2.10 Past Research on Carbon Footprints Analysis	24
2.11 Past Research on Crane Productivity	25
2.12 Double-Jib Tower Crane	26
Chapter 3: Proposed Methodology	29
3.1 Introduction	29
3.2 Methodology	36
3.2.1 Database Development and Integration	39
3.2.2 Crane Selection	41
3.2.3 Location Optimization	54
3.2.4 Crane Stability Analysis	71
3.2.5 Crane Operations Simulation.....	91
3.2.6 Crane Operations Productivity Analysis.....	94
3.2.7 Wind Effect Analysis	103

3.2.8	Environmental Footprint (Carbon Emission) Analysis	106
3.2.9	Cost Analysis	110
3.2.10	Identifying Most Feasible Cranes	114
3.2.11	Integration with Building Information Model (BIM)	116
3.3	Summary	120
Chapter 4: Case Studies		121
4.1	Introduction	121
4.2	Case 1: Pembina Lodge Project, Westlock, Alberta	121
4.3	Case 2: 34-Storey Modular Building, Brooklyn, New York.....	130
4.4	Case 3: Industrial Project, Saskatoon, SK.....	145
Chapter 5: Conclusions		151
5.1	Research Summary.....	151
5.2	Research Contributions	152
5.3	Research Assumptions and Limitations	155
5.4	Recommendations for Future Work.....	156
REFERENCES		158

LIST OF FIGURES

Figure 2.1: Diurnal variation of wind speed	16
Figure 2.2: Heavy-pressure vessel lift using two cranes (current practice)	23
Figure 2.3: Typical load distributions of two crane operation	24
Figure 2.4: Two jibs enhance jib length and safety	27
Figure 2.5: Propellers enhance rotation speed and energy efficiency	27
Figure 3.1: Different types of crane	30
Figure 3.2: Truck crane parameters	32
Figure 3.3: Free body diagram of truck crane (plan view)	32
Figure 3.4: Crawler crane parameters	34
Figure 3.5: Free body diagram of crawler crane (plan view)	34
Figure 3.6: Free body diagram of tower crane.....	35
Figure 3.7: Framework of crane selection decision support system.....	36
Figure 3.8: Proposed crane selection scheme	39
Figure 3.9: Crane 2007 database schema (Hasan et al., 2009b)	41
Figure 3.10: List of available cranes and crane selection	42
Figure 3.11: Rigging equipment	43
Figure 3.12: Crawler/mobile crane: (a) main boom, (b) main boom with luffing jib	45
Figure 3.13: Calculation of minimum clearance for main boom.....	46
Figure 3.14: Calculation of minimum clearance for main boom with luffing jib.	47
Figure 3.15: Rotation processes of a long vessel using single crane (Hermann et al., 2011)	48

Figure 3.16: Vessel-lifting mechanism configuration (Hermann et al., 2011)	50
Figure 3.17: Vessel lift configuration and design form (Hermann et al., 2011)...	51
Figure 3.18: Design results for varying sling lengths E (Hermann et al., 2011) ..	52
Figure 3.19: Mobile crane stability analysis system.....	54
Figure 3.20: Crane location and operations optimization model (Hasan et al., 2012b)	56
Figure 3.21: Available area calculation for possible crane location.....	58
Figure 3.22: Venn diagrammatic representation of the three areas relevant to crane lifting activities	60
Figure 3.23: Simplified path for an object lifted from pick point to its set position	63
Figure 3.24: Simulated site layout in which loading and destination zones are symmetrical with respect to the crane location area	64
Figure 3.25: Moments ratio map at each permitted crane location.....	65
Figure 3.26: Horizontal translation of an object lifted by a luffing-jib crane.....	67
Figure 3.27: Crane configuration form	72
Figure 3.28: Trapezoidal pressure diagram under crawler track	75
Figure 3.29: Triangular pressure diagram under crawler track.....	75
Figure 3.30: Mobile crane support reactions: (a) truck crane; (b) crawler crane .	76
Figure 3.31: Crane swing condition angle input form	77
Figure 3.32: Reaction influence chart with warning of tipping failure (Hasan et al., 2009)	78
Figure 3.33: Reaction influence chart (Hasan et al. 2009)	79

Figure 3.34: Safety warning about supporting material failure (Hasan et al. 2009)	80
.....	
Figure 3.35: Wind acting on mobile crane.....	82
Figure 3.36: Wind acting on tower crane.....	83
Figure 3.37: Crawler track pressure.....	84
Figure 3.38: Tower crane reactions	85
Figure 3.39: Wind direction effects on crawler crane operations.....	85
Figure 3.40: Wind direction effects on tower crane operations.....	86
Figure 3.41: Crane geometric and operations input form.....	87
Figure 3.42: Crawler crane support reaction calculation form with wind speed and direction	87
Figure 3.43: Tower crane support reaction calculation form with wind speed and direction	88
Figure 3.44: GBPE crane selection and input form	89
Figure 3.45: Output ground pressure from GBPE	89
Figure 3.46: Support design crane configuration and input form.....	90
Figure 3.47: Track pressure for a specified position of crane.....	90
Figure 3.48: Crane operations simulation model from Simphony.NET3.5.....	93
Figure 3.49: Double-jib crane operation.....	95
Figure 3.50: Geometrical parameters used for the estimation of mean productivity	96
Figure 3.51: Total rotation angle for a double-jib crane when $\alpha > \pi/2$	97

Figure 3.52: Ratio of single-jib to double-jib crane cycle angle (Hasan et al., 2013)	98
Figure 3.53: Three different scenarios of daily lifts (Hasan et al., 2013)	99
Figure 3.54: Distribution of swing angles for (a) the worst-case, (b) the most likely and (c) the best-case lift scenarios (Hasan et al., 2013).....	101
Figure 3.55: Contours for productivity ratios (double-jib over single-jib crane) for varying values of α_1 and α_2 (Hasan et al., 2013)	102
Figure 3.56: Hourly wind speeds in Saskatoon, 2010	104
Figure 3.57: Wind cumulative frequency	104
Figure 3.58: Sample for cost utility score assessment	114
Figure 3.59: Proposed Building Information Model (BIM)	117
Figure 3.60: Proposed BIM logical diagram (Hasan et al., 2012a)	118
Figure 3.61: BIM-supported visualization model for crawler crane operations .	119
Figure 3.62: BIM-supported visualization model for tower crane operations....	119
Figure 4.1: Pembina Lodge project, (a) site map from Google Maps, (b) proposed building	121
Figure 4.2: Site layout with feasible entrances	122
Figure 4.3: Simulation of Liebherr LTM 1800	123
Figure 4.4: Simulation of Liebherr LR 1300	124
Figure 4.5: Simulation of Liebherr LR1160	125
Figure 4.6: Crane stability analyses	126
Figure 4.7: Reaction influence chart for Scenario 3	126
Figure 4.8: Crawler track pressure diagram at 150° swing for Scenario 3	127

Figure 4.9: Crane support design summary	127
Figure 4.10: Proposed lifting visualization model	128
Figure 4.11: Crane clearances: (a) visualization model, (b) construction site	129
Figure 4.12: Actual lifting sequence photos	129
Figure 4.13: 34-storey modular building construction using (a) single-jib tower crane, or (b) double-jib tower crane.....	131
Figure 4.14: Typical floor plan and crane location.....	132
Figure 4.15: Luffing-jib crane operation on site.....	132
Figure 4.16: Hook-up activity using a platform.....	134
Figure 4.17: Scaffold transfer from one module to another.....	135
Figure 4.18: Simulation model from Simphony.NET3.5	137
Figure 4.19: Different crane work processes	138
Figure 4.20: Number of module installations per day at each floor level for both tower cranes	140
Figure 4.21: Three different simulation options: (a) one 440-ton crawler crane, (b) one 128-ton tower crane on rail, and (c) two 128-ton tower cranes	145

LIST OF TABLES

Table 3.1: Truck crane parameters.....	31
Table 3.2: Crawler crane parameters	33
Table 3.3: Tower crane parameters.....	35
Table 3.4: Crane location moment matrix	61
Table 3.5: Wind effects at different crane operations in Saskatoon on 2010	106
Table 3.6: Crane cost scores	111
Table 4.1: Scenarios with crane information	122
Table 4.2: Total rotation and time for swing to complete various module lifting operations	133
Table 4.3: Energy consumption and CO ₂ emission comparison of luffing-jib and double-jib crane	136
Table 4.4: Possible duration for different types of activities using a single-jib crane at Floor 2	139
Table 4.5: Typical module installation schedule on a given day at 2 nd and 34 th floors using single- or double-jib crane	143
Table 4.6: Utilization of different type of resources at Floor 2	144
Table 4.7: CO ₂ emission calculation for a 440-ton crawler crane at full throttle and while idling.....	147
Table 4.8: Calculation for tower crane's CO ₂ emissions.....	148
Table 4.9: Summary of different analyses	150

LIST OF NOTATIONS

α	swing angle
θ	boom angle
ω	direction of wind
ρ	maximum threshold
A	crane activity duration
A_a	available area for crane location
A_s	site area
A_b	building area
A_c	area for minimum clearances from the building
A_r	restricted area on site
$C1$	boom clearance (radial) from the lifted load
$C2$	boom clearance (radial) from the obstacle
CCE	total amount of CO ₂ emissions
CLA	crane location area
C_i	CO ₂ emission factor
d	distance from the pick or set point to the crane location
d_l	distances between outriggers in the longitudinal direction
d_t	distances between outriggers in the transverse direction
D^c	crane disassembly cost
E	energy consumption
EF	emission factor
EF_i	idling emission factor
F_b	resultant wind force on boom
F_j	resultant wind force on jib

F_t	resultant wind force on tower
F_l	resultant wind force on lifted load
f_{shape}	shape factor
f_w	wind speed multiplying factor
f_e	crawler crane's track pressure due to front or rear moment
f_s	crawler crane's track pressure due to side moment
GC	gross capacity
H	lifting height
H'	minimum lifting height
H_1	obstacle height
H_2	load height
H_3	slings and rigging height
H_w	hook weight
I	impact of delay
I'	crane installation cost
LF	load factor
LF_f	duration of crane full throttle in a day
LF_i	total crane idling time in a day
L_w	lift or object weight
M_u	required ultimate moment
M_{ns}	moment acting around the crane sides
M_{nr}	moment acting around the crane front or rear
M_w	moment created by the wind force
M_{load}	moment created by the lifted load
M_{aw}	moment created by the additional loads, such as slings or hook

M_{sw}	moment created by the movement of the boom, jib, or structure
M_{cw}	moment created by the counterweight.
M^c	crane maintenance cost
N	number of cranes
n	number of crane cycles
OCL	distance from the optimal crane location to the positions of objects
O^c	operator wages
PAs	object pick areas
P_{kw}	average engine power
P_{fb}, P_{fc}	truck crane's front outriggers reactions
P_{rb}, P_{rc}	truck crane's rear outriggers reactions
P_{front}	crawler crane's track pressure at front
P_{rear}	crawler crane's track pressure at rear
P_s	priority scale
P_j	force on the spreader bar (J)
q	wind pressure
R	crane working radius
R_1	boom clearance (horizontal) from the lifted load
R_2	boom clearance (horizontal) from the obstacle
R_w	rigging weight
R^c	crane rental cost
SL_w	sling weight
SP_w	spread bar weight
S_v	length of the variable lifting sling
S^c	crane support system cost

S_i	cost score
T_A	actual lifting start time
T_P	planned lifting start time
T_f	complete lifting cycle time
t_h	duration for hooking
t_{uh}	duration for unhooking
t_a	duration for aligning the lifted object
t_j	duration for to move an object from a pick point to its set point
T^c	transportation cost
T_W	total weight
V_w	wind velocity
v	crawler crane's track pressure due to total vertical load
v_j	speed of jib
V_u	total vertical load
w	crawler track width
W_{load}	lifting load
W_{add}	additional load
W_{design}	design load
W_{sw}	weight of the crane structure
W_{cw}	weight of the counterweight
W_i	wind parameter
x_0	distance between the crane's centerline and the center of rotation
Y	cycle angle for a given lift operation

Chapter 1: Introduction

1.1 Motivation and Background

Cranes are widely used in the construction industry to improve construction efficiency and to facilitate the on-site assembly of prefabricated components. The use of machinery in the construction industry has always been a major cost element, and cranes are among the most expensive types of construction equipment. Construction is one of the most hazardous industries in terms of safety, and in most countries it experiences the highest percentage of fatalities (Suraji et al., 2001). Among numerous factors involved in construction accidents, cranes contribute to as many as 33% of total deaths and injuries experienced in the industry (Neitzel et al., 2001). Careful and detailed planning of crane operations is crucial to the success of any project, which will consist of various tasks; errors in crane lift planning can cause schedule delays and increase project costs. Due to the competitiveness of the construction industry, contractors need to analyze the capacity and capability of key resources in order to reduce the cost and time of construction. A common link among most mobile crane accidents is human-related factors, such as poor design or improper crane selection (www.craneaccidents.com). Use of mobile cranes has represented over 84% of fatalities in the use of cranes (Beavers et al. 2006). In the United States the construction industry accounts for 19.4% of work place fatalities and 12.3% of occupational injuries and illnesses, in spite of the fact that construction workers represent only 4.8% of the U.S. work force (Abudayyeh et al. 2003). This fact is critical considering that cranes maintain a central role in building

projects, and mobile cranes in particular have dominated the North American market (Shapira et al. 2007).

Although wind is often ignored as one of the governing factors for crane operations; crane operation safety and failure analyses identify wind as an important factor (Shapira and Lyachin, 2009). Existing crane selection models do not consider construction stoppage due to high wind as a selection factor, even though high wind speed affects a crane's lifting operations and creates safety hazards. According to crane manufacturers' information on maximum allowable wind speeds, tower cranes have the advantage of usability in higher wind speeds (on average 9-14 m/s for mobile crane compared to 15-20 m/s for tower crane). It is thus necessary to consider wind as a factor while selecting a crane for a project, especially if the construction site faces significant wind exposure. Considering the effect of wind is not only important in terms of the instability of crane, but also in regards to lift scheduling, especially when the wind speed rises above the allowable limit set by crane manufacturers.

At present, planning of crane operations is primarily performed manually by experts based on experience. Efficient utilization of cranes greatly depends on skilled judgments that account for a number of technical, scheduling, and financial factors. As the number of work tasks and the demand for crane operations increases, planners may be required to make decisions regarding job conditions for a particular situation. Although lift planning and crane selection have received considerable attention from practitioners in recent decades, the developed approaches to select the best possible crane do not necessarily result

in an optimum crane selection. Several researchers have developed approaches for optimizing site layout. In these approaches specific constraints such as safety, time, and cost are taken into account in order to determine optimum crane locations. However, none of these studies have considered the crane support reactions and possible crane instability due to lifting different loads in variable radius. Thus, using these developed approaches to select the most appropriate crane and location will not necessarily result in a best crane selection.

To select the most appropriate crane, this research presents a mathematical model which identifies the ideal crane location and provides the maximum capacity required to lift all given loads by minimizing the ultimate moment created on the crane base due to different load pick points, set points, or weights of the lifted loads. Given that careful planning of crane lift operations is essential to the success of construction projects, since errors in planning could cause schedule delays and cost overruns, lifting schedules can be enhanced through the optimization of source location and crane swing.

1.2 Research Objective

The hypothesis of this research is

“Improving the crane selection process and designing crane support systems for large construction projects by evaluating wind and environmental impacts and optimizing crane location, which could reduce the risk associated on crane operations.”

The research hypothesis will be accomplished by the following process:

- (i) Identifying the most suitable crane, considering technical factors, wind effects, environment (carbon footprint), productivity and cost;
- (ii) Evaluating the stability of the selected crane due to the critical loads;
- (iii) Analysing the crane instability due to heavy winds;
- (iv) Identifying the best possible crane location;
- (v) Developing decision support system which can assist in selecting the most appropriate crane.

1.3 Organization of the Thesis

The thesis is organized into five chapters; Chapters 2-5 are outlined below:

Chapter 2 (Literature Review) includes a summary of the previous research related to lift planning and selection of cranes for construction. The application of simulation, database management, and 3D animation for crane planning in the construction field are described in this chapter. **Chapter 3** (Proposed Methodology) presents a crane selection decision support system satisfying stability, wind, productivity, carbon footprint and cost. **Chapter 4** (Case Studies) describes the usefulness of the proposed methodology by describing three case examples. **Chapter 5** (Conclusion and Recommendations) summarizes this work and outlines research contributions and specific limitations. This chapter also lists several research directions which merit further investigation to broaden the application of this research.

Chapter 2: Literature Review

2.1 Introduction

The literature review for this research was conducted on the basis of the need for lift planning tools. Lift planning for heavy lifts on major industrial construction projects is time-consuming, and traditional industrial project management processes are often deficient in terms of the sharing of information among different workers or parties. In order to address these challenges, engineers and researchers utilize computer technology to automate the crane planning process and develop visualization models. This chapter presents a summary of the existing research related to crane selection, visualization, and site-layout optimization, and provides the roadmap for the development in this research of decision support system for crane selection which analyzes crane stability.

2.2 Past Research on Crane Selection Process

Current research in the domain of construction cranes focuses primarily on developing tools to assist practitioners in the crane selection process. Furusaka and Gray (1984) developed a model for the selection of the optimum crane for any given specific construction site. Gray and Little (1985) developed a crane selection model where each possible choice was financially evaluated and the final choice was made on practical and economic grounds. The authors also developed a computer-based expert system which greatly simplified the crane selection process. The developed system has two components. First, the graphics routine is used to consider the implications of the building's shape, load

distribution and possible crane location. This information is then used as input during the second part, which asks a series of questions to work through the decision flowcharts described in the paper. Output is presented as the best option for each selected type of crane, which is then evaluated financially to enable the least cost option to be selected. Alkass et al. (1997) described a methodology for crane selection for construction projects. The methodology is incorporated into an integrated computer system capable of advising users on the selection of appropriate cranes for their construction projects. Expert's knowledge has been captured, classified and coded in the system's knowledge-base. The system integrates a knowledge-base with algorithmic programs, and commercially available tools such as: database management, spreadsheet applications, graphics and simulations. The system utilizes Object Oriented Programming characteristics of the abstraction, inheritance, modularity, and encapsulation of data. The system allows for the stored data and knowledge to be accessed by all parties involved in the crane selection process. It is also capable of facilitating user friendly interface. Description of the methods and current practices used for cranes selection for construction projects is also presented. A fuzzy logic approach to selecting the best crane type for a construction task from a list of selected crane types was established by Hanna and Lotfallah (1999). Relational database management systems (DBMSs) are widely used to model data using a simple table-type structure without having to predefine the inter-data-relations. Al-Hussein et al. (2000) developed a database designed to house information related to cranes, their geometric lifting configuration specifications, and their

lifting capacities based on the information provided by manufacturers in crane lifting capacity charts. Al-Hussein et al. (2001) described a methodology for crane selection for construction projects. The methodology is incorporated into an integrated computer system capable of advising users on the selection of feasible cranes from a previously developed crane database. Sawhney and Mund (2002) developed a prototype integrated crane selection tool, IntelliCranes, based on adaptive probabilistic neural networks, which assists in both crane type and crane model selection. Al-Hussein et al. (2005) developed an optimization algorithm for the selection and location of mobile cranes on construction sites. The developed algorithm and its optimization module provide practitioners with a powerful, accurate, and instant evaluation tool for assessing lift configurations retrieved from the crane's database. It overcomes the limitations arising from the use of the limited information provided by the cranes' manufacturers in the form of lift-capacity charts. The algorithm has been implemented and coded using the Microsoft Visual Basic programming language and its optimization module developed using Microsoft Solver. Taghaddos et al. (2010) developed a simulation-based approach for the heavy lift planning of industrial projects which assists practitioners in selecting mobile cranes, locations, and configurations for different lifts, and producing a schedule to reduce total cost and overall construction time. Furthermore, Hermann et al. (2011) proposed a crane selection methodology for lifting long vessels in industrial projects. Usually, crane selections for lifting heavy-pressure vessels are based on the heaviest lift and/or the largest lift radius, and the potential crane and pick

position are identified by an experienced lift engineer. For two-crane lift operations, there are few written guidelines or published scholarly articles. Hermann et al. (2011) did propose a guideline for making two-crane lifts with only one crane. However, none of the developed methodologies for crane selection have considered crane location optimization during the selection process. Moreover, in order to obtain the most appropriate crane, this research presents a methodology in which the crane location and selection optimizations are carried out simultaneously.

2.3 Past Research on Simulation and Visualization of Crane Operations

Current research in the domain of crane simulation focuses primarily on developing tools to assist practitioners in the crane scheduling process. Leung and Tam (2003) demonstrated that simulation can be used to improve the scheduling strategies and reviewing the floor construction schedule. Appleton et al. (2002) developed a special purpose simulation model using priority rating logic. Shi and AbouRizk (1997) presented a resource-based modeling method for construction simulation. Shi (1999), for instance, developed a simulation method based on construction activity. Kamat and Martinez (2001) demonstrated that process-based simulation could be used to analyze crane operations by modeling the dynamic movement of cranes as well as the interaction between the crane and the lifted material during a given operation. Computer models for planning heavy and critical lifts have also been made available using integer programming and optimization techniques (Lin and Haas 1996). All these simulation models are helpful in better understanding construction operations.

However, these researchers have not considered continuous flow in their simulation models which reduces the waiting time and increase the productivity of crane operations. In order to introduce continuous flow into crane operation planning, productivity improvement strategies can be applied in conjunction with lean principles. Lean theory has been used by the manufacturing company for several years. The goal of Lean is to provide products or services to customers with the highest quality, at the lowest cost, and in the shortest time by eliminating waste. Lean principles can improve crane operation performances, along with the quality of the work performed. Hasan et al (2010b) presented an integrated system dynamics model with Lean concepts to simulate tower crane operations.

Where jobsites are tightly congested, using a series of 2D or 3D drawings helps engineers to select and plan for mobile cranes. Al-Hussein et al. (2006) noted that 3D visualization is helpful in the verification and validation of crane operations, and can be a useful tool to improve the productivity of crane operation. A basic 4D Computer-aided design (CAD) simulation model, meanwhile, allows users to visualize the expected evolution of building structures during a given period of construction based on the schedule of activities. In specific, these drawings show where cranes are expected to be located at different periods of time during the construction process (Akinici et al., 2003). Sivakumar et al. (2003) developed an approach for coordinating motions of multiple cooperative cranes during material lifting operations based on a robot path planning algorithm. Kamat and Martinez (2004) developed VITASCOPE

for the purpose of generating and displaying 3D animations of the motion of pieces of equipment during construction based on a simulation model. An integrated system has been proposed by Hermann et al. (2010) which selects the crane position, optimizes the crane scheduling, and object placement, and provides a 4D animation function. Wu et al. (2011) incorporated the designed algorithm to select mobile cranes for integration into the 3D computer-aided system. AlBahnassi and Hammad (2012) presented a framework for near real-time motion planning of cranes which satisfies safety requirements and efficiently considers the dynamic properties of construction sites. A data-driven remote monitoring and alarming system for tower crane operations has also been developed which integrates field data and 3D simulation (Li and Liu 2012). However, none of the developed visualization models for crane operations identify the possible crane instability caused by strong winds. This research thus presents a methodology to implement the safe operation of cranes by identifying possible crane instability caused by strong winds using Building information modeling (Hasan et al. 2012).

2.4 Past Research on Crane Safety

Construction is one of the most hazardous industries in terms of safety, as in most countries it experiences the highest percentage of fatalities (Suraji et. al. 2001). North America is no exception in this regard, where the highest percentage of work related fatalities takes place in construction (Behm 2005). According to a study by the Occupational Safety and Health Administration (OSHA), in the United States crane accidents claim 50 lives every year, with

over 500 construction workers having perished in crane accidents between 1984 and 1994. A report by Workers Compensation Board shows that construction constitutes 34.4% of all occupational fatalities in Alberta, which is by far the highest among all industries. Safety in construction is therefore considered a major issue for many years now; however, hazard rate in the industry still remains high. Construction entails many complex and dynamic processes involving numerous resources and equipment, and crane is certainly one of the most important equipment used in the industry. Approximately 125,000 cranes of various types and sizes are used among all sectors of the United States construction industry (Neitzel et. al. 2001). Increasing size and complexity in construction these days, calls for performing challenging maneuvers within tight schedule and budget. This is even more prominent in the case of crane use because of high cost of the equipment, and the site management tends to strive finishing the crane related tasks as quickly as possible. In order to prevent crane failures, it is essential to understand the types and causes failures. This can be obtained after investigation of an accident. Many literatures address the factors involved in crane accidents. Shapira et. al. (2009), Neitzel et. al. (2001), Beaver et. al. (2006), Vivian et.al. (2010) analyze different types of crane failure and the contributing factors. OSHA, WCB also have their own classification system, which is not completely similar to the other literatures. Ambiguities are even found when distinguishing between the failures themselves and its causes. This is because there exists no unified classification system for crane failures, nor there is any unified reporting system. It is certain that many of the accidents are

preventable, and analysis of previous accidents is very important to take effective precaution. Reporting takes time, investigation even more, so finding the cause takes too much time. Faster process can help us prevent future accidents.

Clearly additional efforts must be made to reduce the number of crane-related fatalities in construction industry. In this regard, new technologies have been applied to crane operations in order to improve efficiency and enhance safety. Bernold et al. (1997) developed a crane monitoring system capable of warning an operator who enters a danger zone due to critical loading conditions. Shapira et al. (2008) proposed a tower crane-mounted live video system which enhances safety and productivity of crane operations. Shapira and Simcha (2009) addressed quantitative measurements and risk scales of safety hazards on construction sites such as overlapping cranes, operator proficiency due to tower crane operations. Lee et al. (2012) introduced a newly developed tower crane navigation system using various sensors and BIM. Tantisevi and Akinci (2009) proposed an approach to generate mobile crane motions automatically in order to support conflict detection, which extended existing approaches in product and process modeling and visualization of construction operations.

2.5 Past Research on Crane Stability

Crane support design is commonly carried out by the rental company, the general contractor, or a third party; designers use rules of thumb to make outrigger reaction and support design calculations. However, it is not economical to design support for a maximum reaction that may not be encountered in all

situations. It thus becomes important to calculate the exact reaction in each outrigger when the crane is in motion. Some geo-technical engineers use the traditional soil-bearing capacity calculation for building foundations to design the crane mat. However, the duration of loading for a crane is relatively short and the allowable settlements for cranes are higher than for building foundations (Liu 2005). Dynamic loading, due to crane motion and load, are the key factors associated with the failure to maintain stability, and they must be considered in crane selection (Hasan et al., 2009a). Sochacki (2007) showed that the dynamic stability of a truck crane can be compromised for specified geometrical and load conditions. Jerman (2006) proposed a mathematical model for investigating the dynamic loading of a slewing crane, and identified the dynamic forces which act upon the crane's steel structure during load transport. Not only do the structures of the crane and external loads affect the dynamic behaviour of mobile cranes, but the body motion and drive system of the crane are also responsible for dynamic stability (Sun and Kleeberger, 2003). Moreover, in order to reduce the dynamic effect on crane operations, the swing operation must be effectively controlled. In this regard, Klosinski (2005) developed a mathematical model including numerical simulations and experimental investigations of mobile crane operations in order to ensure minimization of crane swings. Maczynski and Wojciech (2003), meanwhile, developed an optimization algorithm of drive functions for mobile crane slewing. Still, in practice mobile cranes may become unstable as a result of rapid penetration of the outriggers into the ground (Tamate et al., 2005) which can be observed in many cases, such as about 20%

of overturning incidents occurred when the hook load was less than the net rated load. The necessary ground conditions for setting up mobile cranes are not specifically prescribed in regulations. Chin et al. (2001) have demonstrated the causes of crane instability during payload motion, and have developed a mathematical algorithm for equilibrium and dynamic solutions of crane motion. Jeng et al. (2010) proposed a linear programming simplex method for evaluating allowable reaction forces of multiple outriggers with stability constraints. Hasan et al. (2010a) presented an integrated system to prevent crane accidents and select feasible cranes based on stability. Kim et al. (2011) have developed an automatic optimal algorithm to design the foundation of tower cranes based on secure stability and minimum cost. Finally, Hong et al. (2012) proposed a management process for tower crane selection and support design, through stability analysis and lateral support design. Calculation of ground pressure due to dynamic involvement of the mobile crane has typically been carried out manually except in the case of the system developed by Manitowoc Cranes, Inc., which provides the option to calculate the ground pressure for the Manitowoc crawler crane only. Also, it does not assist in the controlling of crane swing and design the supporting system. This research presents a decision support system to aid practitioners in the process of preparing lift studies by selecting feasible crane and calculating ground pressure.

2.6 Past Research on Wind Effects on Crane Operations

Analyses of past crane failures show that a considerable percentage have involved high wind (Shapira and Lyachin 2009, Neitzel et al., 2001; Beavers et

al., 2006). Among the two types of cranes most commonly used in industrial construction, mobile cranes are more vulnerable to high wind-related failures than are tower cranes (Shapira and Lyiachin, 2009). Several research studies have shown that maximum sustained wind speed normally occurs during daytime (Vining and Gregory, 2011; Danish Wind Industry Association, 2011). Figure 2.1 illustrates the diurnal variation of wind speed, which is plotted from the historical hourly wind speed data for Saskatoon, Saskatchewan, Canada (Environment Canada, 2011). Hourly variation of wind speed data for other Canadian cities shows similar patterns in this regard (Weather stats Canada, 2011; Li and Li, 2005). It is noted that the maximum sustained wind speed can affect daytime crane operations, and thus should be considered in selecting a crane for a given task. Daily average wind speed is averaged over the entire 24-hour period, and hence this data does not reflect whether or not the maximum wind speed at any time during the day is higher than the allowable. High wind speed affects the crane's lifting operations and creates safety hazards. For instance, one of the most devastating crane accidents ever to have occurred, the Big Blue collapse on the Miller Park Stadium project, was primarily caused by wind and poor ground conditions (Ross et al., 2007). However, consideration of the effect of wind on during lift analyses of crane operations is not widely practiced. Considering the effect of wind is not only important in terms of the instability of crane, but also in regards to lift scheduling, especially when the wind speed rises above the allowable limit set by crane manufacturers. Thus this

research presents a methodology to implement the safe operation of cranes by identifying possible crane instability caused by strong winds.

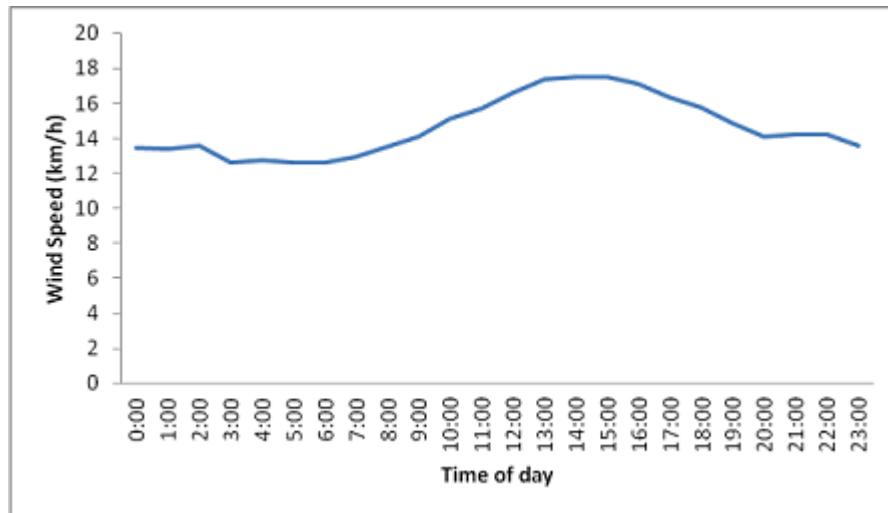


Figure 2.1: Diurnal variation of wind speed

2.7 Past Research on Site Layout Optimization

Many researchers have developed approaches to assist practitioners in optimizing site layout (Lim et al., 2005; Sivakumar et al., 2003; Tam et al., 2001; Chung, 1999). In these approaches some constraints, such as safety, time, and costs, are taken into account in order to determine the best possible location. Rodriguez-Ramos and Francis (1983) introduced a mathematical model to optimize the location of single crane, which aims to minimize the total transportation cost between the crane and construction supportive facilities that are serviced by the crane. Zhang et al. (1999) presented a computerized model to optimize location of a group of tower cranes, which consists of three models: (1) a location generation model, which produces an approximate task group for each crane; (2) a task assignment model, which adjust the task groups; and (3) an

optimization model, which finds an exact crane location for each task group. These works did not involve supply location optimization, and therefore the selected crane location may not be the optimized one if the supply location changes. Tam et al. (2001) used a genetic algorithm to optimize the tower crane and supply locations in high-rise building construction. Tam and Tong (2003) has proposed a model to select locations for tower cranes in high-rise public housing, adopting artificial neural networks (ANN) and genetic algorithms (GA) techniques. Sivakumar et al. (2003) developed an approach for coordinating motions of multiple cooperative cranes during material lifting operations based on a robot path planning algorithm. Ali et al. (2005) proposed a genetic algorithm approach for automated path planning of mobile cranes. Reddy and Varghese (2002) also developed a tool using configuration space (C-space) to identify the crane lift paths and optimize them within a constrained search space. These approaches identify the spatial conflicts at discrete time steps and at every single location within the boundary of a site. In such cases, however, site layout optimization can be time-consuming in large construction areas where several lifts need to be performed. Safouhi et al. (2011) proposed an algorithm to determine the workspace area on site for mobile cranes which satisfies the required crane-fitting distance by calculating the crane body area to a given clearance distance. Lei et al. (2011) applied a robotic motion planning method to solve crane path planning problems. Chang et al. (2012) developed a method to plan the erection path automatically for single and dual cranes which converted the scene of crane erection into a configuration space and adopted the

probabilistic road map (PRM) method to search the collision-free path. However, none of these approaches considered the crane support reactions due to the lifting of different loads. Thus, using these developed approaches to select the best possible crane and location cannot necessarily result in an optimum crane selection. This research thus presents a methodology which optimizes crane and source locations by minimizing moments created on the crane base, which can reduce the support reactions and assist in selecting the most feasible crane.

2.8 Past Research on Building Information Model for Crane Operations

Building Information Modeling (BIM) is one of the most promising recent developments in the Architecture, Engineering and Construction (AEC) industry, where virtual digital models are created in order to facilitate project-related activities at various phases (Eastman et al., 2011). It allows better information sharing among the project stakeholders, and thus can improve safety, productivity, cost, schedule, and resource management for the project. BIM helps to facilitate a 3D visualization of the project to detect clashes or errors (Eastman et al., 2011). The traditional document-based project delivery method is archaic, error-prone, litigation-prone, high-risk, and reliant upon very inefficient, hard to predict construction processes that result in owners taking over projects with little information on how to operate and maintain their building (Neeley, 2010). According to the International Organization for Standardization (ISO), BIM is to describe and display information required in the design, construction, and operation of construction facilities (ISO 29484-1

2010). It is also helpful to reduce or eliminate the need for the many paper documents currently in use. As Hasan et al. (2012) have summarized, BIM generally addresses laws and regulations, material information and specifications, procurement information, facility information, construction information, simulation results, 2D/3D drawings, and visualization/animation models. Eastman et al. (2008) have introduced a mode of BIM which provides methods to increase total project quality, improve accuracy of schedule timetables, yield quantity take-offs, and reduce total project costs. The partial or whole BIM models have been used to generate a number of effective solutions related to clash detection, quantity take-off, cost estimation, and scheduling throughout the modeling of a project (Koo and Fisher 2000; Manrique et al. 2007; Kang et al. 2007; Russell et al. 2009; Yan et al. 2011, Han et al. 2011; and Gökçe 2012). In this regard, various research and development efforts have been made to extend the use of BIM, addressing different application areas. Bynum et al. (2012) have investigated perceptions of the use of BIM for sustainable design and construction among designers and constructors. Goedert and Meadati (2008) have extended the use of BIM throughout the construction phase of the project life cycle by documenting 3D as-builts, producing a 4D as-constructed model, and capturing and storing construction documents for the owner. Abudayyeh and Al-Battaineh (2003) have used BIM to manage information in order to support bridge maintenance. Gökçe et al. (2012) proposed a new type of product catalogue structure that complies with the data schema of the IFC standard, allowing for coherent integration of product and cost information. New

methodologies to produce energy estimates and interoperability between simulation engine and BIM tools have also been introduced (Kim and Anderson 2012; Gökçe et al. 2012). Even though BIM is widely used in AEC industries to obtain networked-based environments for effective inter-organizational project collaboration, Kam and Fischer (2002) have found some limitations of BIM: (1) lack of information exchange between different software products; (2) time consuming when transferring file exchange of the model because of large file size; (3) practically impossible to achieve versioning and controlling user right in file exchange. To overcome these limitations, a standardized BIM approach, based on the Industry Foundation Classes (IFC) model of BuildingSMART, is utilized for construction management purposes (Halwafy et al. 2005; Chen 2004; Gökçe et al. 2012; and Edwin 2010). Although heavy equipment such as cranes, trucks, dozers, and tractors used in construction projects play a critical role in efficient project management, current BIM applications do not support associated information for the design of heavy equipment operations which is critical to facility construction tasks. In the current practice, only 3D visualization—one of the BIM functions—is used to identify collision-free paths by detecting and eliminating errors in the equipment schedule before constructing (Al-Hussein et al. 2005; Hasan et al. 2012; and Han et al. 2012), and many applications to plan heavy equipment operations are not supported by formal, standardized and comprehensive models for information exchange between domain applications. The construction industry is seeking a new innovative approach to integrate all the information needed to describe buildings

throughout the whole design, construction and management process. As such, BIM should contain all relevant information in a single model.

2.9 Past Research on Complex Industrial Lifts

Industrial projects, including oil refineries, usually involve a lengthy and complex process; efficient crane operation can have a significant positive impact on the overall scheduling, cost, and safety of these projects. Usually, crane selections for lifting heavy-pressure vessels are based on the heaviest lift and/or the largest lift radius, and the potential crane and pick position is identified by an experienced lift engineer. For two-crane lift operations, there are few written guidelines and published literature. Experienced lift engineers select cranes based on an individual crane's capacity to lift the heavy vessel. The current industry practice for lifting large, heavy vessels has typically been carried out utilizing two cranes. With each crane hooked to one end of the vessel, the lifting process starts simultaneously, maintaining the vessel at a horizontal position. Then, the main lift crane raises the top of the vessel while the tail crane holds the bottom of the vessel close to the ground. After being rotated into a vertical position, the vessel is placed into position as shown in Figure 2.2. However, two-crane lifts have certain difficulties, such as the following:

1. Side loading from an out-of-plumb load line can affect crane operation. This may happen when the deviation from plumb is near right angle to the boom, such as when one crane swings and is permitted to pull the second crane with it (Shapiro et al. 1999);

2. Bouncing movement (sometimes called jerking) of the heavy vessel can occur when the lifting operation is not properly coordinated and when the speeds of the cranes are different. As such, the tail crane receives additional undesired stresses which can cause accidents;
3. Swinging movement of the vessel can take place toward the tail crane's travel direction. Lifted objects with high surface areas are sensitive to wind, and at certain elevations, wind forces can displace the object in the air and create swinging movements;
4. Fleeting effect happens due to multi-crane operations where the load periodically moves off-center from the lifted hook. Lattice boom cranes are designed to carry the load perpendicular to the ground, and any additional force acting on the structure in a different direction may create significant safety concerns. Fleeting effect can arise at the lift stage when the lift crane lifts and the tail crane walks, which causes forward and backward motions; and
5. Booms tip collision can occur during a tandem lift of an object. Such an incident can take place at the end of the two-crane operation when the load carried by the tail crane is transferred to the lift crane. Any open-air load transfer from one crane to another during a lifting operation could be critical.
6. The load transfer from the tail crane to the lift crane happens within the last few degrees of the rotation and can lead to impact loading if released too quickly. If not handled properly, the load transfer can momentarily cause the tail crane to take nearly the full load of the vessel.

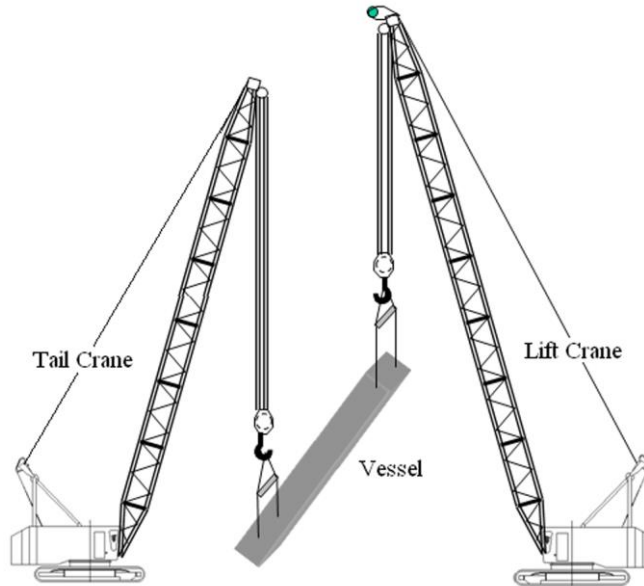


Figure 2.2: Heavy-pressure vessel lift using two cranes (current practice)

The typical load transfer from the tail crane to lift crane has been shown in Figure 2.3. However, during the operation, the tail crane may take full load due to the fault of either crane operator and an accident may occur. Therefore, two-crane lifting requires a detailed and costly analysis of each lift to ensure that the objectives of the lift are being met and the safety of the crew is maintained. As cranes are a major cost item in the construction process, the industry is always seeking to optimize the utilization of the resource. The limitations of current approaches suggest the need for a new methodology to select one crane for performing heavy-vessel lifts at construction sites.

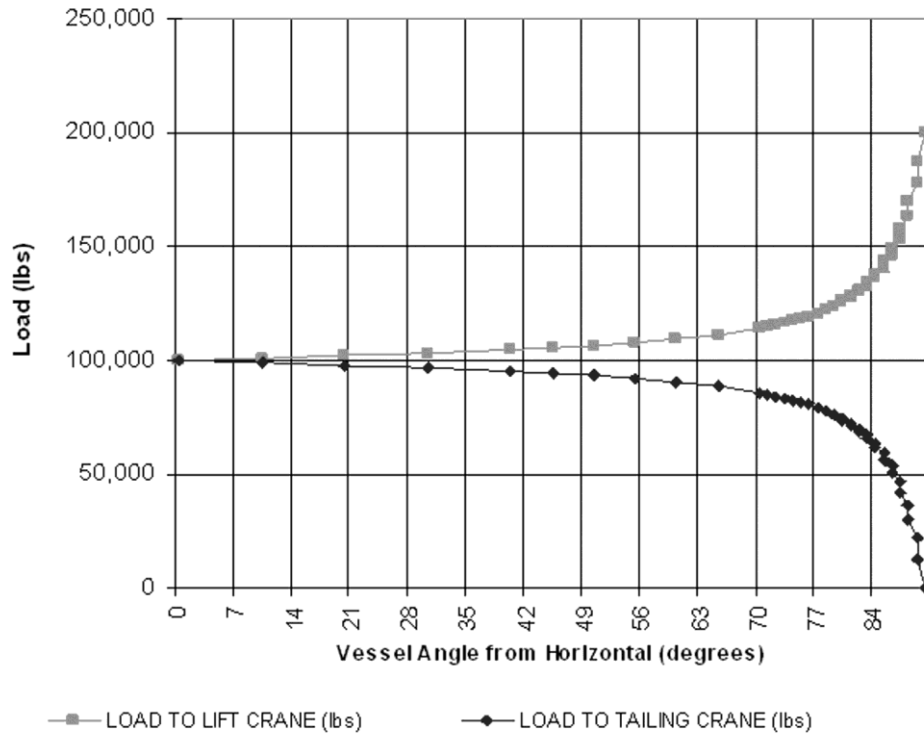


Figure 2.3: Typical load distributions of two crane operation

To overcome the limitations of current approaches and to reduce the cost and time of large-scale construction projects (such as oil sands projects), a methodology has been developed to utilize one crane rather than two for the lifting of heavy-pressure vessels (Hermann et al. 2011)

2.10 Past Research on Carbon Footprints Analysis

The construction industry has become increasingly aware of the sector's contribution to climate change. The construction industry's energy use causes significant environmental impacts (Hendrickson and Horvath, 2000). Carbon footprint quantification, analysis, and reduction cannot be ignored. Cranes maintain a central role in construction projects, and tower cranes in particular have dominated high-rise building projects. Construction cranes consume great

amounts of energy and emit significant volumes of CO₂ on site. Since 2006, the Government of Canada has been introducing regulations to reduce emissions from key sources (Environment Canada, 2010). Cranes were listed in the U.S. Environmental Protection Agency's (EPA) non-road vehicles and equipment category as one of the main sources of emissions (EPA, 2005). Due to the large amount of diesel used on site, the U.S. EPA published a Non-road Diesel Program to advance emission control technologies for engines used in non-road equipment (EPA, 2004). However, the NONROAD model data were only intended to predict average emissions for a fleet of vehicles. Similar data are needed to quantify the CO₂ emission generated by on-site crane engines. At a time when the environment is of utmost importance, every opportunity to minimize a project's carbon footprint is vital. Minimizing crane operations on construction sites will lead to faster construction and eliminate unnecessary CO₂ emissions. The construction industry is seeking innovative approaches to minimize the carbon footprint of crane operations. This research presents a methodology that focuses on the selection of cranes for high-rise building construction projects based on carbon footprint impact.

2.11 Past Research on Crane Productivity

It is important to analyze the capacity and capability of key resources to improve the productivity of on-site operations. Thomas and Yiakoumis (1987) separated factors affecting productivity into four categories: environmental, site, management, and design. 3D visualization is helpful in the verification and validation of crane operations (Al-Hussein et al., 2006) and can be a useful tool

to improve the productivity of crane operation. However, measuring the productivity of construction machinery remains difficult. Park et al. (2005) introduced a standard construction productivity metrics system (CPMS). The proposed CPMS is a standard construction productivity data collection tool and provides a framework to report industry norms to benchmark construction productivity. Crane productivity analysis does not receive much attention by practitioners. Lee et al. (2006) proposed a wireless technology to improve the productivity of the traditional tower crane. In practice, planning for crane operations is performed mostly intuitively and informally. The construction industry is seeking innovative approaches to improve the productivity of crane operations. This research presents a methodology that focuses on the selection of cranes for high-rise building construction projects based on crane productivity performance and carbon footprint impact. This research also presents a comparison analysis between the use of a single-jib tower crane and a new type of tower crane that operates using two jibs, referred to in this paper as a “double-jib” tower crane (Hasan et al., 2010b).

2.12 Double-Jib Tower Crane

In 1968, Gaspard Gillis, founder of the GG Crane Group, designed, patented, and built cranes with two jibs in Belgium. The idea consisted of a central tower with jibs placed on both sides of the tower (see Figure 2.4), with the jibs rotating around the central tower by use of propellers mounted at the end of each jib (see Figure 2.5). These propellers also rotate to provide braking operation to the jib.

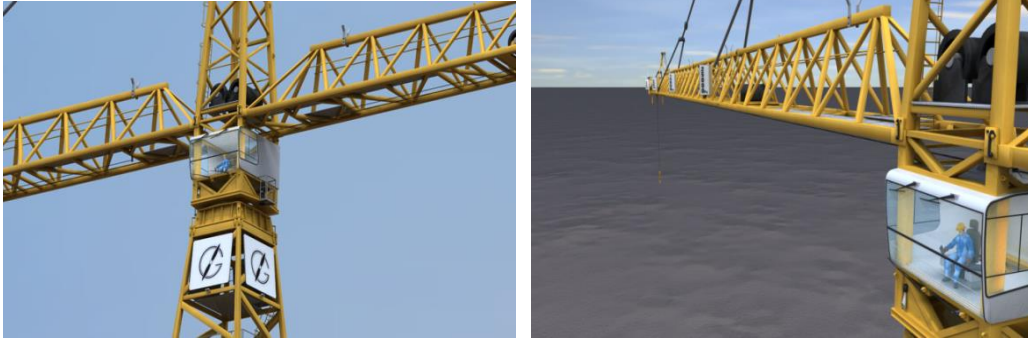


Figure 2.4: Two jibs enhance jib length and safety

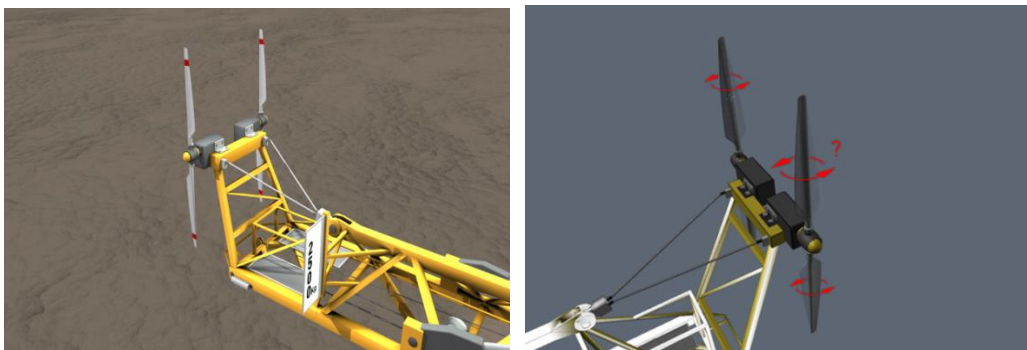


Figure 2.5: Propellers enhance rotation speed and energy efficiency

This technique has the advantage of eliminating the torque forces generated by the tower (what is also known as the mast of the tower crane). The elements of the tower and jib are built to improve assembly and disassembly, and the dimensions of the elements are aligned to the legal dimensions for freight transport on public roads. The objectives to increase the performance and application of the current tower cranes are to: (1) enhance work efficiency; (2) enhance lifting capacity; (3) enhance the jib lengths; (4) increase the rotational speed; (5) enhance the rotating and braking power; (6) eliminate torsion forces; (7) neutralize the wind load; (8) improve energy efficiency; (9) enhance safety; (10) enhancing reliability; and (11) reduce assembly, disassembly, and

transportation costs. The jib lengths of the GG Crane are greater than on conventional cranes. Having the propellers positioned at the ends of the jibs, driven by an electric motor, means that the force to turn the jib is being exerted at that point, rather than at the central tower as with conventional cranes. This crane is more energy-efficient, since less force is required to turn and break the swinging operations of the tower crane.

Chapter 3: Proposed Methodology

3.1 Introduction

The aim of the research presented in this thesis is to assist practitioners in selecting and planning detailed crane operations with the help of decision support system which integrates different mathematical models. The types of mobile cranes available vary due to the different types of booms (telescoping or lattice) and undercarriages (on wheeled or crawler-tracked) used. The basic types of mobile cranes are: Boom Truck, Carry Deck, Crawler, Mobile Conventional, Mobile Hydraulic, Rough Terrain, Sky Horse, Tower Crawler, Transi-Lift, and Traveling Ringer. To simplify the analysis process, in this research mobile cranes have been classified into two categories: truck crane and crawler crane. A crane is called a truck crane if the rotating superstructure of the mobile crane is mounted on a wheelbase (rubber) or outrigger base, and when the superstructure of the crane is mounted on a crawler carrier it is referred to as a crawler crane (see Figure 3.1). There are several methods of support for static mount tower cranes such as: in-situ anchor bolt base, in-situ expendable base, knee braced base, guyed tower crane with spread footing, braced tower crane and internal climbing crane. In this research, tower cranes with four support points (anchor bolt) are considered (see Figure 3.1).

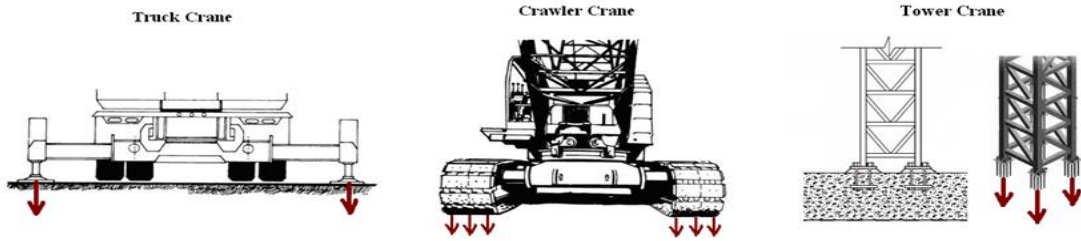


Figure 3.1: Different types of crane

The geometric configurations needed to perform the calculations are not ordinarily given in the crane manufacturer’s literature. Crane owners, users, or installation designers can, however, request needed data from the crane manufacturer. Unfortunately, manufacturers supply information about their cranes in inconsistent and paper-based formats. To address this deficiency, researchers have developed a database to replace and store the existing paper-based crane load charts and geometric information in a standardized computer-based format. In this research, the “D-Crane” and “Crane 2007” databases have been used to store information about crane geometry. Based on the type of crane under study, the geometric configuration module interacts with the crane database to retrieve the information. For the truck crane, the variables used in the analysis process are listed in Table 3.1 and are shown in Figures 3.2 and 3.3.

Table 3.1: Truck crane parameters

Type	Notation	Description
Constant Parameter	t	Distance between Boom pin and center of rotation.
	x_o	Distance between outrigger centerline and axis of rotation.
	d_t	Distance between outriggers in the transverse direction.
	d_l	Distance between outriggers in the longitudinal direction.
	θ	Boom angle to the ground
	W_r	Weight of the suspended hoist ropes, hook block and Slings.
	W_b, W_j	Weight of the boom & weight of the jib
	L_b and θ_b	Position of boom center of gravity (CG)
	J_j and μ_j	Position of jib CG
	L	Boom length
	W_{u1}, d_{u1}	Upper-structure weight & CG distance to center of rotation
	W_{u2}, d_{u2}	Counterweight weight & CG distance to center of rotation
	W_c, d_c	Carrier weight & CG distance to center of rotation
	W_m, d_m	Machine weight & CG distance to center of rotation
	W_a	Additional weight
	User defined parameter	V
α		Boom horizontal swinging angle
W		Weight of the lifted load
Calculated parameter	R	Lifting radius
	P_{fb}	Reaction of front outrigger on the boom side
	P_{fc}	Reaction of front outrigger on the counteract weight side
	P_{rb}	Reaction of rear outrigger on the boom side
	P_{rc}	Reaction of rear outrigger on the counteract weight side

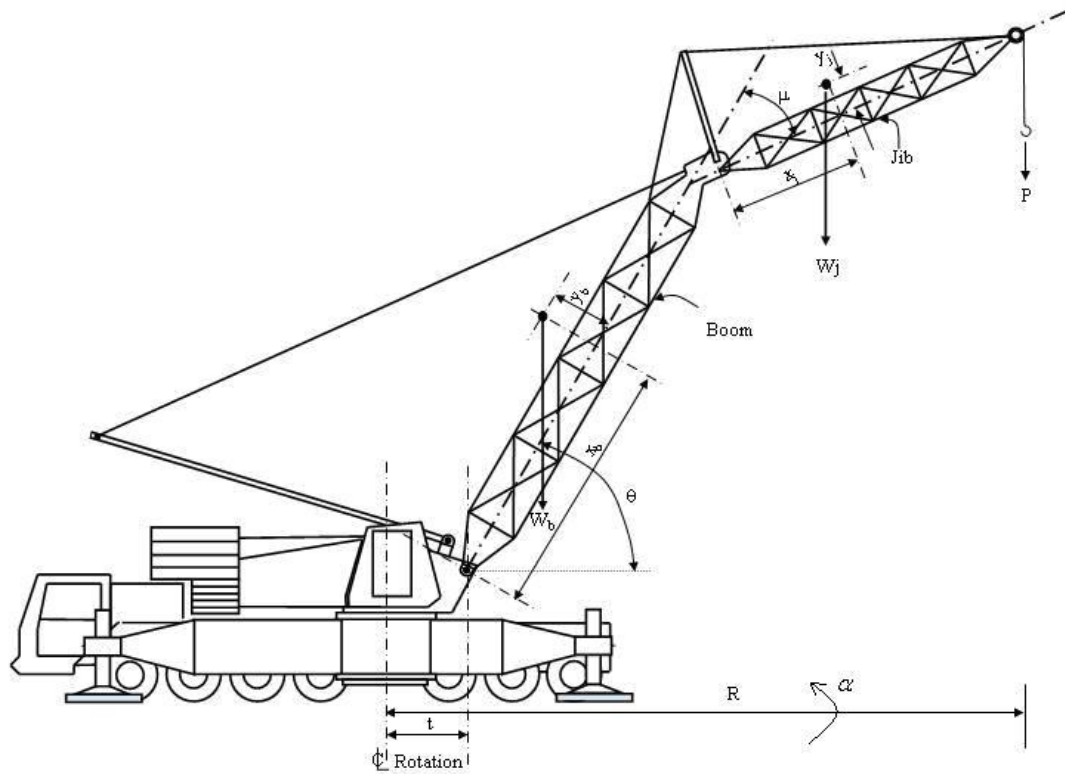


Figure 3.2: Truck crane parameters

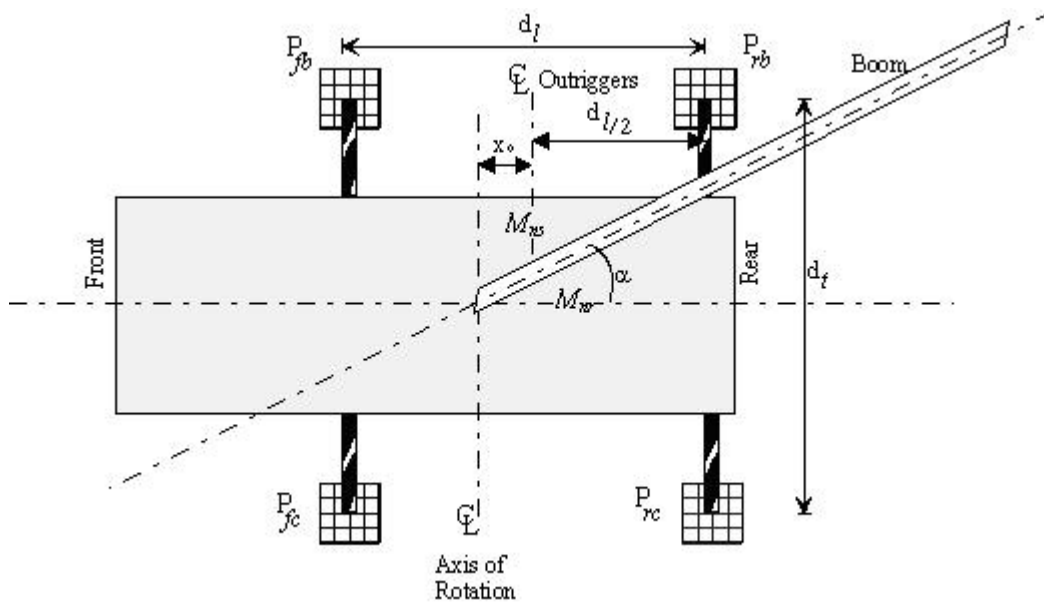


Figure 3.3: Free body diagram of truck crane (plan view)

For the crawler crane, the variables used in the analysis process are listed in Table 3.2 and are shown in Figures 3.4 and 3.5.

Table 3.2: Crawler crane parameters

Type	Notation	Description
Constant Parameter	t	Distance between Boom pin and center of rotation.
	x_o	Distance between outrigger centerline and axis of rotation.
	d_t	Distance between tracks in the transverse direction.
	d_l	Crawler bearing length.
	θ	Boom angle to the ground
	W_r	Weight of the suspended hoist ropes, hook block and Slings.
	W_b, W_j	Weight of the boom & weight of the jib
	L_b and θ_b	Position of boom center of gravity (CG)
	J_j and μ_j	Position of jib CG
	L	Boom length
	W_{u1}, d_{u1}	Upper-structure weight & CG distance to center of rotation
	W_{u2}, d_{u2}	Counterweight weight & CG distance to center of rotation
	W_c, d_c	Carrier weight & CG distance to center of rotation
User defined parameter	V	Total weight of the crane and the lifting load
	α	Boom horizontal swinging angle
	W	Weight of the lifted load
Calculated parameter	R	Lifting radius
	P_{fron1}	Front track pressure on boom side
	P_{rear1}	Rear track pressure on boom side
	P_{front2}	Front track pressure on counterweight side
P_{rear2}	Rear track pressure on counterweight side	

For the tower crane, the variables used in the analysis process are listed in Table 3.3 and are shown in Figure 3.6.

Table 3.3: Tower crane parameters

Type	Notation	Description
	d_t	Distance between two anchor pins (supports) in the transverse direction.
	d_l	Distance between two anchor pins (supports) in the longitudinal direction.
	W_r	Weight of the suspended hoist ropes, hook block and Slings.
	W_T, W_j	Weight of the tower and weight of the jib
	J_j and μ_j	Position of jib CG
	L	Tower length
	W_{u1}, d_{u1}	Structure weight & CG distance to center of rotation
	W_{u2}, d_{u2}	Counterweight weight & CG distance to center of rotation
	W_a	Additional weight
	V	Total weight of the crane and the lifting load
User defined parameter	α	Boom horizontal swinging angle
	W	Weight of the lifted load
	R	Lifting radius
Calculated parameter	P_{fron1}	Front support reaction on jib side
	P_{rear1}	Rear support reaction on jib side
	P_{front2}	Front support reaction on counterweight side
	P_{rear2}	Rear support reaction on counterweight side

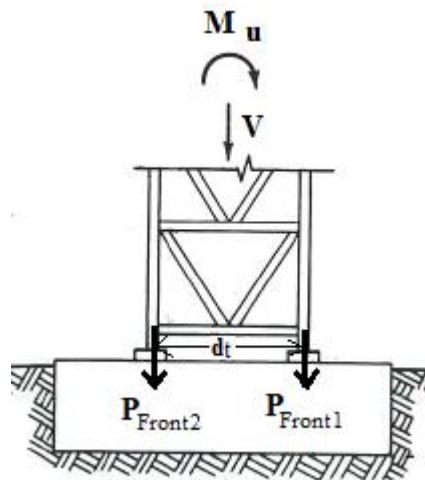


Figure 3.6: Free body diagram of tower crane

3.2 Methodology

The purpose of the methodology employed is to improve operations for both tower cranes and mobile cranes. The aim of the research presented in this thesis is to assist practitioners in selecting and planning detailed crane operations by developing decision support system and mathematical models. The proposed decision support system comprises the following three modules as shown in Figure 3.7: (1) crane selection and location optimization, (2) stability analysis, (3) advanced analysis, and (4) integration with Building Information Model.

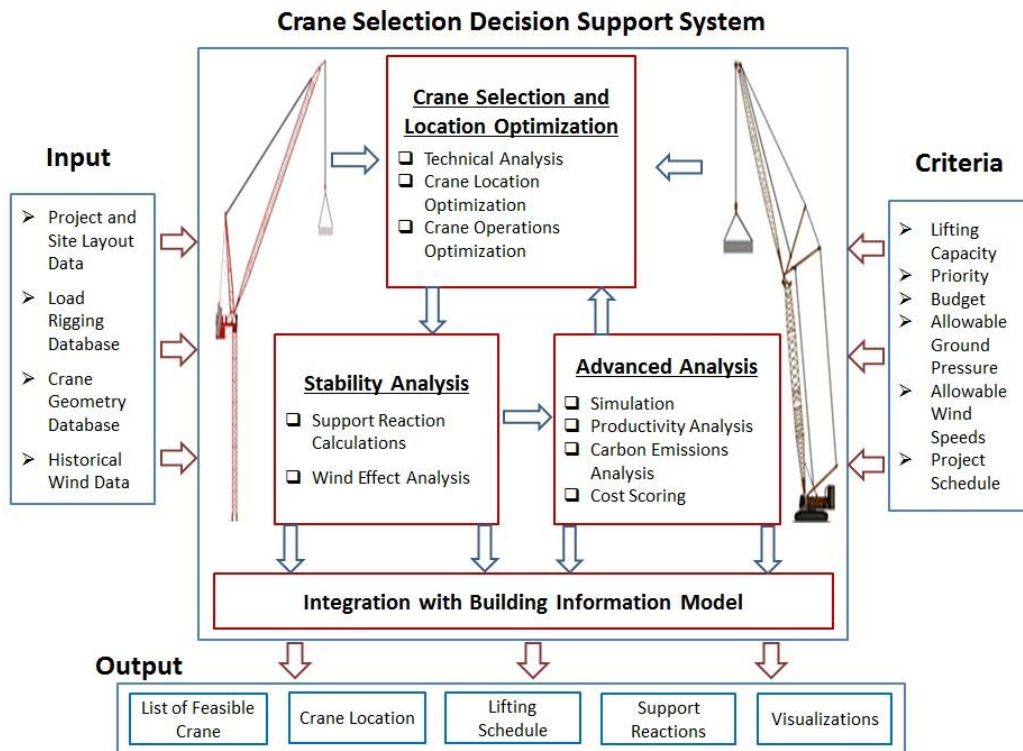


Figure 3.7: Framework of crane selection decision support system

The crane selection and location optimization module has the following components: technical analysis, crane location optimization and crane operations optimization. The technical analysis assists in selecting a technically feasible

crane by assessing the: (1) crane capacity, (2) lifting radius, (3) lifting height, and (4) clearances. The stability analysis facilitates safe operation of cranes by identifying possible crane instability caused by improper selection or strong winds. The advance analysis module has the following components: simulation, productivity analysis, carbon emissions analysis and cost scoring. The advanced analysis assists in identifying productive and energy efficient cranes. Finally the integration with Building Information Model allows visualizing the conflict free paths of crane operations and scheduling lifting activities. The selection process is based upon the following criteria: (1) lifting capacity; (2) budget; (3) soil bearing capacity; (4) allowable wind speeds; and (5) project schedule. The integrated model output includes the following five components: (1) crane selection, either optimum or feasible, based on the selection criteria; (2) crane location, which identify the best possible crane and loading source (pick point) locations in the construction site; (3) support reactions, which are determined by calculating the reactions for truck and tower cranes, as well as the shapes and values of the track pressure for the crawler crane; (4) lifting schedule, which provides the detailed crane schedule satisfying the wind affects and soil bearing capacity; and (5) visualizations, which shows the lift activities with respective crane support reactions due to varying wind speeds and directions.

A crane selection scheme is described as shown in Figure 3.8. The first step is to select an appropriate technically feasible crane to perform the required lifts. In this case, cranes must be selected based on known configurations which encompass capacity, boom-jib lengths, counterweight, crane layout, and other

crane geometric information. Once the crane has been selected, based on the type of crane the geometric information module interacts with the crane database to retrieve the crane's geometric information. Once the technically acceptable cranes have been identified, the next step is to identify the best suitable location for crane and loading source. After identifying the perfect location, all the technically feasible cranes need to satisfy the stability constraints. The identified feasible cranes need to satisfy project schedule parameters which can be identified using a simulation model. After simulating the lifting operations based on priority, schedule, and crane configurations, the simulation model provides information about the number of cranes required. Crane productivity need be analysed during the crane selection and planning process. Once the technically acceptable and productive cranes have been identified, the final steps are to determine which is most suitable based on the specific factors, namely, wind, carbon footprint, and cost. Finally, crane operations and conflict-free paths are identified using visualization models integrated with Building Information Model.

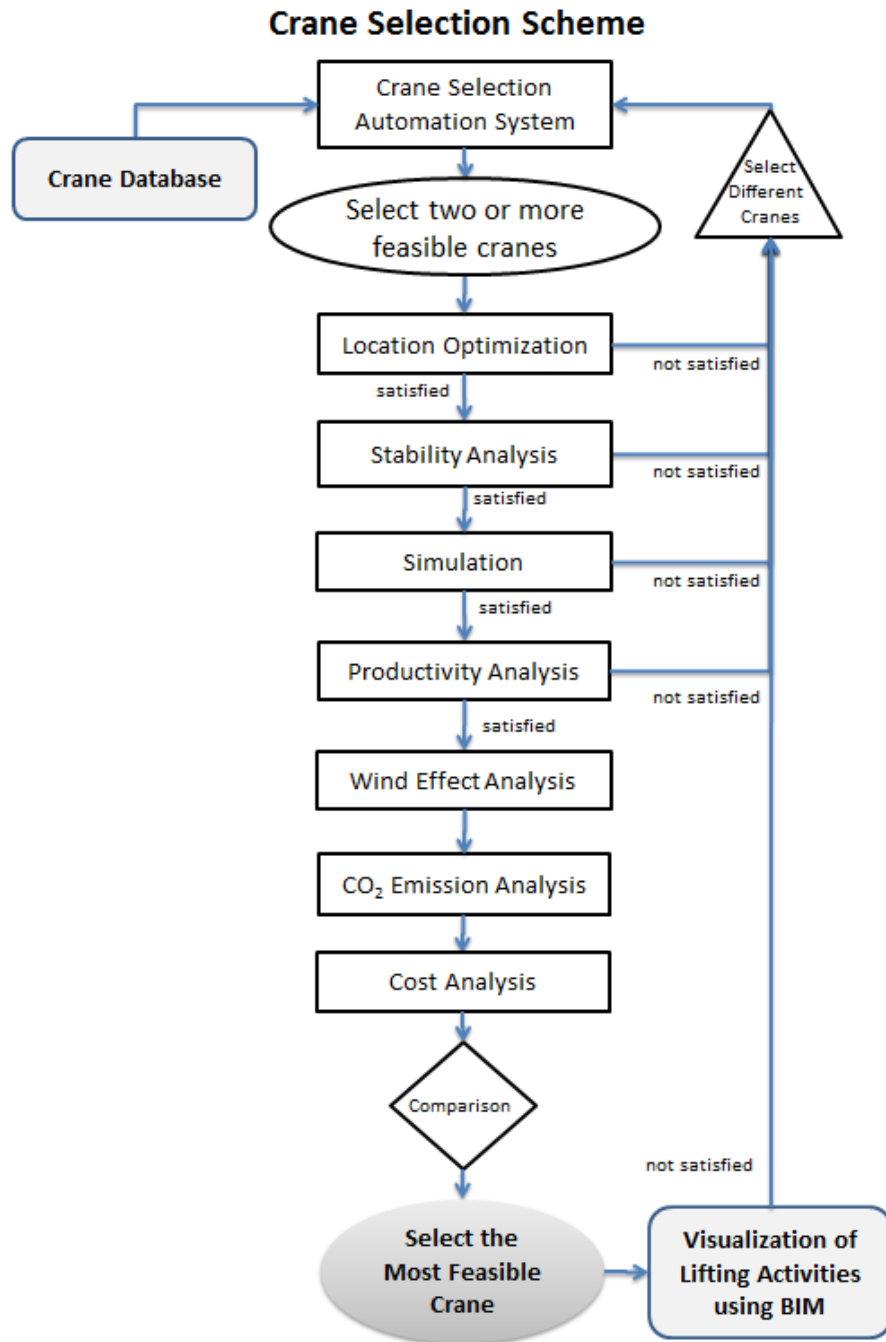


Figure 3.8: Proposed crane selection scheme

3.2.1 Database Development and Integration

Relational database management systems (DBMSs) are widely used to model data using a simple table-type structure. The use of such a system eliminates the

need to predefine the inter-data-relations. Mobile crane geometric specifications, load information, and other data supplied by the manufacturer for 195 different cranes have been stored in the Crane 2007 database (Hasan et al., 2009b). The types of mobile cranes available vary due to the different types of booms (telescopic or lattice) and undercarriages (wheeled or crawler-tracked) used. The basic types of mobile cranes available in the Crane 2007 database are: boom truck, carry deck, crawler, mobile conventional, mobile hydraulic, rough terrain, sky horse, tower crawler, transi-lift, and traveling ringer. The database has been developed in such a way that it offers three important attributes: (1) simplicity and user-friendliness; (2) functionality with other systems that require crane information; and (3) compatibility with the new crane information to be added. The database consists of 8 different tables with hundreds of fields as well as user-friendly forms. Among these fields, certain variables are needed in order to calculate the ground pressure. Conveniently, the developed system interacts with the database to retrieve these variables. Finally, a database schema is used to characterize and map the relationships among the required entities as shown in Figure 3.9 (Hasan et al., 2009b). The developed system has also been integrated with the “D-Crane” database which has been previously developed by Al-Hussein et al. (2000). The developed crane selection system interacts with the crane databases to retrieve the crane geometry information once a crane with a capacity to carry the design load has been selected.

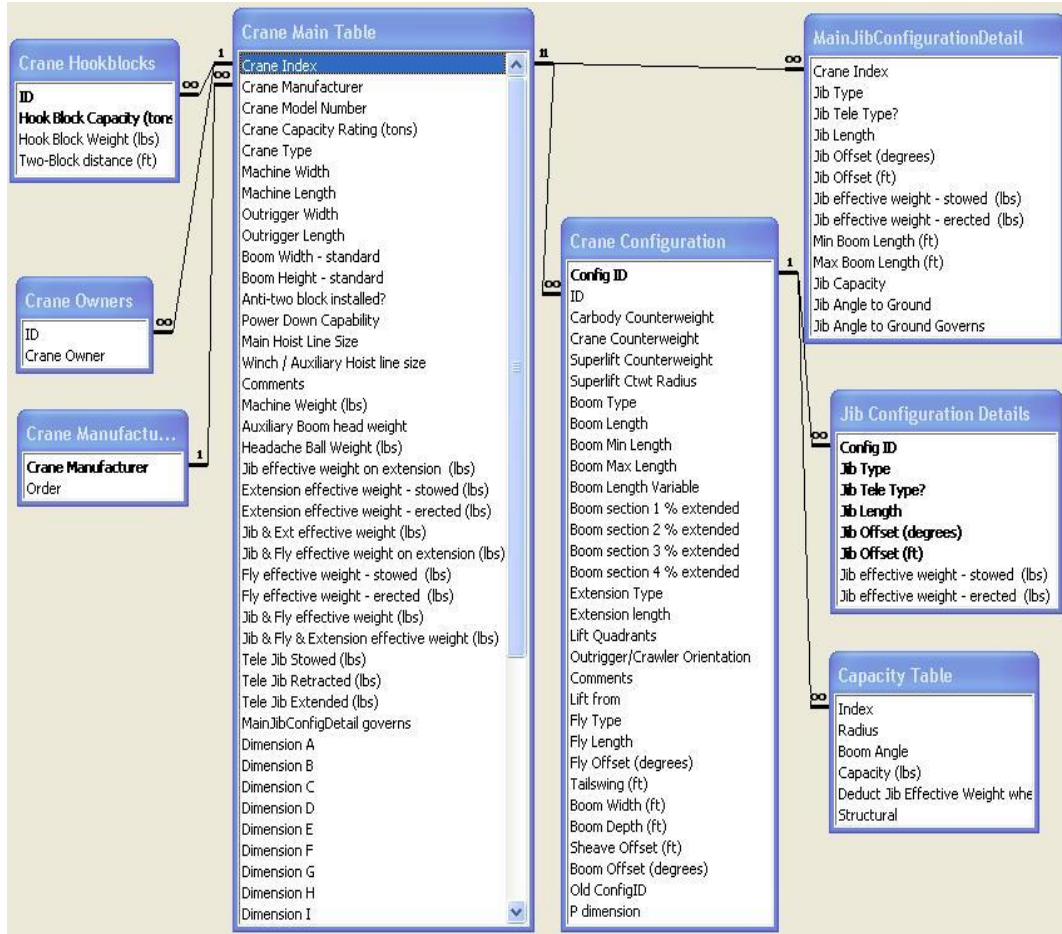


Figure 3.9: Crane 2007 database schema (Hasan et al., 2009b)

3.2.2 Crane Selection

The crane selection automated system assists in selecting a crane which can be obtained in three different ways: by (1) manually selecting a crane, (2) selecting from the crane database, or (3) using a crane selection system (The developed system has been integrated with the D-Crane database and Crane 2007 database.) One of the first steps in selecting a crane for lift operations is to identify the maximum load to be lifted. Once the lifted load has been identified, the user can assume the weight of the rigging equipment based on the size and weight of the lifted load. To ensure safe operations, the user must input the maximum

threshold based on the particular job conditions. This includes such conditions as: soft, uneven, or un-level ground; high winds; side loads; jerking or sudden stopping of loads; or other hazardous conditions. Usually for the tower crane operation 85% and for mobile crane operations 75% thresholds are assumed. The design load can be calculated using Equation (3.1) and shown in Figure 3.10.

$$W_{design} = (W_{load} + W_{add}) / \rho \quad (3.1)$$

where W_{load} , W_{add} , W_{design} are the lifting load, additional load, and design load, respectively, and ρ is the maximum threshold.

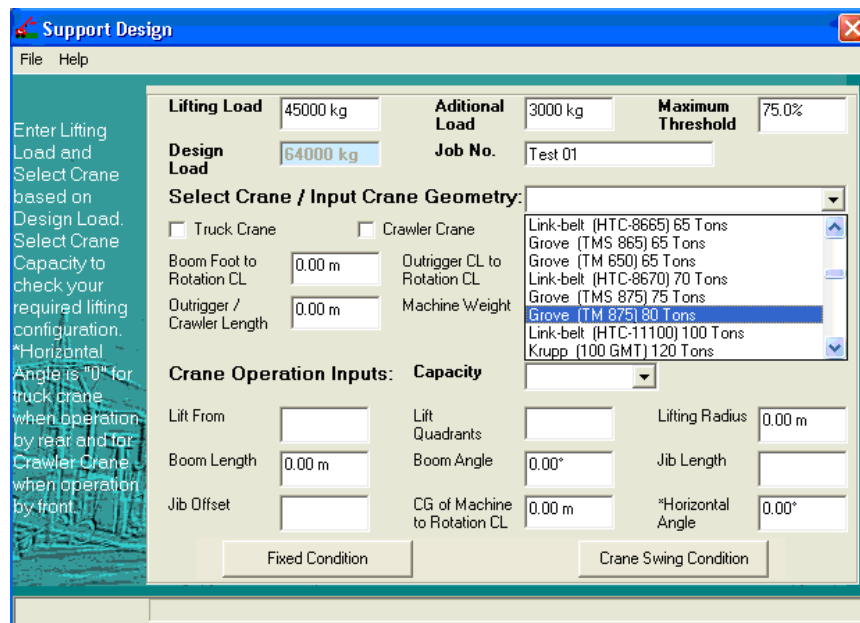


Figure 3.10: List of available cranes and crane selection

A crane with a capacity to carry the design load can be selected from the list of available cranes in the database using the list menu of the configuration form as shown in Figure 3.10. Once the crane has been selected, based on the type of crane, the geometric information system interacts with the crane databases to retrieve the crane geometry information. The user must select a configuration

based on the crane capacity. To select a suitable crane the following four configurations must need to be satisfied: (1) lifting capacity, (2) lifting radius, (3) lifting height, and (4) clearances. If the given configuration cannot meet the requirements, then the user must select a higher-capacity crane. The user also has the option to alter the given configuration.

Lifting Capacity Assessment

The lifting capacity chart provided by manufacturers is used for calculations to select the appropriate crane. The crane capacity associated with any given configuration should be greater than or equal to the total lift weight. The crane's lifting capacity must satisfy Equation (3.2).

$$GC \geq T_w = L_w + H_w + SL_w + SP_w \quad (3.2)$$

where GC = gross capacity; T_w = total weight; L_w = lift or object weight; R_w = rigging weight; H_w = hook weight; SL_w = sling weight; SP_w = spread bar weight. Figure 3.11 illustrates a typical four points rigging system.

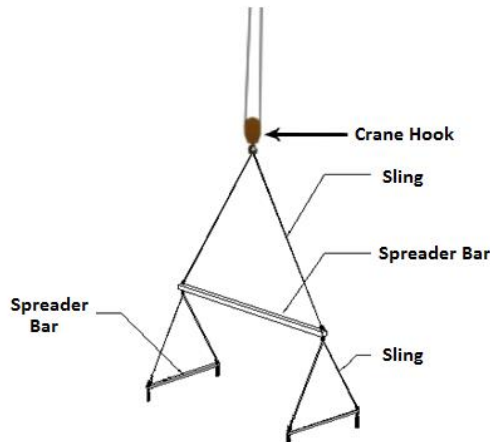


Figure 3.11: Rigging equipment

Lifting Radius Assessment

The crane working radius must be greater than or equal to the distance from the optimal crane location to the positions of objects (local), satisfying Equation (3.3).

$$R \geq OCL \quad (3.3)$$

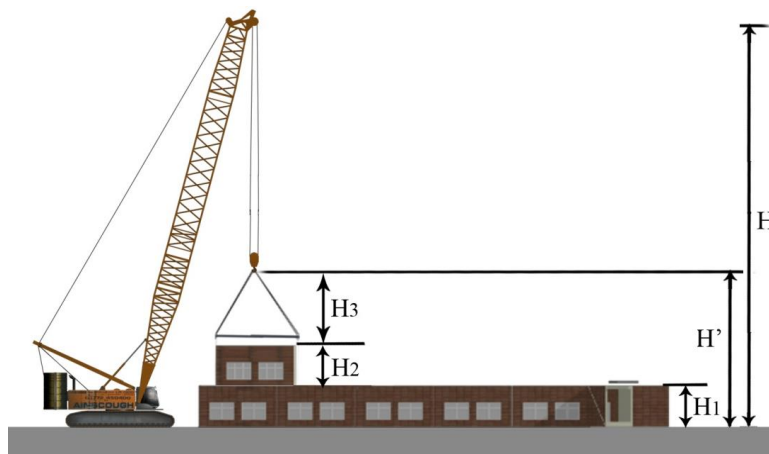
Where R = crane working radius; and OCL = distance from the optimal crane location to the positions of objects defined in the crane location section.

Lifting Height Assessment

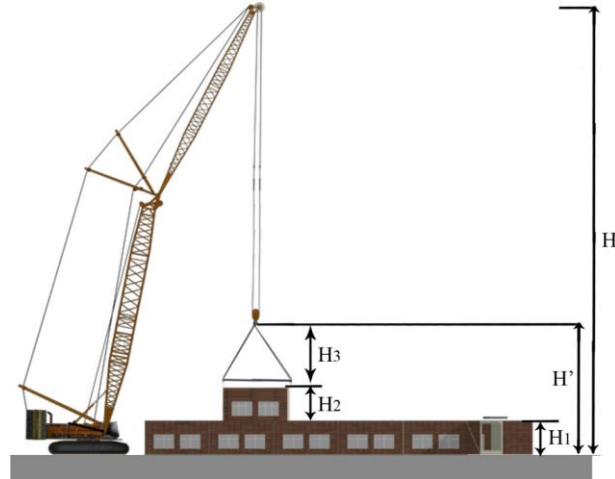
The lifting height is calculated under different boom and jib combinations. There are two types of boom and jib combinations: the main boom configuration (see Figure 3.12a) and the main boom with luffing jib configuration (see Figure 3.12b). The lifting height (H) must be greater than the minimum lifting height (H'), satisfying Equation (3.4).

$$H > H' = H_1 + H_2 + H_3 \quad (3.4)$$

where H_1 , H_2 , and H_3 are the obstacle height, load height, and sling and rigging height, respectively.



(a) Main boom configuration



(b) Main boom with luffing-jib configuration

Figure 3.12: Crawler/mobile crane: (a) main boom, (b) main boom with luffing jib

Assessment of Clearances

Generally, pieces of heavy equipment with diameters of 4 to 6 m, and in some cases up to 10 m, have the possibility of colliding with the main boom or jib of the crane (Wu et al., 2011). The calculation of minimum clearance consists of two steps: (1) distance between crane boom/jib and building (C_1) and (2) distance between crane boom/jib and the lifted load (C_2). Depending upon the given crane configuration, whether main boom and main boom with luffing jib, the calculation of clearances varies. As shown in Figure 3.13, for lifts utilizing a main boom configuration, the minimum clearances can be calculated using Equations (3.5) and (3.6).

$$C_1 = R_1 \times \sin \theta \geq \text{default values defined by users} \quad (3.5)$$

$$C_2 = R_2 \times \sin \theta \geq \text{default values defined by users} \quad (3.6)$$

$$\text{and } \theta = \tan^{-1} \frac{(H - Z_1)}{R}$$

where θ is the boom angle, R_1 is the distance between Points B and C, R_2 is the distance between Points D and E, and Z_1 is the height of the boom rotation point.

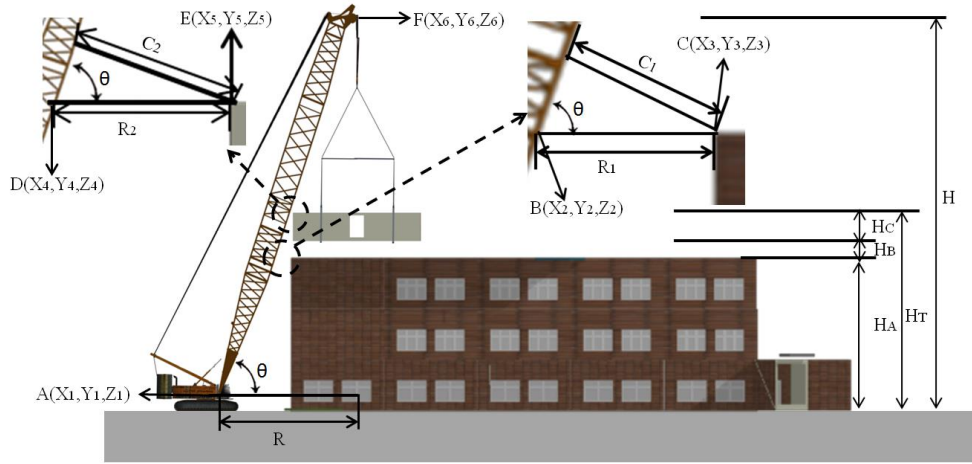


Figure 3.13: Calculation of minimum clearance for main boom

As shown in Figure 3.14, for lifts using a luffing jib, the minimum clearances can be calculated using Equations (3.7) to (3.9).

$$C_1 = R_1 \times \sin \theta \geq \text{default value defined by users} \quad (3.7)$$

$$C_2 = R_2 \times \sin \theta \geq \text{default value defined by users} \quad (3.8)$$

$$C_2 = R_2 \times \sin \beta \geq \text{default value defined by users} \quad (3.9)$$

$$\text{where } \beta = \tan^{-1} \frac{H_{Tr}'}{R_3}$$

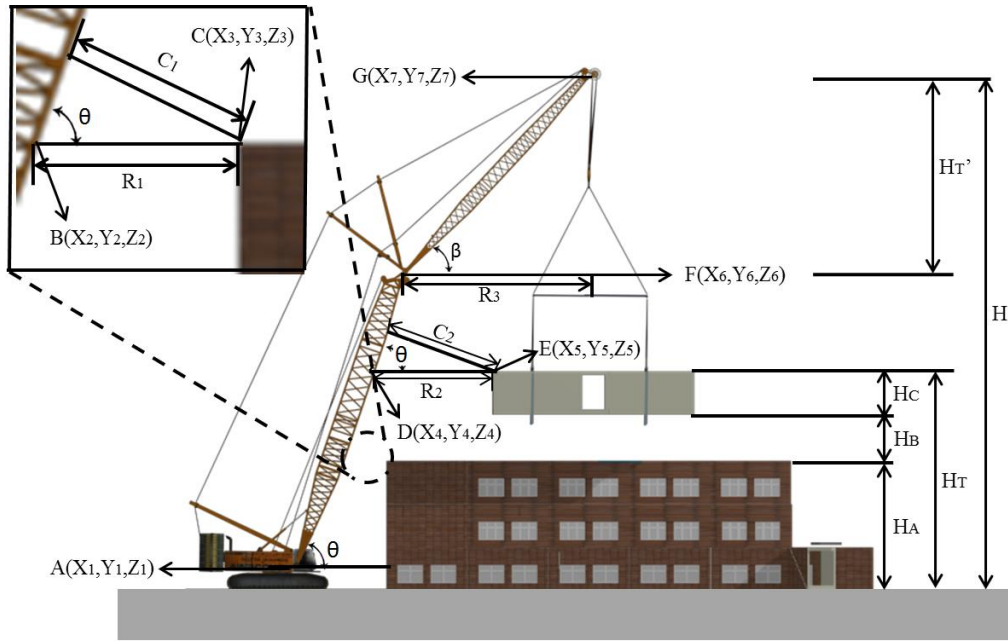


Figure 3.14: Calculation of minimum clearance for main boom with luffing jib

The developed automated system assists the user in the selection of a technically feasible crane to lift and rotate long heavy-pressure vessel lifts on construction sites. This automated system can optimize the vessel lift configuration (Hermann et al., 2011). The proposed methodology has been designed to carry out a heavy-vessel lift utilizing only one crane instead of utilizing current industry practice, two cranes lift. This method utilizes a lifting mechanism where the lift operator needs to shorten one of the side slings in order to rotate the vessel into a vertical position before placement. Having independent control over both slings from the lifting point of the crane, the sling connected to the vessel top will start to pull (shorten) using a secondary load line suspended from the boom tip and running through a sheave mechanism to rotate the vessel until it reaches its final vertical position as shown in Figure 3.15. The body of the vessel is not designed to withstand any pressure from the cables while lifting. Therefore, in order to

protect it from any damage, a custom spreader bar is utilized to provide a minimal clearing distance between the body of the vessel and the cables during the rotation of the vessel. In Figure 4, the ends of the spreader bar (J) are connected to the vessel's lift lugs through fixed length slings (E and F). The spreader bar is also connected to the lifting point through two slings (Sf and Sv). The sling running to the tail lug (Sf) is of fixed length, and the sling to the top lift lug (Sv) is of variable length.

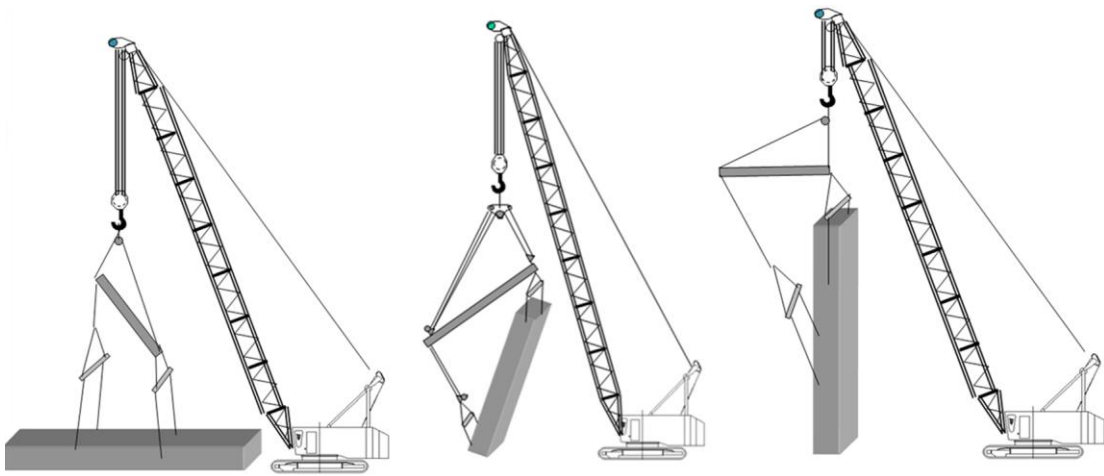


Figure 3.15: Rotation processes of a long vessel using single crane (Hermann et al., 2011)

There are physical constraints related to the structure of the spreader bar that have to be observed while finding the proper configuration of sling lengths. One consideration includes the angle between the spreader bar (J) and the lifting slings (Sf and Sv) which needs a minimum of 25° to operate/function. Any configuration of a known set of lengths for the slings and the spreader bar that will satisfy the lifting constraints is considered a solution. However, the objective of this methodology is to find the optimal configuration that will minimize the pulled length (shortening) of the variable sling (Sv) that is needed

to complete the full rotation of the vessel from horizontal ($\alpha = 0^\circ$) to vertical ($\alpha = 90^\circ$) and satisfying Equations (3.10) to (3.15):

$$\delta > 25^\circ \quad (3.10)$$

$$\gamma > 25^\circ \quad (3.11)$$

$$15' < F < 25' \quad (3.12)$$

$$20' < S_v < 30' \text{ at } \alpha = 90^\circ \text{ (i.e. final vertical position)} \quad (3.13)$$

$$P_j > 0 \text{ (i.e. always under compression)} \quad (3.14)$$

$$\text{Clearance between Spreader Bar and Vessel} > 3' \quad (3.15)$$

where,

δ = the angle between the spreader bar (J) and the fixed lifting sling (S_f)

γ = the angle between the spreader bar (J) and the variable lifting sling (S_v)

F = the length of the side sling F

S_v = the length of the variable lifting sling

P_j = the force on the spreader bar (J)

The system is developed to calculate the maximum and minimum lengths of sling S_v (see Figure 3.16) in order to complete the full rotation of the vessel from 0° to 90° . The input parameters are the properties of the vessel, spreader bar length (trial), and all the slings' lengths (trial), except the length of S_v . The design process is based upon the following criteria: (1) the angles δ and γ of the slings (S_f and S_v) with the spreader bar (J) must be greater than what the user has defined, e.g., 25° ; and (2) the maximum and minimum forces on the slings should be within an acceptable range based on the materials' properties. The user

needs to input all the slings' lengths (except S_v), vessel dimensions, and the spreader bar length in order to design a rotation as shown in Figure 5.4. All outputs should satisfy the constraints; otherwise, the system will warn the user by highlighting the unsafe output in red. The crane selection system will not be activated unless the 90° rotation of the vessel is found to be safe to be performed (see Figure 3.17).

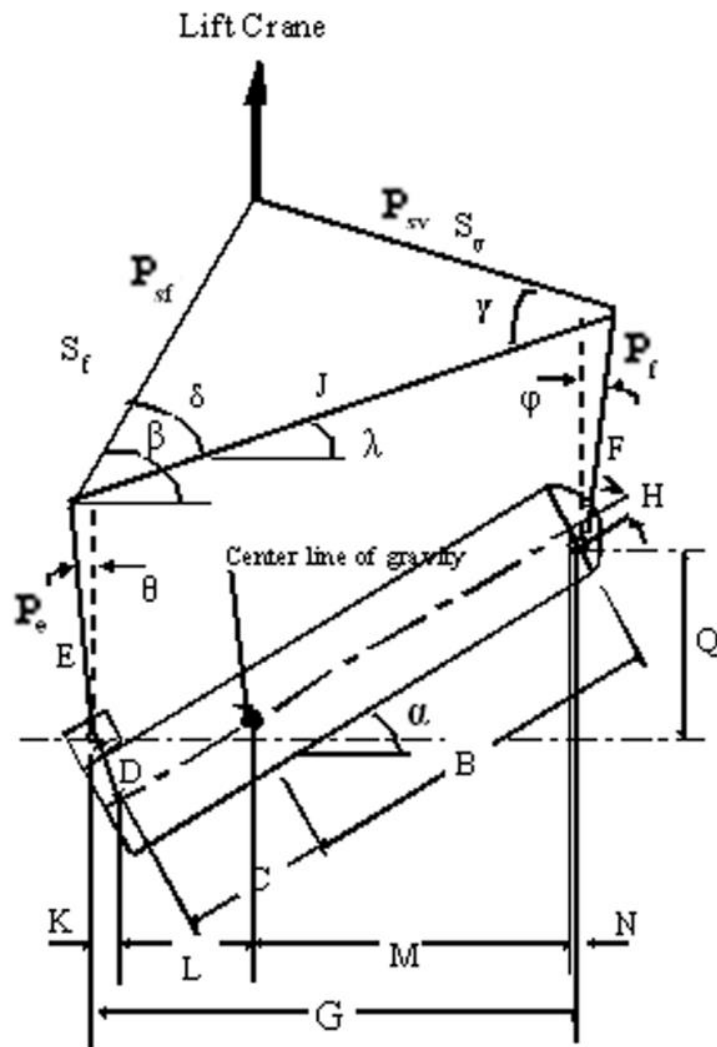


Figure 3.16: Vessel-lifting mechanism configuration (Hermann et al., 2011)

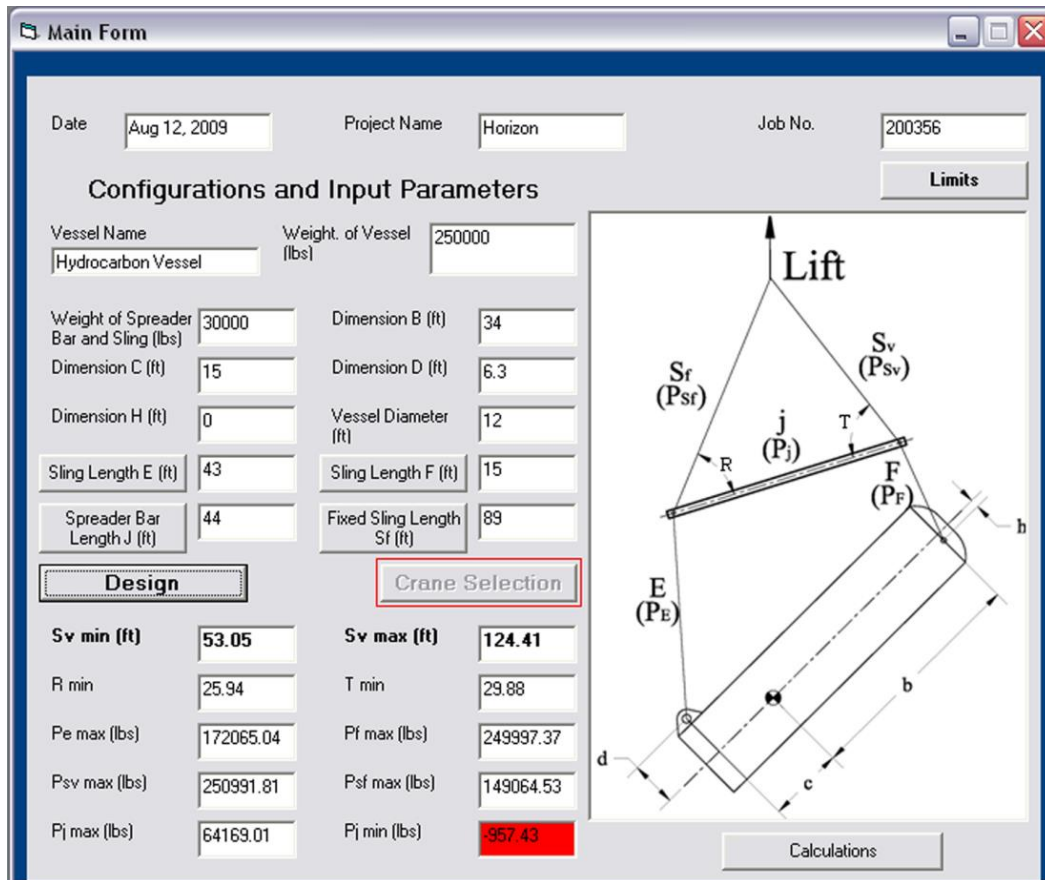


Figure 3.17: Vessel lift configuration and design form (Hermann et al., 2011)

The user also has the option to observe the summary of design results by varying the individual lengths of Slings E, F and S_f or of the spreader bar (J) as shown in Figure 3.17 by simply clicking on the buttons on each sling or spreader bar. For example, for the varying lengths of Sling E, the user can view the design results as well as observe the graphics of the lifting position on that configuration by clicking on the corresponding length of Sling E on the table (see Figure 3.18). The user can observe all the design results and can select a safe configuration simply by double-clicking on any row on that table. The main form will display the design results for that configuration. The developed system provides default allowable limits for the forces acting on the spreader bar and each sling. The user

can modify the allowable limits based on manufacturer specifications. When the output forces are unsafe, the user will be promoted to select a different configuration. If all the design results are under the allowable limit, the crane selection option will be enabled. Changes to the input configuration, such as increasing the size or weight of the vessel, will lead to new design results, and as long as all the design results are acceptable, the user can select a feasible crane. Obviously, increasing the weight of the vessel requires a higher-capacity crane.

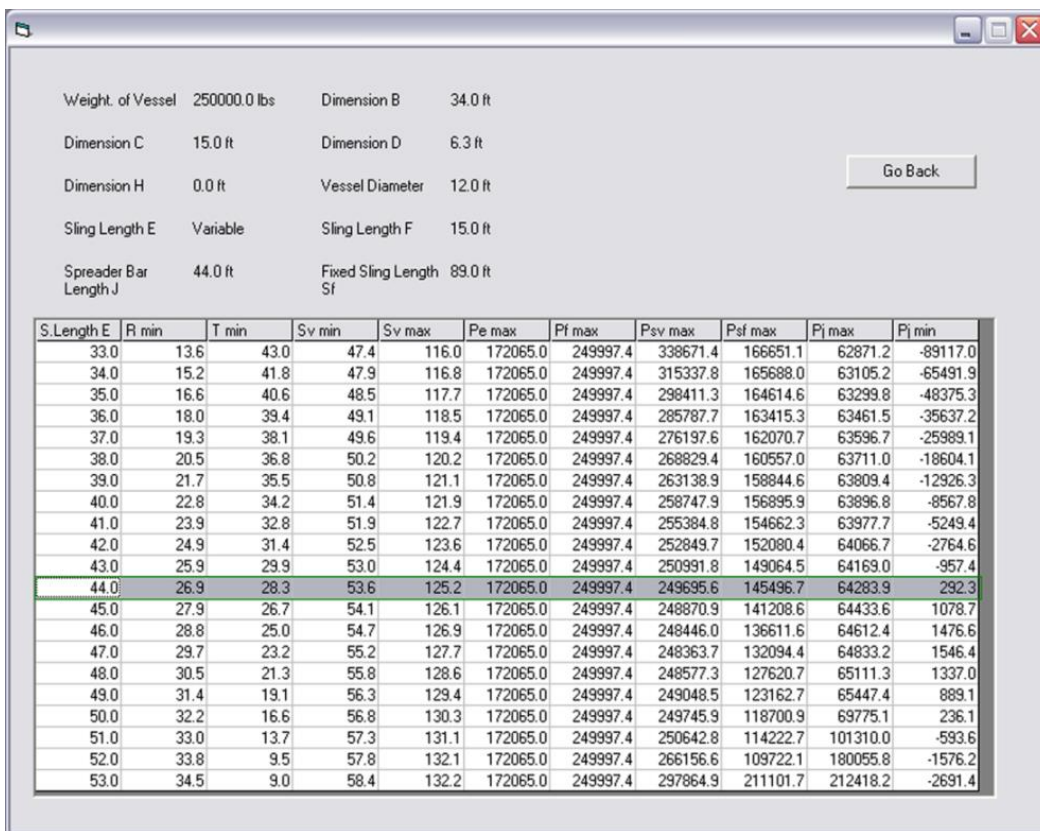


Figure 3.18: Design results for varying sling lengths E (Hermann et al., 2011)

The results provide the pulling length of Sling S_v , as well as the forces acting upon each sling and spreader bar. The user needs to select the type of spreader bar and slings to be used depending on market availability. Manufacturers usually provide the maximum allowable stresses for their spreader bars and

slings. Utilizing the ASME B30.20 design method with a factor of safety of 5 (Hermann et al., 2011), the user can determine the width and thickness for the spreader bar and diameter for the slings. One limitation of the system is the need to avoid overloading the secondary load line used to modify the variable length sling S_v as the vessel approaches the vertical position. For very long and heavy vessels, the design and capacity of the spreader bar make it impractical and the added weight reduces the crane's capacity.

By simply clicking on the Crane Selection button, the crane selection system will be displayed as shown in Figure 3.19, and will retrieve all the required components from the database. Once the crane has been selected, and the crane configuration has been added the next step is to identify the perfect position of the crane. If one or all of the selected cranes need to be fixed in the project location (i.e. can't walk in the site) then a location optimization needs to be performed before the crane stability analysis. An optimization model is developed to identify the perfect crane location.

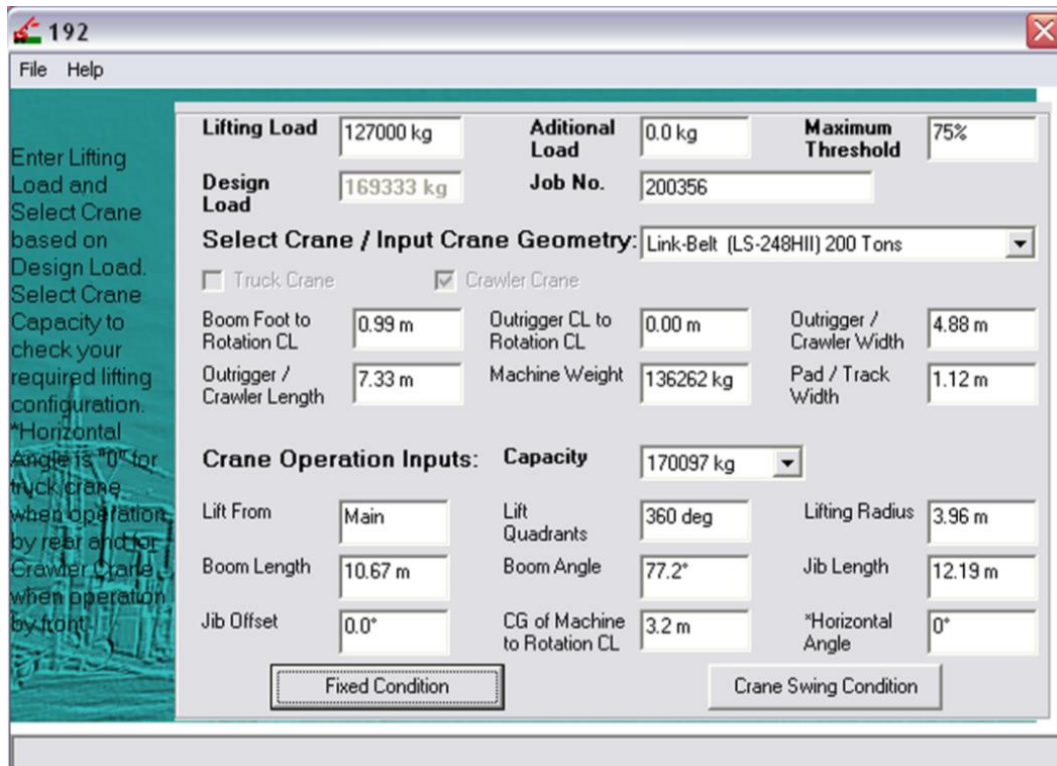


Figure 3.19: Mobile crane stability analysis system

3.2.3 Location Optimization

Cranes are selected through analyzing several parameters which are chosen by the practitioner based on a variety of quantitative and qualitative parameters. These parameters include (i) source location, also known as pick point location where the objects will be delivered or stored to lift by the crane; (ii) destination location, also known as set point location where the lifted object will be unhooked and installed; (iii) weight and size of the lifted objects; (iv) crane capacity; (v) crane jib length; (vi) jib slewing speed; and (vii) reach or the crane radius. Crane is involved in many different tasks and most of the activities in major construction site directly or indirectly rely on crane operation. Thus all the activities which rely on crane need to be ranked on a priority scale (1 to 5) based

on the importance of the task and impact on the schedule in which high priority tasks must proceed first. Thus priority setting is an important constraint and need to be considered while optimizing the lifting activities. Figure 3.20 illustrates the proposed algorithm for crane location and operation optimization which has three major steps: (1) crane location optimization, (2) source location optimization, and (3) crane operation optimization. The optimization process is based upon the following constraints: (1) lifting priority; (2) project schedule; (3) crane stability; and (4) constraints related to construction site. The proposed algorithm output includes the following three components : (1) crane location, either optimum or feasible depends on the selected crane; (2) source location, which identifies the optimum pick points in the construction site; and (3) lifting schedule, which provides the most feasible crane operations by minimizing crane swing and considering lifting priorities. Although the optimization procedure consists of a three-step algorithm, *cf.* Figure (3.20), it is important to note that all steps are interconnected, since the underlying parameter of the optimization routine is the loads' moments at the crane base. In other words, any change in pick point or crane location is likely to have a direct impact on “*pick*” and “*set*” moments, and swing angles.

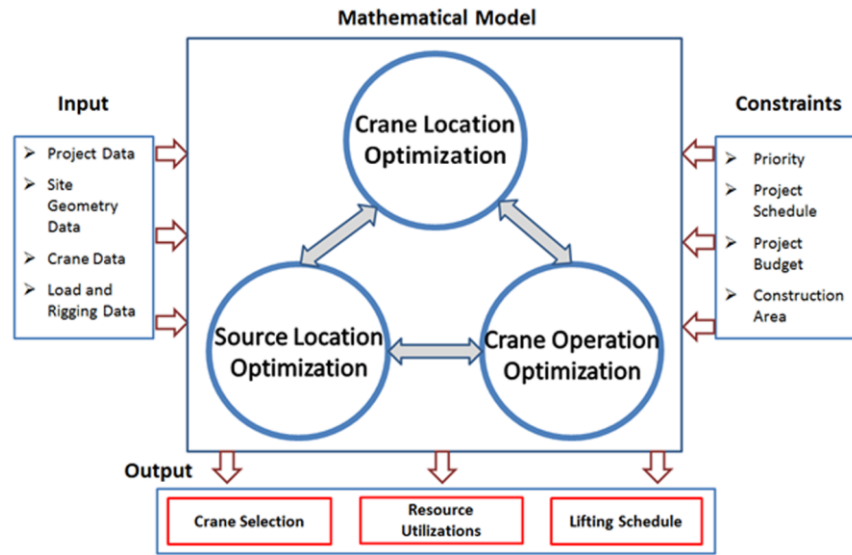


Figure 3.20: Crane location and operations optimization model (Hasan et al., 2012b)

The first phase examines all available crane locations from which the optimal location is selected based on the weights of objects to be lifted and their distances (radii) from the crane tower. The ultimate objective is to minimize the moments created at the crane base. Then the source locations (pick points) for each load are optimized using the loads' moments as the objective function. It is worth noting that although the destination points (set points) are fixed, the moments calculated for these points must be considered during the optimization process in order to avoid a biased crane location, i.e., a location which is too close to the pick area and too far from the set area. Finally, the last phase consists of optimizing the crane activities, which essentially involves minimizing unnecessary delays introduced by large swinging angles.

Crane and Source Locations Optimizations:

The moments of loads to be lifted play a central role in the proposed optimization procedure since minimizing moments is equivalent to minimizing the support reaction around the crane base (Hasan et al., 2010), which in turn increases the safety of the crane operation. The required ultimate moment M_u can be calculated satisfying Equation (3.16):

$$M_u = M_{load} + M_{aw} + M_{sw} + M_{cw} \quad (3.16)$$

where

M_{load} is the moment created by the lifted load;

M_{aw} is the moment created by the additional loads, such as slings or hook;

M_{sw} is the moment created by the movement of the boom, jib, or structure; and

M_{cw} is the moment created by the counterweight.

The lifted load moment (M_{load}) is a function of the weight to be lifted (W_{load}) and its distance from the pick or set point to the crane location (d). Thus

M_{load} can be calculated satisfying Equation (3.17):

$$M_{load} = W_{load} \times d \quad (3.17)$$

A crane can be selected based on lifted load moments or ultimate moments. The corresponding algorithms for this selection have been developed by Hasan et al. (2010). To select the optimum crane, lifted load moments need to be optimized for all loads, a process which can be achieved through two steps: (1) optimizing crane location, and (2) optimizing source locations, where it is assumed that the destination locations are already fixed.

The objective function is to minimize M_u by satisfying Equation (3.18)

$$\text{Minimize } M_{load} = W_{load} \times d \quad (3.18)$$

Satisfying the following constraint:

1. Crane location must need to be inside the site boundary,
2. Crane location cannot be too close to the proposed building area (need to maintain a safe clearance from the building)
3. Destination (delivery) points of each object are fixed and cannot be changed.

The available area for crane location (A_a) can be calculated satisfying Equation (3.19) (see also Figure 3.21).

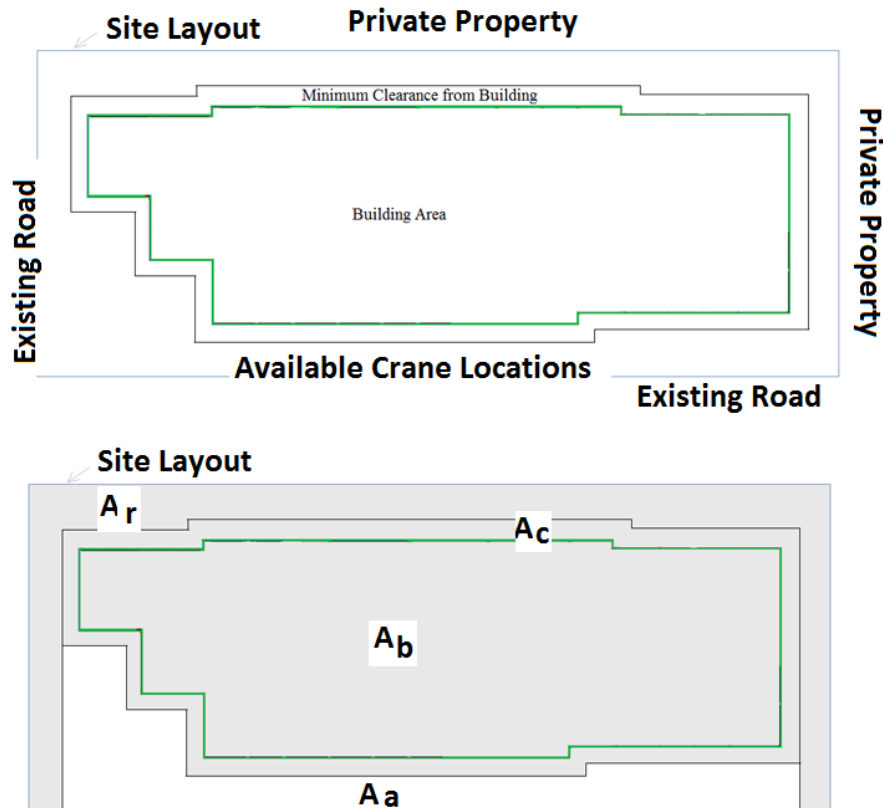


Figure 3.21: Available area calculation for possible crane location

$$A_a = A_s - (A_b + A_c + A_r) \quad (3.19)$$

where

A_s is the total site area;

A_b is the building area;

A_c is the area for minimum clearances from the building; and

A_r is the restricted area on site.

The possible crane position can be anywhere within the space, A_a , as shown in Figure 3.21. The distance of a load's pick point or set point to the crane location can be calculated satisfying Equation (3.20):

$$d_i = \sqrt{(x_i - x_1)^2 + (y_i - y_1)^2} \quad (3.20)$$

where

x_1, y_1 is the crane location; and

x_i, y_i is the pick point or set point of a load i .

In order to provide a generic approach to the problem at hand, the process begins with an abstract model which describes the spatial parameters of crane lifting problems. As mentioned above, three input parameters are fundamental to crane operation analysis, and hence are required for optimal scheduling: (i) crane location, (ii) pick point(s), and (iii) set point(s). Figure 3.22 provides a Venn diagram of the spatial parameters.

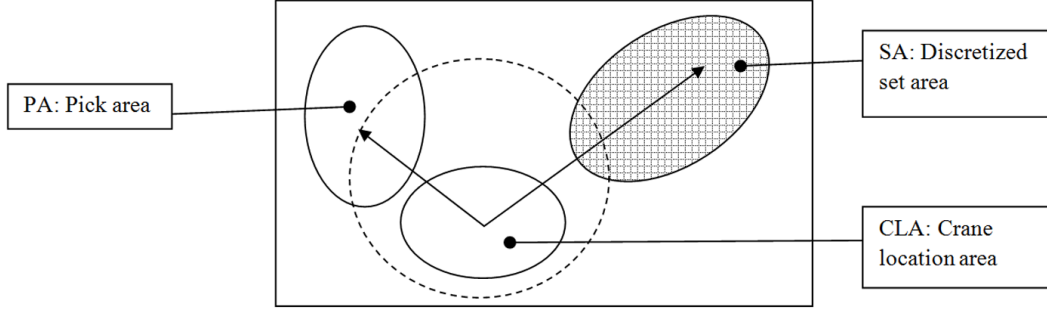


Figure 3.22: Venn diagrammatic representation of the three areas relevant to crane lifting activities

In order to optimize the crane operation, it is necessary to proceed with homogenizing the above-described problem by discretizing the pick areas (PAs) and crane location area (CLA) depicted in Figure 3.22, allowing them to be represented by two sets of points N^{PP} and N^{CL} . The set area (SA) is, by default, represented by a discrete set of points since each load must be located at a fixed location. Consequently, the degree of freedom underlying the optimization procedure is essentially provided by the pick points and the crane locations. Using the k^{th} crane location as the origin of the coordinate system, the pick and set points are defined as $(x_{k,i}, y_{k,i}, z_{k,i})_{i=1,2,\dots,N^{PP}}^{PP}$ and $(x_{k,l}, y_{k,l}, z_{k,l})_{l=1,2,\dots,N^{SP}}^{SP}$, where the component, $u_{a,b}$, represents the difference, $u_b - u_a$. As mentioned above, broadly speaking the proposed optimization procedure aims to select the crane location and pick points in order to minimize the moments of all the loads (calculated using the pick and set points). To enhance readability, it was instructive to provide a step-by-step description of the optimization procedure rather than an obscure mathematical formula which would place the burden of implementation on the reader. For each crane location, a moment matrix similar

to that presented in Table 3.4 is constructed. Note that if a load cannot be picked from a given location in the PA, due either to its geometric constraints or to the limited reach of the crane, an infinite moment is assigned to that location for that particular load.

Table 3.4: Crane location moment matrix

Crane location: (x_k, y_k, z_k)				
	W_1	W_2	W_L
Pick point #1	$\mu_{1,1,k} = w_1 \times d_{k,1}$	$\mu_{1,2,k} = w_2 \times d_{k,1}$	∞
Pick point #2	$\mu_{2,1,k} = w_1 \times d_{k,2}$	$\mu_{2,2,k} = w_2 \times d_{k,2}$	$\mu_{2,L,k} = w_L \times d_{k,2}$
Pick point #3	$\mu_{3,1,k} = w_1 \times d_{k,3}$	$\mu_{3,2,k} = w_2 \times d_{k,3}$	∞
Pick point #4	∞	$\mu_{4,2,k} = w_2 \times d_{k,4}$	$\mu_{4,L,k} = w_L \times d_{k,4}$
.....
Pick point # N^{SP}	∞	∞	$\mu_{N^{SP},L,k} = w_L \times d_{k,N^{SP}}$
Smallest moment	$\min(\{\mu_{i,1,k}\}_{i=1,2,\dots,N^{SP}})$	$\min(\{\mu_{i,2,k}\}_{i=1,2,\dots,N^{SP}})$		$\min(\{\mu_{i,L,k}\}_{i=1,2,\dots,N^{SP}})$
List of points	$P_{1,k}^{\min}$	$P_{2,k}^{\min}$	$P_{L,k}^{\min}$

Having constructed the above moment matrix in reference to crane location k , the next step consists of extracting a list of the smallest moments and corresponding pick points, i.e., the last two rows in Table 3.4. Each crane location leads to a set of minimal “pick moments” and a set of corresponding pick points which need to be sorted by means of an appropriate metric. For this purpose, the crane locations are ordered from most to least suitable by combining the “pick moments” and “set moments” into a single coordinate tuple

$(\mu_{i,1,k}^{\min}, \mu_{i,2,k}^{\min}, \dots, \mu_{i,L,k}^{\min}, \hat{\mu}_{1,k}, \hat{\mu}_{2,k}, \dots, \hat{\mu}_{L,k})$ representing a point in the Euclidean space, \mathbb{R}^{2L} . Note that the last L -coordinates correspond to the “*set moments*”, hence involving only two indices: the load number and the crane location. At this point, the optimal crane location(s) and pick points are those with a minimal Euclidean distance, which can be achieved satisfying Equation (3.21):

$$\min \left(\sqrt{\sum_{j=1}^L (\mu_{i,j,k}^{\min})^2 + \sum_{j=1}^L (\hat{\mu}_{j,k})^2} \right), \quad k = 1, 2, \dots, N^{CL} \quad (3.21)$$

From a practical point of view, the above equation may lead to a number of equivalent solutions which need to be segregated according to another factor before being presented to the lift engineer. Since this contribution aims to improve both safety and efficiency, the swing angle has been chosen as the secondary sorting criterion. However, the swing angle criterion does not consider that the swinging of an object with a larger moment carries a greater risk than that of an object with a smaller moment. As a result, the secondary discriminating factor is defined satisfying Equation (3.22):

$$\varpi_{\bullet,j,k}^{\min} = \mu_{\bullet,j,k}^{\min} (R_{\bullet,j,k}^{\min} \times \theta_{\bullet,j,k}^{\min}) + \max \left[0, \int_{R_{\bullet,j,k}^{\min}}^{R_{\bullet,j,k}^{\text{set}}} (W_j x) dx \right] = \mu_{\bullet,j,k}^{\min} (R_{\bullet,j,k}^{\min} \times \theta_{\bullet,j,k}^{\min}) + \max \left[0, W_j \frac{(R_{\bullet,j,k}^{\text{set}})^2 - (R_{\bullet,j,k}^{\min})^2}{2} \right] \quad (3.22)$$

where

$\varpi_{\bullet,j,k}^{\min}$: is the penalty for moving load j from the pick point at which its “*pick moment*” is minimal relative to its final resting location. The first term represents the contribution due to the load rotation, whereas the second is an additional penalty corresponding to an increase in the moment if the load requires an

outward translation, (Figure 3.23). Note that for an inward translation, the translation penalty is zero.

$\mu_{\bullet,j,k}^{\min}$: is the moment of load j at the pick point where it is minimal.

$\theta_{\bullet,j,k}^{\min}$: is the swing angle for load j from the pick point at which the moment is minimal relative to its resting position.

$R_{\bullet,j,k}^{\min}$ and $R_{\bullet,j,k}^{\text{set}}$ are the distances from the crane location to load j at pick point i , and to the set point, respectively.

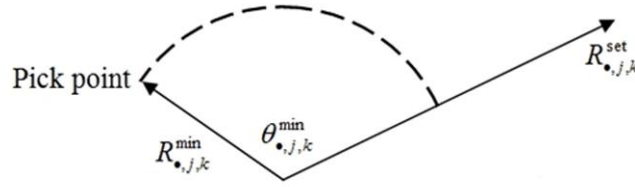


Figure 3.23: Simplified path for an object lifted from pick point to its set position

In Equation (3.22), the swing angle $\theta_{\bullet,j,k}^{\min}$ between pick points at which the “pick moment” for load j is minimal (represented by a dot), evaluated with respect to crane location k , is introduced. Under the assumption that $\theta_{\bullet,j,k}^{\min} \leq 180^\circ$, the swing angle can be calculated satisfying Equation (3.23):

$$\theta_{\bullet,j,k}^{\min} = \cos^{-1} \left[\frac{(x_{\bullet,j}^{\min} - x_k)(x_j^{\text{set}} - x_k) + (y_{\bullet,j}^{\min} - y_k)(y_j^{\text{set}} - y_k) + (z_{\bullet,j}^{\min} - z_k)(z_j^{\text{set}} - z_k)}{\sqrt{(x_{\bullet,j}^{\min} - x_k)^2 + (y_{\bullet,j}^{\min} - y_k)^2 + (z_{\bullet,j}^{\min} - z_k)^2} \sqrt{(x_j^{\text{set}} - x_k)^2 + (y_j^{\text{set}} - y_k)^2 + (z_j^{\text{set}} - z_k)^2}} \right] \quad (3.23)$$

in which (x_k, y_k, z_k) , $(x_{\bullet,j}^{\min}, y_{\bullet,j}^{\min}, z_{\bullet,j}^{\min})$ and $(x_j^{\text{set}}, y_j^{\text{set}}, z_j^{\text{set}})$ are the coordinates of the crane location, the pick point at which the “pick moment” is minimal, and the set point for object j , respectively. Before considering a case study, it is instructive

to begin with a simulated experiment which entails full control of the data. In the first case, a simple construction site is considered in which the PAs and SAs are symmetrically located with respect to the crane location sites (Figure 3.24).

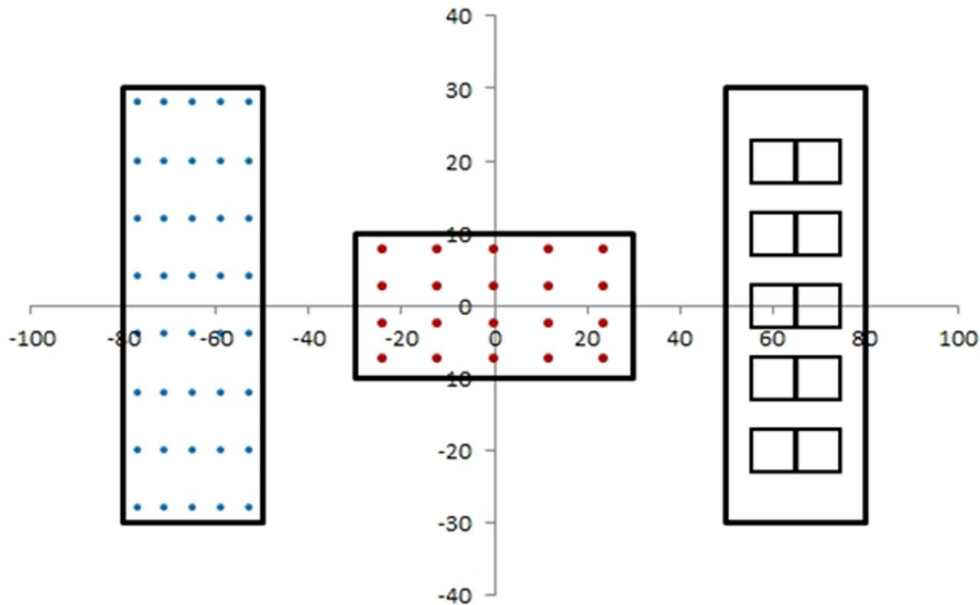


Figure 3.24: Simulated site layout in which loading and destination zones are symmetrical with respect to the crane location area

Note that the SA is an oversimplified representation of a three-storey building, with storey heights of 0, 4, and 8 metres, respectively. Accordingly, the simulation uses 30 objects with weights that are assumed to be described by the normal distribution, $N(\mu=3000, \sigma=500)$. As a result of the optimization process, a moment map is obtained for each potential crane location (Figure 3.25) which represents the ratio of corresponding Euclidean distances, as calculated using Equation (3.21), to the largest one.

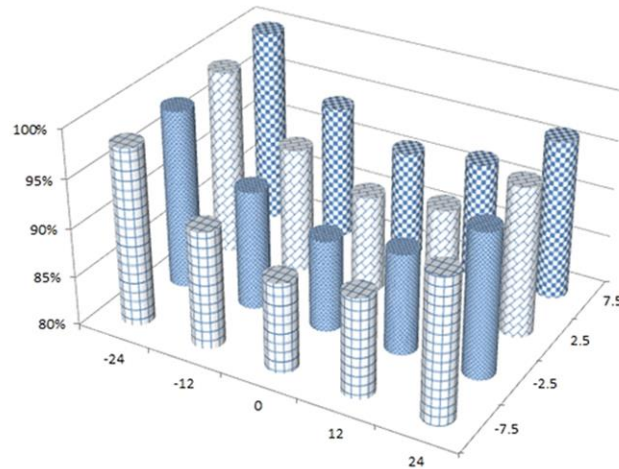


Figure 3.25: Moments ratio map at each permitted crane location

Since the simulated case is symmetrical, the optimal crane positions are located approximately in the middle of the PA. Note that the above map can be color-coded for highly dense positions, thus allowing the practitioner to immediately identify the most appropriate crane location.

When optimizing crane and pick point locations, the developed approach begins with identification of the locations that minimize pick moments and set moments, since these quantities are paramount to the safety of crane operations. However, in the vast majority of cases, the chosen crane's capacity is larger than the calculated moments. As a result, all locations satisfying the crane's capacity threshold are stored and sorted based on the smallest swing angle. Thus, rather than providing a single answer, the above paradigm provides a mosaic of information which assists the practitioner in making an informed decision based on optimal moments (see previous section), swing angle penalties (see previous section), or a time factor. In fact, since time is the parameter required to determine project schedule, the transformation allows the user to relate the swinging and translation of a lifted object to time, as described below. Using the

notation of Equation (3.21), and with reference to Figure 3.26, the time required for an object to be moved from its pick point to final destination (not considering the “constant time” corresponding to tasks such as hooking or loading/unloading) is calculated satisfying Equation (3.24) for a saddle-jib crane:

$$t_{i,j,k}^{\leq T} = \frac{\theta_{i,j,k}^{\leq T}}{\omega} + \frac{|R_{i,j,k}^{\text{set}} - R_{i,j,k}^{\leq T}|}{\nu} \quad (3.24)$$

where

$t_{i,j,k}^{\leq T}$ is the time required to lift object j from the pick point i at which the pick moments and set moments are below the capacity threshold T when the crane is located at position k ; and

ω, ν are, respectively, the average angular and linear velocities of the jib (when rotating) and the object (when moving horizontally from $R_{i,j,k}^{\leq T}$ to $R_{i,j,k}^{\text{set}}$).

It should be noted that in the case of a double-jib crane, Equation (3.24) still applies. However, once an object is set at its final position, the next object to be lifted can be moved by means of the second arm, which may require a smaller swing angle to reach the next object in the list.

In the case of the luffing-jib crane, the translation of the object is ensured by booming up and down the jib (Figure 3.26). As a result, using the same notation as in Equation (3.24), the time required to move an object from pick point i to its destination is given by Equation (3.25):

$$t_{i,j,k}^{\leq T} = \frac{\theta_{i,j,k}^{\leq T}}{\omega} + \frac{\cos^{(-1)}\left[\frac{\min(R_j^{\text{set}}, R_{i,j,k}^{\leq T})}{R}\right] - \cos^{(-1)}\left[\frac{\max(R_j^{\text{set}}, R_{i,j,k}^{\leq T})}{R}\right]}{\omega'} \quad (3.25)$$

where ω' is the average velocity of the jib when booming up or down and R is the jib length (Figure 3.26).

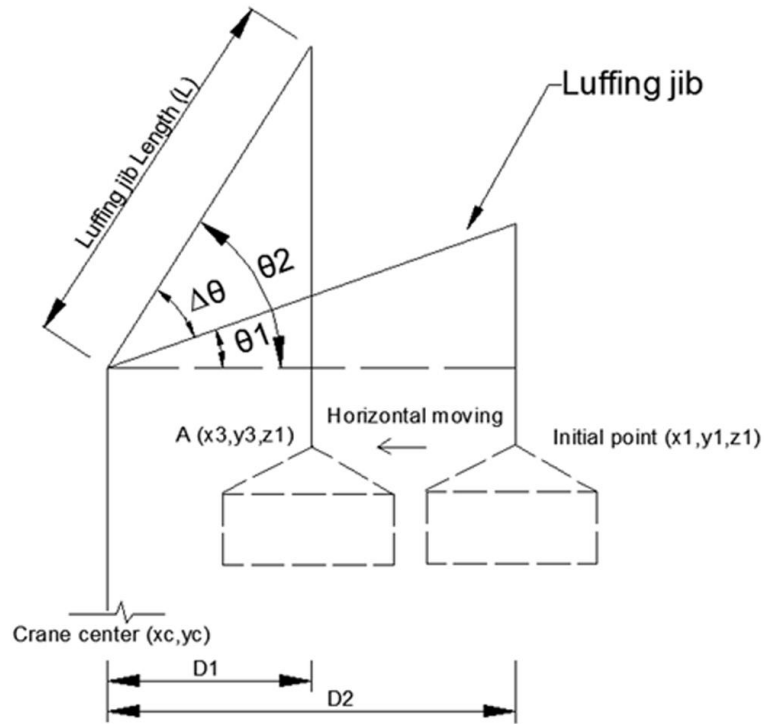


Figure 3.26: Horizontal translation of an object lifted by a luffing-jib crane

For a given crane location and set of source and destination points (the latter being fixed), the total time can be calculated using Equations (3.24) and (3.25), assuming that the order in which the objects are to be lifted is known beforehand.

Crane Operations Optimization

In the previous section, formulas allowing the lift planner to calculate using Equations (3.24) and (3.25) the time it requires for a crane to move an object from a pick location to its final destination. However, this time does not include the overhead time corresponding to tasks such as hooking and un-hooking. As a

result the overall time t_j necessary to move object j is defined satisfying Equation (3.26),

$$t_j = t_h + t_{i,j,k}^{\leq T} + t_{uh} + t_a \quad (3.26)$$

in which t_h, t_{uh}, t_a are respectively the durations for hooking, unhooking and aligning the lifted object. Using Equation (3.26), lifting each activity or work package is associated with a time that is used by the planner to setup a daily lifting schedule. In practice, crane activities are generally segregated into two main categories referred to as primary and secondary. For instance, in the case of modular construction, the primary activity of a crane is to lift the modules whereas any other activity e.g. lifting rebar or equipment for installation, is considered secondary. However, secondary activities are as equally important as their primary counterparts since they must be executed prior to becoming elements on the critical path.

Using a terminology common to the so-called Critical Path Method (CPM), secondary activities are characterized by their free-float since they are not critical. As a result while they offer flexibility in their execution, an aging secondary activity increases its probability of becoming critical. In order to analyze this aspect of the crane operation, activities are ranked on a priority scale (P_s) from 1 to 5 predefined by the project manager in which high priority tasks must proceed first. At this point, it is instructive to highlight the similarity which exists between a computer CPU and a crane on a construction site. Since efficiency is at the core of computer science, a wealth of CPU scheduling algorithms were devised during the past few decades. One of such algorithm is

known as “priority scheduling” in which processes are ranked according to their priority which allows the CPU to run critical, i.e. high priority, processes first. Although this contribution builds on the priority scheduling concept, it is important to emphasize that in contrast to a computer CPU, cranes cannot interrupt a task after it starts. In addition to this and as mentioned above, in the construction industry, non-critical tasks are characterized by their flexibility in terms of execution (free float) but they cannot be left to age beyond a certain point since they will become critical. While establishing priorities are practically controlled by the lift engineer, this contribution suggests a default ranking procedure which is based on the shortest lift time (see Equation 3.26). In other words, shorter times are given higher priorities. However, to avoid the danger of aging tasks, a parameter measuring their distance to criticality is associated with each of these tasks. As a result and for the purpose of modeling and computation, the system of crane activities is represented by a two-dimensional matrix as given by Equation (3.27),

$$\begin{array}{l}
 t = 0 \\
 t = t_1 \\
 \vdots \\
 t = t_m
 \end{array}
 \rightarrow
 \begin{bmatrix}
 \Delta_{0,0} = 0 & \Delta_{0,1} & \Delta_{0,2} & \cdots \\
 \Delta_{1,0} = 0 & \Delta_{1,1} & \Delta_{1,2} & \cdots \\
 \vdots & \vdots & \vdots & \ddots \\
 \Delta_{m,0} = 0 & \Delta_{m,1} & \Delta_{m,2} & \cdots
 \end{bmatrix}
 \quad (3.27)$$

In Equation (3.27) the time allowed for a given day is discretized based on the primary activities whose distances to criticality is set to zero since they cannot be delayed. In fact, it is important to understand that in many modular construction projects, time is discretized according to the frequency of delivery of the modules which constitute the primary activity of the crane. For instance for the

case study described in the next section, each module required approximately 30 minutes to be delivered to the construction site whereas the lift and installation took on average 25 to 35 minutes depends on the complexity of the module location. As a result, the number of lines in the matrix representation given in Equation (3.27) corresponds to the number of time intervals, i.e. the number of modules, per working day. As for the columns, they represent the tasks to be performed. The matrix elements represent the distance to criticality which for primary activities (column labeled “0”) is set to zero which translates into a high priority (infinity). Secondary activities on the other hand have free float which allows them to be delayed until their distance to criticality becomes zero in which case their priority jumps to infinity. To optimize the crane operations with regards to non-critical activities, a metric is defined to quantify the overall impact of delay on the schedule satisfying Equation (3.28),

$$I = \max(0, T_A - T_P) \times P_s \quad (3.28)$$

where $(T_A - T_P)$ is the difference between the actual time representing the time at which the scheduling algorithm selects the task to be executed and the time it was initially scheduled. Note that in Equation (3.28), if a task is performed before schedule, we chose to set its impact to zero in order to avoid counterbalancing delays by starting some tasks ahead of schedule. In the case where one needs to also penalize ahead of schedule activities, an alternative to Equation (3.28) is expressed as $I = |T_A - T_P| \times P_s$. For optimal scheduling, it is tried to minimize the overall impact of the activities as per Equation (3.29),

$$I_{Total} = \min \left[\sum_{j=1}^L \max(0, T_{j,A} - T_{j,P}) \times P_{j,s} \right] \text{ subjected to } \Delta_j \geq 0 \quad (3.29)$$

where the index j runs over all non-critical loads to be lifted.

The internal relationship between the crane location optimization and operations optimization algorithms is that optimizing crane location provides a foundation for optimizing lifting schedule. The proposed algorithm is developed using MS Excel to optimize crane location, which provides an initiative for the subsequent lifting schedule optimization.

3.2.4 Crane Stability Analysis

Once the crane and the location have been selected the user can check the crane stability and calculate the support reactions. The developed system provides two options (see Figure 3.27) to calculate the crane support reactions: (1) Fixed Condition, where reactions are calculated for a specific boom angle and horizontal angle and for a specific load, and (2) Crane Swing Condition, where reactions are calculated for up to 360° of rotation of the boom and for different boom angles.

Figure 3.27: Crane configuration form

The outrigger reactions and the track pressure are a function of the respective weights of the lift and crane components and their moments around the center of rotation of the crane. These moments are divided into two categories due to the horizontal and vertical displacement of the boom: one acting around the crane sides M_{ns} and the other acting on the crane rear or front M_{nr} . (for free body diagram please see Figure 3.3 and 3.5). These moments are calculated satisfying Equations (3.30) and (3.31):

$$M_{ns} = M_u \sin \alpha \quad (3.30)$$

$$M_{nr} = M_u \cos \alpha - V_u x_o \quad (3.31)$$

where

M_u is the required ultimate moment;

α is the horizontal swinging angle;

V_u is the total vertical load; and

x_0 is the distance between the crane's centerline and the center of rotation (see Figure 3.3 and 3.5).

The total required ultimate moment M_u satisfying Equation (3.16) and vertical load V_u are calculated satisfying Equation and (3.32).

$$V_u = W_{load} + W_{add} + W_{sw} + W_{cw} \quad (3.32)$$

where

W_{load} is the weight of the lifted load;

W_{add} is the weight of the additional load for the slings and rigging;

W_{sw} is the weight of the crane structure, e.g., boom or tower, jib, machine;

W_{cw} is the weight of the counterweight;

The reaction under the truck crane's four outriggers—two front, P_{fb} , P_{fc} , and two rear, P_{rb} , P_{rc} (see Figure 3.3)—are calculated satisfying Equations (3.33) to (3.36) (Shapiro et al., 1999).

$$P_{fb} = \frac{V_u}{4} + \frac{1}{2} \left(\frac{M_{ns}}{d_t} - \frac{M_{nr}}{d_l} \right) \quad (3.33)$$

$$P_{fc} = \frac{V_u}{4} - \frac{1}{2} \left(\frac{M_{ns}}{d_t} + \frac{M_{nr}}{d_l} \right) \quad (3.34)$$

$$P_{rb} = \frac{V_u}{4} + \frac{1}{2} \left(\frac{M_{ns}}{d_t} + \frac{M_{nr}}{d_l} \right) \quad (3.35)$$

$$P_{rc} = \frac{V_u}{4} - \frac{1}{2} \left(\frac{M_{ns}}{d_t} - \frac{M_{nr}}{d_l} \right) \quad (3.36)$$

where d_t and d_l are the distances between outriggers in the transverse direction and in the longitudinal direction, respectively (see Figure 3.3).

For tower crane with bolt anchorage support the reactions for four legs are calculated using the same methodology as described for truck crane satisfying Equations (3.33) to (3.36).

For crawler crane, pressures under the tracks are denoted as P_{front} and P_{rear} (see Figure 3.5). Due to the vertical load, front or rear moment, and side moment around the center of rotation, track pressure can be sub-divided into three categories (Shapiro et al., 1999), v , f_e and f_s , which can be calculated satisfying Equations (3.37) to (3.39):

$$v = \frac{V_u}{2wd_l} \quad (3.37)$$

$$f_e = \frac{3M_{nf}}{w(d_l)^2} \quad (3.38)$$

$$f_s = \frac{M_{ns}}{wd_l d_t} \quad (3.39)$$

where w is the crawler track width and d_l , d_t are the length of each track and the distance between the tracks, respectively.

The track pressure diagram will assume either a trapezoidal or a triangular shape as shown in Figures 3.28 and 3.28. If $v + f_s > f_e$, then the pressure diagram is trapezoidal (see Figure 3.28).

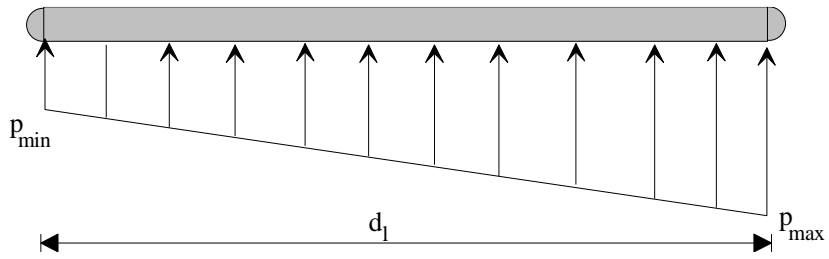


Figure 3.28: Trapezoidal pressure diagram under crawler track

The pressure for the track on the boom (load) side can be calculated satisfying

Equations (3.40) and (3.41):

$$p_{\max 1} = v + f_s + f_e \quad (3.40)$$

$$p_{\min 1} = v + f_s - f_e \quad (3.41)$$

The pressure for the track on the counterweight side can be calculated satisfying

Equations (3.42) and (3.43):

$$p_{\max 2} = v - f_s + f_e \quad (3.42)$$

$$p_{\min 2} = v - f_s - f_e \quad (3.43)$$

If $v + f_s < f_e$, then the pressure diagram in the triangular form over length l will appear as shown in Figure 3.29, and the side can be calculated satisfying

Equation (3.44):

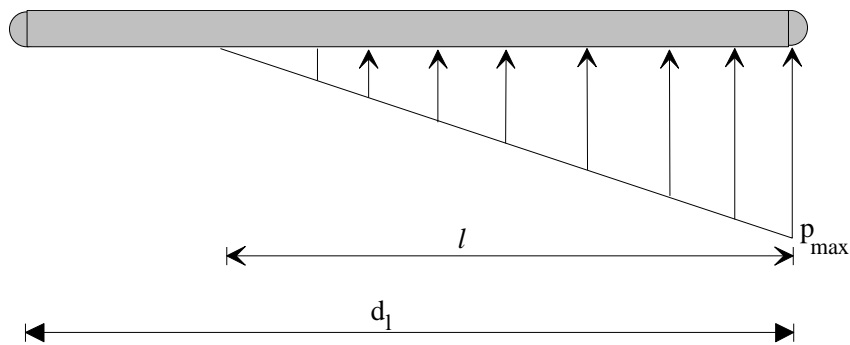


Figure 3.29: Triangular pressure diagram under crawler track

$$l = 1.5d_t - \frac{3M_{nf}}{V} \quad (3.44)$$

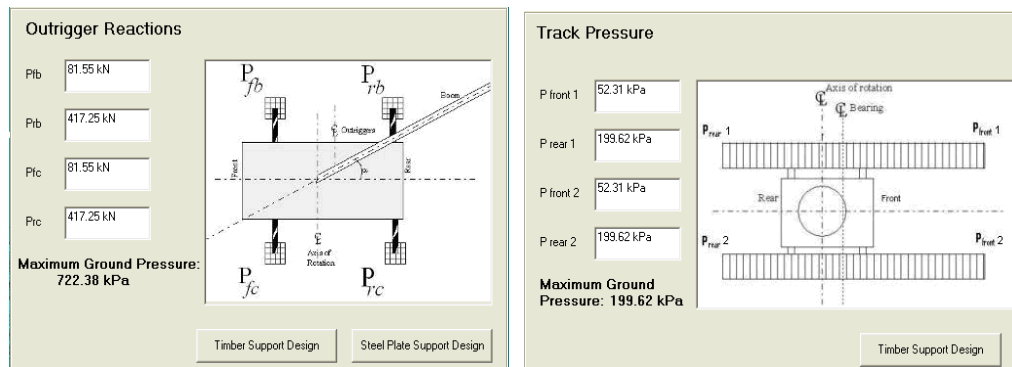
The pressure for the track on the load side (P_{front1}) (see Figure 3.5) can be calculated satisfying Equation (3.45):

$$p_{front1} = \frac{V + 2\left(\frac{M_{ns}}{d_t}\right)}{wl} \quad (3.45)$$

The pressure for the track on the counterweight side (P_{front2}) (see Figure 3.5) can be calculated satisfying Equation (3.46):

$$p_{front2} = \frac{V - 2\left(\frac{M_{ns}}{d_t}\right)}{wl} \quad (3.46)$$

In the fixed condition, the reaction under the truck crane's four outriggers—two front (P_{fb} , P_{fc}) and two rear (P_{rb} , P_{rc})—and the pressures under the front and rear (P_{front} , P_{rear}) of each track of the crawler crane are calculated (see Figure 3.30). In addition, the maximum ground pressure for that particular position of crane is displayed. Also, this system generates a supporting system design using either timber or steel based on the maximum ground pressure (Hasan et al., 2010a).



(a) (b)
 Figure 3.30: Mobile crane support reactions: (a) truck crane; (b) crawler crane

In the swinging condition, the four outriggers' reaction values or the pressure of the two tracks (depending on the crane) can be calculated in each position of crane swing up to 360°. The mobile crane has the option to swing over 360°, over front/rear, or over side In order to control the crane swing the system provides a “Lift Quadrants” option in the crane operations input form as shown in Figure 3.10. Based on the “Lift Quadrants” option, the user must provide the initial and final swing angles in the support reaction calculation form as shown in Figure 3.30. The user can also change the angle of the crane boom to the ground by setting the minimum and maximum boom angles to be at the ground and by specifying the required increments of change of these angles (see Figure 3.31).

The screenshot shows a software window titled "Support Design" with a menu bar containing "File" and "Help". The main area contains several input fields and buttons:

Swing Angle Initial	0	Boom Angle Min	60	Reaction Chart
Swing Angle Final	360	Boom Angle Max	70	
Increment	5	Increment	1	Go Back

Figure 3.31: Crane swing condition angle input form

A reaction influence chart for up to 360° of swing, in increments predetermined by the user, is also integrated into the system (Hasan et al., 2009a). The reaction influence chart provides the four outrigger reaction value for truck cranes or the maximum and minimum pressure of tracks for crawler cranes for each swing angle of the crane for a particular boom angle to the ground. The reaction influence chart changes with a change in boom angle, and the user can view different charts for different boom angles to the ground. In addition to being displayed in the chart, this information is also shown in a tabulated format which

the user can view using a standard spreadsheet; the maximum values from that table are highlighted, available for reference by the user as shown in Figure 3.32. Cases of unsafe rotation are also highlighted in this table, including any case in which the outrigger reaction value becomes negative. Both the influence chart and the table show where the crane can swing safely and where there is the possibility of tipping failure. Finally, the maximum pressure on the ground due to all changing conditions of boom is displayed, and the system provides an allowable design pressure value which reflects a safety factor sensitive to the type of crane (truck / crawler) in order to design the supporting system using either timber or steel (see Figure 3.32) (Hasan et al., 2009b).

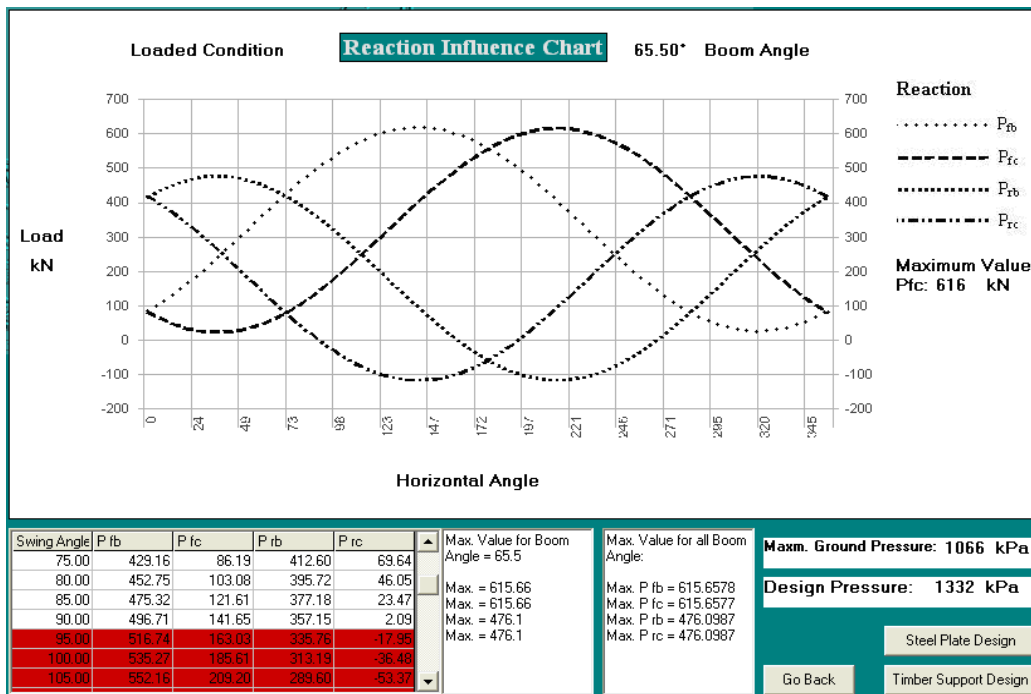


Figure 3.32: Reaction influence chart with warning of tipping failure (Hasan et al., 2009b)

Instability accidents due to tipping of mobile cranes have generally resulted from faulty decisions to perform lifts which either exceed the lifting capacity of the crane or swing in an area that is not permitted by the crane load chart. The proposed system does not allow the user to design for a load that exceeds the crane's capacity or violates swing constraints. If the 'lift quadrants' of the crane configuration displayed are "over side and rear" as shown in Figure 3.10 and the user has designed it for a 360°-swing (see Figure 3.31), the support reaction may become negative just after the 90° swing, as shown in Figure 3.32. In this case the user must maintain the crane swing from -90° to +90° as shown in Figure 3.33.

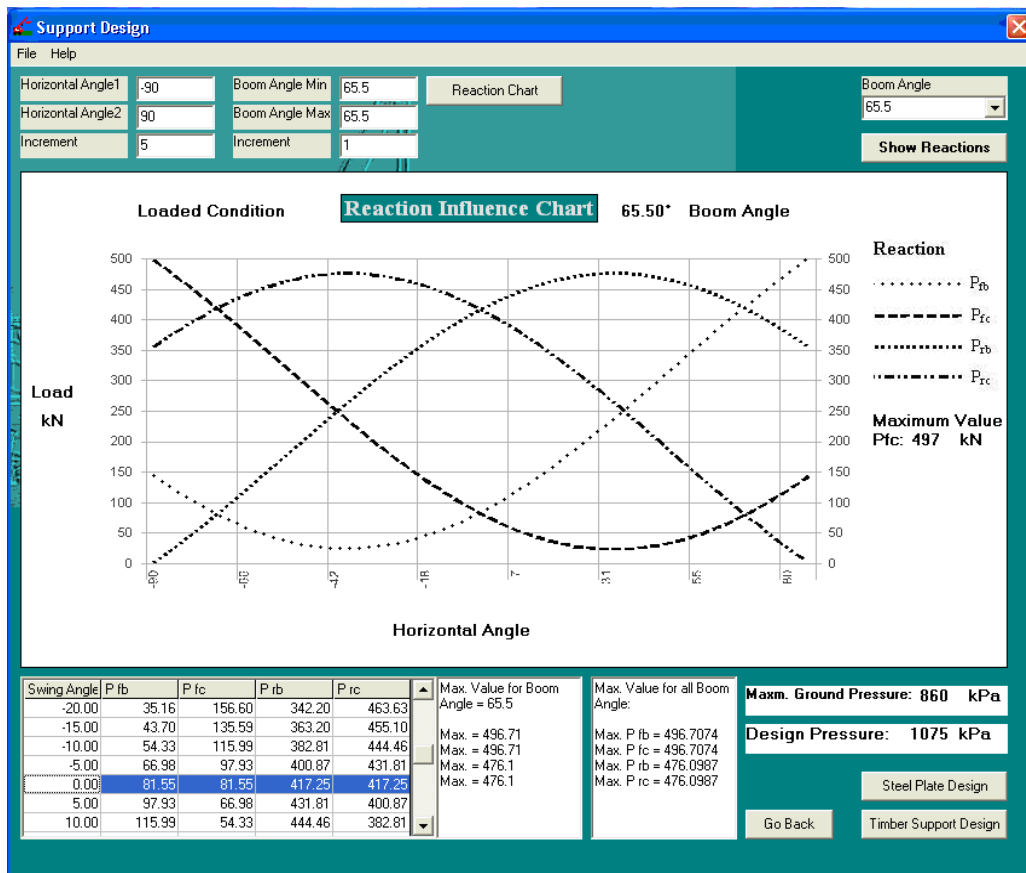


Figure 3.33: Reaction influence chart (Hasan et al. 2009b)

Crane instability may also occur due to the lack of a proper crane support system. Accordingly, this system also provides the design of crane supports (Hasan et al., 2010a), based on the maximum ground pressure given by the system, the allowable bearing capacity of the soil, and the allowable bending and shear stress of the material to be used. The system provides the actual stresses of the materials and compares these values with the allowable stress values for the selected type of material. The result is highlighted if the discrepancy is such that the design is determined to be unsafe as shown in Figure 3.34. In the case of a failure, the user is prompted with a message indicating the type of failure, at which point the user is presented with the option to either increase the material size and select another material type, or reinforce the soil.

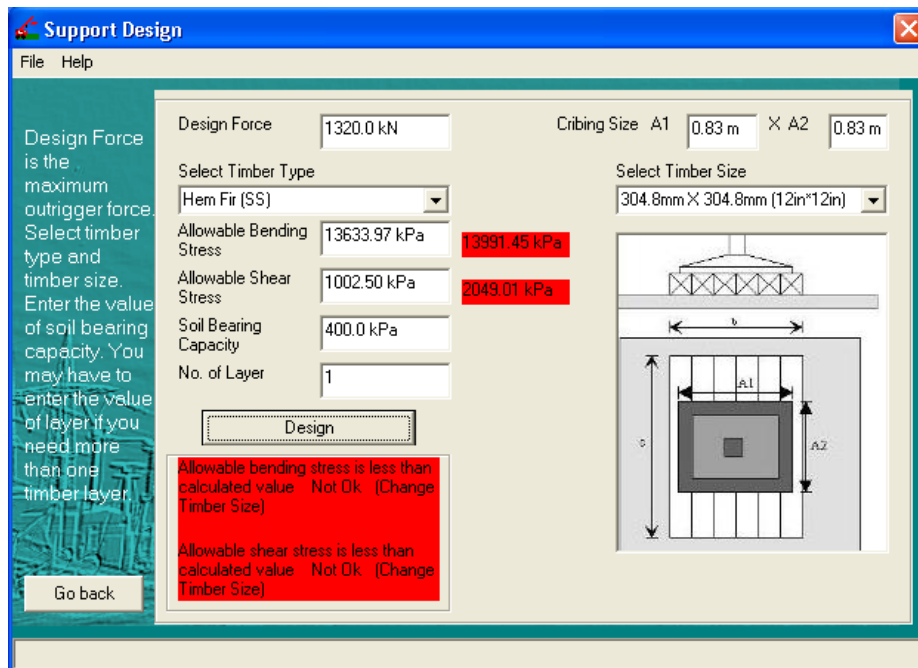


Figure 3.34: Safety warning about supporting material failure (Hasan et al. 2009b)

High wind speed affects the crane's lifting operations and also can create crane instability. This research develops a methodology to incorporate wind speed data

into lift analysis, from which crane support reactions are calculated during each lifting operation and stability is checked. Due to high wind speed an additional moment which is called here the wind moment, is developed at the crane base. The wind moment M_w is a function of the wind velocity and pressure. The wind pressure can be calculated as follows:

$$\text{Wind Pressure} = \frac{1}{2} (\text{density of air}) (\text{wind speed})^2 (\text{shape factor}).$$

The density of air is about 1.25 kg/m³. The shape factor (drag coefficient) depends on the shape of the body. It has order of magnitude 1 (assume) and is dimension less. Thus,

$$\text{Wind Pressure} = (1.25/2) (\text{wind speed})^2 = 5/8 (\text{wind speed})^2$$

If the wind velocity is V_w then the wind pressure q can be calculated satisfying Equation (3.47):

$$q = \frac{5V_w^2}{8} \quad (3.47)$$

where V_w represents metres per second and q represents Newtons per square metre. The height or lift elevation is an important factor in this regard, since the wind speed is measured at 10 m above the ground. The Construction Plant-hire Association (2009) suggests wind speed multiplying factors (f_w) for lifting operations higher than 10 meters above the ground. Thus the wind pressure q can be calculated satisfying Equation (3.48):

$$q = \frac{5V_w^2}{8} f_w \quad (3.48)$$

where V_w represents metres per second and q represents Newtons per square metre.

To simplify the wind moment calculation it is assumed that the surface of the boom or tower and jib is solid and rectangular. Therefore, resultant wind forces are calculated based on the surface area and wind pressure acting on that surface, e.g., wind force on boom (F_b) or tower (F_t), jib (F_j) and lifted load (F_l) (see Figure 3.35 and 3.36). Due to negligible surface area, the wind pressures acting upon the crane rigging, gantry, and other parts are considered to be negligible. Figure 3.35 and 3.36 present the different steps for calculating wind forces on a mobile crane and tower crane respectively. The wind moment M_w is calculated satisfying Equation (3.49):

$$M_w = F_b H_b + F_j H_j + F_l H_l \quad (3.49)$$

where H_b , H_j , and H_l are the height of the resultant wind forces acting upon the boom, jib, and lifted load, respectively.

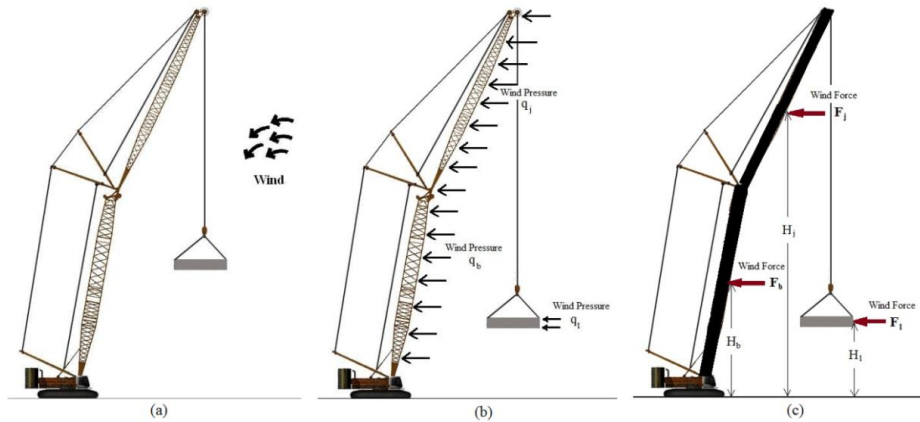


Figure 3.35: Wind acting on mobile crane

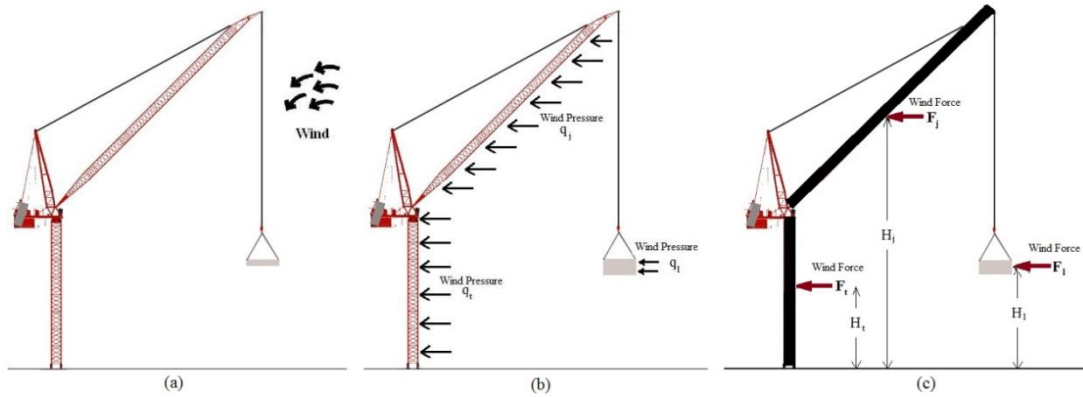


Figure 3.36: Wind acting on tower crane

The resultant wind force on boom (F_b) or tower (F_t), jib (F_j) and lifted load (F_l) can be calculated satisfying Equation (3.50).

$$F = (A \times B) q f_{shape} \quad (3.50)$$

Where A and B is the dimension of the object's surface (boom, tower or the load) where the wind pressure acting and f_{shape} is the shape factor. For a solid surface $f_{shape} = 1$.

Wind moment affects the total moments acting around the crane sides M_{ns} , as well as those acting on the crane rear or front M_{nr} . Thus these moments are calculated satisfying Equations (3.51) and (3.52):

$$M_{ns} = M_u \sin \alpha + M_w \sin(\alpha - \omega) \quad (3.51)$$

$$M_{nr} = M_u \cos \alpha + M_w \cos(\alpha - \omega) - V_u x_o \quad (3.52)$$

where

M_u is the ultimate moment;

M_w is the moment created by the wind force;

ω is the direction of wind measured counter-clockwise from the north;

α is the horizontal swinging angle;

V_u is the total vertical load; and

x_0 is the distance between the crane's centerline and the center of rotation.

Support reactions satisfying Equations (3.33) to (3.36) need to be calculated using the updated crane side moment M_{ns} and rear or front moment M_{nr} . Figure 3.36 and 3.37 show the effect of wind on crawler crane track pressure and tower crane reactions respectively in the reaction influence chart (Hasan et al., 2010). The crawler crane used in this analysis (Figure 3.37) is a Liebherr LR 1300 and the tower crane is used in this analysis (Figure 3.38) is Wilbert WT2405L lifting a 30-ton load within a 30 m radius.

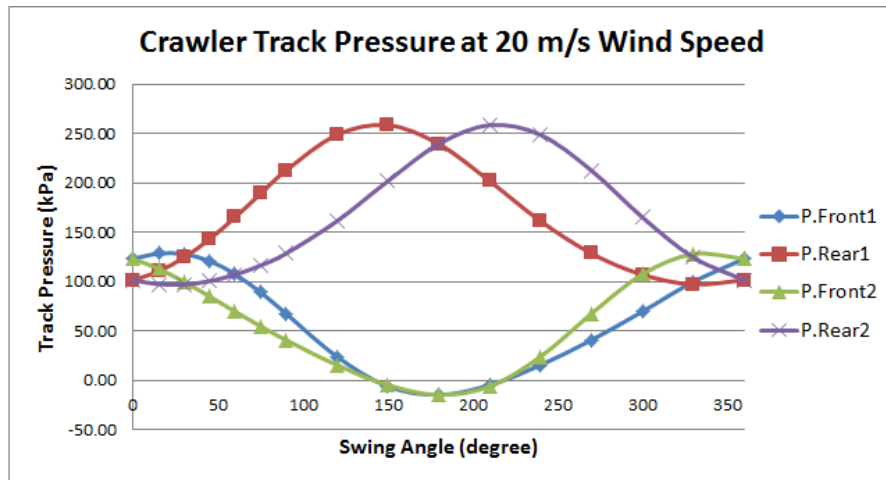


Figure 3.37: Crawler track pressure

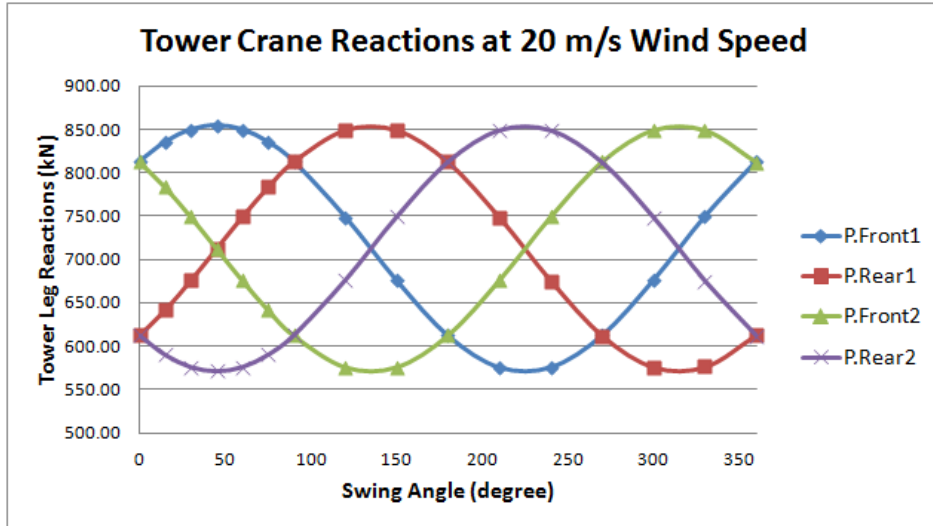


Figure 3.38: Tower crane reactions

Wind direction plays an important role in calculating the support reactions. Figure 3.39 and 3.40 present the crawler track pressure of P_{Front1} at 13.9 m/s wind speed and tower reaction of P_{Front1} at 20 m/s wind speed respectively at different wind directions and within 360° of rotation with a lifted load of 30 tons at 30 m radius.

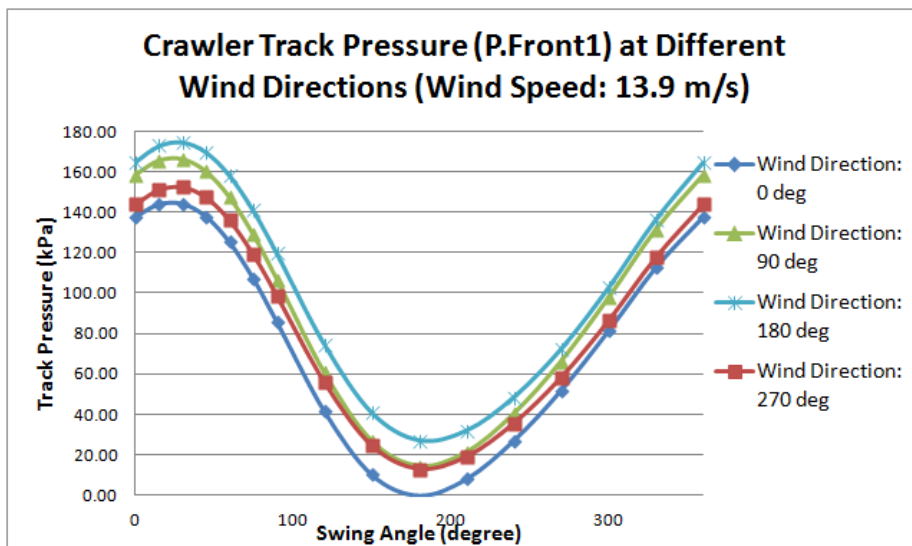


Figure 3.39: Wind direction effects on crawler crane operations

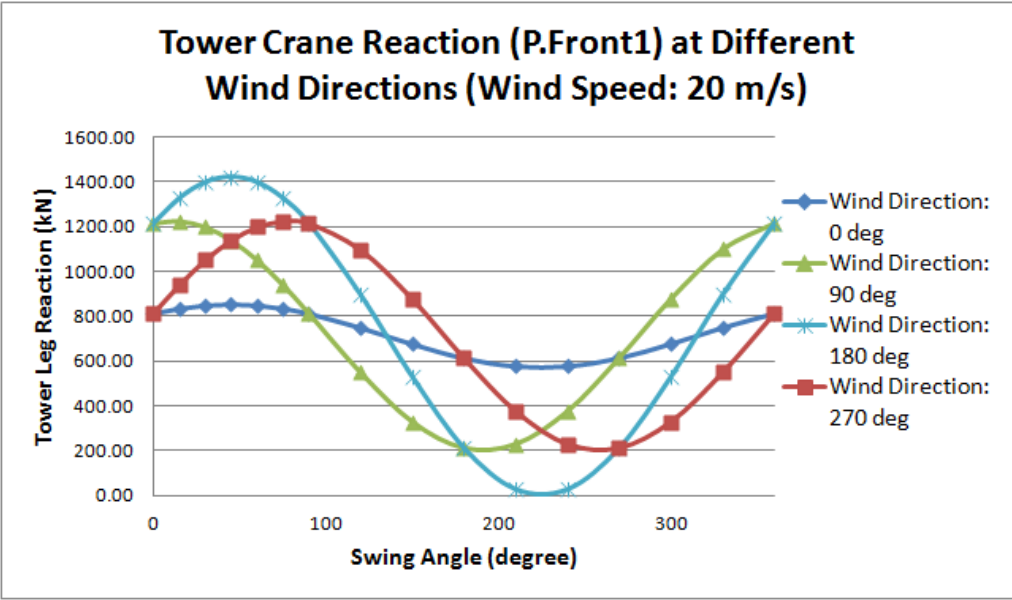


Figure 3.40: Wind direction effects on tower crane operations

MS-Excel spreadsheets are developed to calculate the support reactions with respect to wind speed, direction, and the lifting height for mobile crane and tower crane. The user needs to first input the crane geometric and operations information in a spreadsheet as shown in Figure 3.41. The user must then specify the wind speed, direction, and the lifted load information, along with the lifting height, in another spreadsheet. Figures 3.42 and 3.43 illustrate the support reactions for 360° rotation along with wind speed and direction for crawler crane and tower crane, respectively.

Crane Geometry and Operations Input

Please Input the value of following Parameters	
CL Rotation to Boom Foot (m)	1.70
CL Rotation to CL Crawler Bearing (m)	0.00
Crawler Width (m)	8.00
Crawler Length (m)	9.65
Boom Length (m)	32.00
Boom Weight (kg)	18845.00
Boom Foot to CG of Boom (m)	16.00
Angle of Boom CG	0.00
Jib Offset	50.00
Jib Weight (kg)	13290.00
Jib Foot to CG of Jib (m)	16.00
Angle of Jib CG	0.00
Jib Length (m)	32.00
Structure Weight (kg)	22360.00
Distance from CL Rotation to CG of Structure (m)	0.00
Counterweight (kg)	124000.00
Distance from CL Rotation to CG of Counterweight (m)	6.90
Carrier Weight (kg)	57000.00
Distance from CL Rotation to CG of Carrier (m)	2.00
Additional Load (kg)	0.00
Crawler Track Width (m)	1.20
Boom Angle	88.00
Lifting Radius (m)	29.00
Horizontal Swing Angle	0.00
Lifting Load (kg)	30000.00

Figure 3.41: Crane geometric and operations input form

Wind Speed (m/s)	20
Direction (deg)	0
Boom Angle (deg)	88
Jib Offset	50

Boom Width (m)	3
Jib Width (m)	2
Load Length (m)	8
Load Height (m)	3
Lifting Height (m)	10



Swing Angle	Crawler Tracks Pressure (kPa)				Maximum Pressure (kPa)
	P.Front1	P.Rear1	P.Front2	P.Rear2	
0	123.16	101.70	123.16	101.70	123.16
15	128.52	110.68	113.12	97.42	128.52
30	127.96	124.58	99.91	97.27	127.96
45	120.93	143.09	85.07	100.65	143.09
60	107.66	165.15	69.82	107.10	165.15
75	89.29	189.05	54.98	116.41	189.05
90	67.69	212.54	40.94	128.56	212.54
120	24.13	248.68	15.65	161.27	248.68
150	-5.96	258.51	-4.66	201.84	258.51
180	-14.53	239.40	-14.53	239.40	239.40
210	-4.66	201.84	-5.96	258.51	258.51
240	15.65	161.27	24.13	248.68	248.68
270	40.94	128.56	67.69	212.54	212.54
300	69.82	107.10	107.66	165.15	165.15
330	99.91	97.27	127.96	124.58	127.96
360	123.16	101.70	123.16	101.70	123.16

Figure 3.42: Crawler crane support reaction calculation form with wind speed and direction

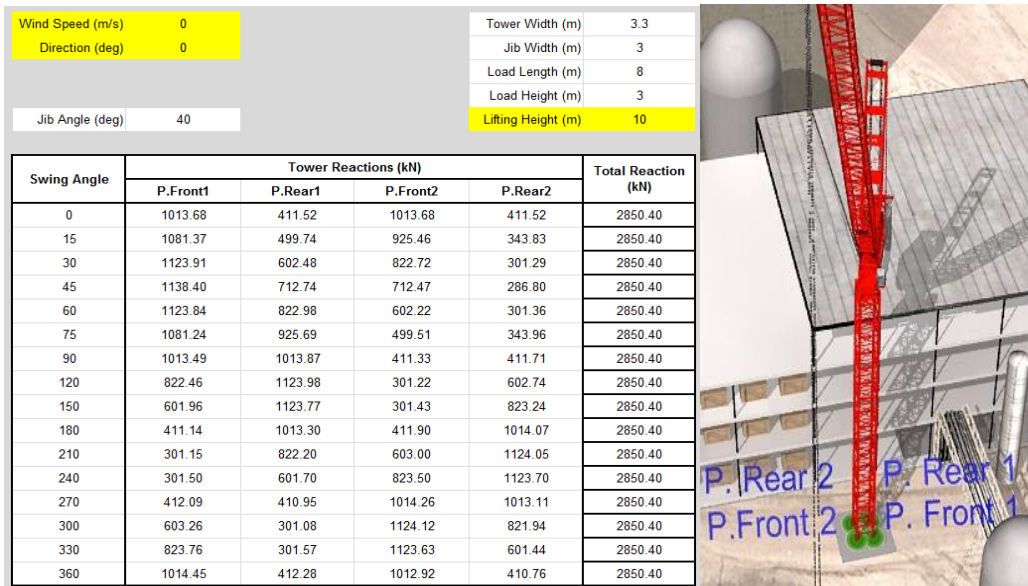


Figure 3.43: Tower crane support reaction calculation form with wind speed and direction

The developed crane stability analysis system performance has been verified with another system, the Ground Bearing Pressure Estimator (GBPE), provided by Manitowoc Cranes, Inc. GBPE provides the option to calculate the ground pressure for the Manitowoc crawler crane only. In comparing the ground pressure results for a Manitowoc 4600 (Series 3) crane lifting a total load of 162,000 kg within a radius of 5.49 m using the GBPE (see Figure 3.44), for instance, the output maximum ground pressure when operating over the front (0° swing angle) is 402 kPa, while at the critical position (151° swing angle) the value is 436 kPa (see Figure 3.45).

Ground Bearing Pressure Estimator



INITIAL CRANE SPECIFICATION

Step - 1
First select the desired model number from the list below. Then adjust the basic option(s) associated with the model number selected.

Model Number	DESCRIPTION	Basic Options
4800 Series 2		Crawler (Ext. / Retr. / Fixed) Fixed Counterweight 110,000-LB (49,841-KG) <small>Includes: Caterpillar D-379 Engine</small> Gantry Position Gantry Up Operating Surface Soft

Step - 2
Second, based on the model stated above, adjust the below primary, secondary and/or third attachment options respectively.

Attachments	DESCRIPTION	Length
Primary :	#27 BOOM OTT	80FT (24.4M)
Secondary :	#123 JIB	40FT (12.2M)

Step - 3
Third, fill in the blanks for the following ...
The total Lift load is 162000 kgs. The load radius is 5.49 and is measured in meters. Next, please indicate the point from which the load is suspended:

#27 BOOM OTT
 #123 JIB
 NO ATTACHMENT

Step - 4
Finally, is there a specific swing angle?
 No
 Yes - Please specify 45 in degrees.

When you have finished answering the above questions, press the CONTINUE button.

CAUTION: Not to be used for crane rating purposes !

Figure 3.44: GBPE crane selection and input form

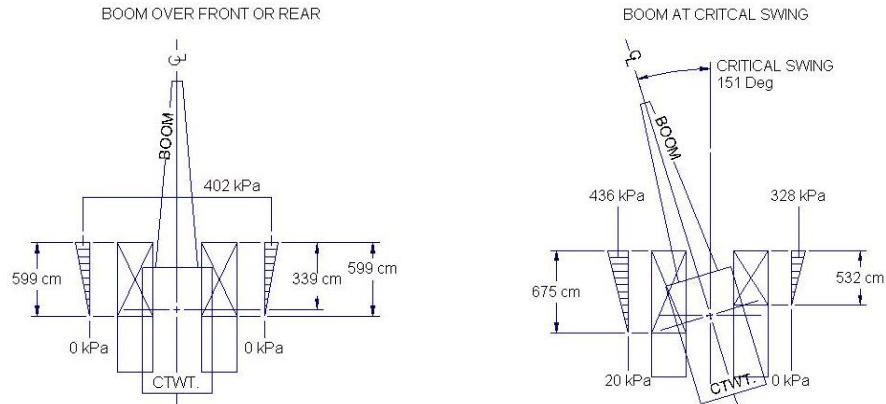


Figure 3.45: Output ground pressure from GBPE

Performing the same configuration in the proposed system as shown in Figure 3.46, the output maximum design pressure when operating at a 0° swing angle is 417 kPa (ground pressure 363 kPa) (see Figure 3.47) while at a 151° swing angle the value is found to be 469 kPa (ground pressure 408 kPa).

Figure 3.46: Support design crane configuration and input form

While GBPE is only applicable to Manitowoc crawler cranes, the proposed system provides the ground pressure values for 195 different cranes, including a reaction influence chart for 360° swing with varying boom angles, also in a tabulated format with the potential to design a crane supporting system using either timber or steel.

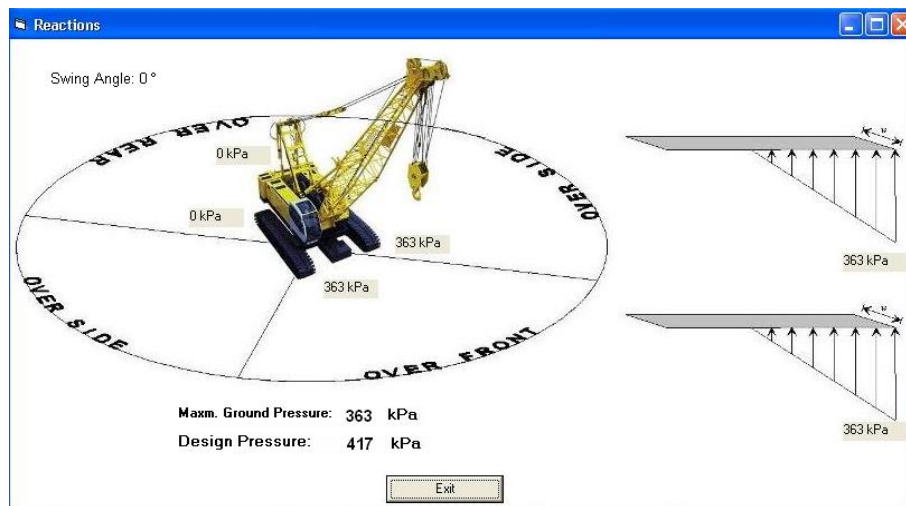


Figure 3.47: Track pressure for a specified position of crane

3.2.5 Crane Operations Simulation

After analysing the crane stability and designing the crane support system, the user need to simulate the crane activity to obtain a detailed schedule and identify the number of crane required. Crane operations can be broken down into separate activities which are dependent on: (1) source location (location of the load when delivered to the site); (2) destination location (final design location); (3) weight and size; (4) priority setting; (5) crane location; (6) boom/jib length; (7) rotating/hoisting speed; and (8) reach (required lifting radii). In order to simulate the lifting operation, travel speeds for hoisting, radial, and horizontal trolley movements also need to be considered. A simulation model has been developed using Symphony.NET3.5 (Hajjar and AbouRizk, 1999) as shown in Figure 3.48. The Symphony software allows users to select different kinds of distribution models depending on the uncertainty of the activity. For example, for construction sites, if the change of source location is slight, the user can select the “uniform” distribution for the crane hook swing activity. However, if the change of source location is significant then the user needs to select a different distribution for hook swing activity which can accommodate the uncertainty of the reallocation (i.e., triangular or normal distribution). Based on the project activity schedule, the construction site necessitates that a crane complete any remaining lifting activities. The following steps describe the total time required to perform an activity:

- a. Lifting requirement is described by the activity schedule.

- b. All activities which require lifting are added to a waiting list for the next available crane.
- c. The crane operator selects a lift (object) based on the project schedule.
- d. The crane hook moves from the last location to the source location of the load (t_{s1}).
- e. Hoist-down without any load ($t_{h-down1}$).
- f. Hook the load ($t_{hooking}$).
- g. Hoist-up the load (t_{h-up1}).
- h. Perform radial (swing) movement (t_{s2}).
- i. Perform horizontal (trolley) or vertical (luffing) movement of the load (t_l).
- j. Hoist-down the load ($t_{h-down2}$).
- k. Position and unhook the load ($t_{un-hooking}$).
- l. Hoist-up without the load (t_{h-up2}).
- m. The crane hook moves to another source location to pick a load based on the lifting schedule.
- n. If no activities are waiting for a crane, the hook moves to a predefined parking location and the simulation stops.

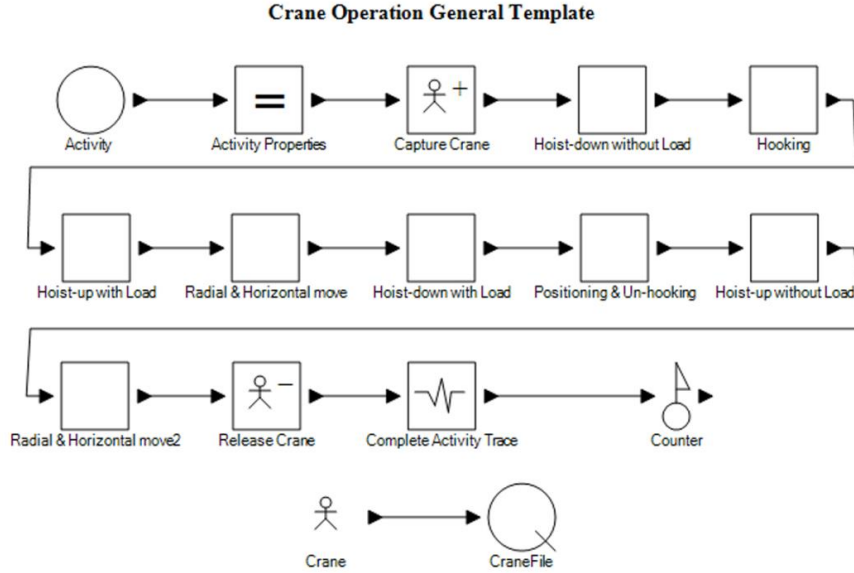


Figure 3.48: Crane operations simulation model from Symphony.NET3.5

Most of the activities vary based on the complexity of the work and on crew performance. Swing activity depends on the radial distance between the source location of the load to the destination location and the crane's swinging speed. Similarly, hoist-up and hoist-down activities depend upon the hoisting speed of the crane with and without the load, and the height of the destination location. The developed simulation model provides the possible time for each lifting cycle. The total time spent by a crane on a full lifting cycle operation (T_f) can be calculated satisfying Equation (3.53)

$$T_f = t_{s1} + t_{s2} + t_{h-down1} + t_{hooking} + t_{h-up1} + t_l + t_{h-down2} + t_{un-hooking} + t_{h-up2} \quad (3.53)$$

The number of cranes required for project (N) can be calculated satisfying Equation (3.54):

$$N = \left\lceil \frac{T_f \times n_A}{T_O} \right\rceil \quad (3.54)$$

where the notation $\lceil x \rceil$ means that x is rounded up to the closest integer value, n_A is the number of lifting activities/cycles per day and T_O is the total operation time of the project on a typical day. The idle time of the crane is waste, and thus it is not considered in determining the number of crane required

Most of the critical planning as well as productivity analysis for crane operations need to be performed during the crane selection process. If it is found that the selected crane remains idle for most of the work duration (non-productive), then the planning engineer needs to select a different crane in order to avoid schedule delays and/or cost overruns.

3.2.6 Crane Operations Productivity Analysis

Crane productivity analysis does not receive much attention by practitioners. This research proposes to analyze the productivity of lifting operations during the crane selection and planning process. Traditionally, tower cranes are mainly used in high-rise building construction and mobile cranes are used for heavy industrial construction projects. There are different ways to analyse and improve the crane operations productivity. Technology such as wireless control video monitoring system and radio frequency identification (RFID) can be used to improve the productivity of both tower crane and mobile crane operations. Lean principles, which have been used by the manufacturing company for several years, can be used to improve the crane operations productivity as well. This thesis provides an opportunity to improve the productivity of tower crane

operations by using double-jib instead of single jib. Two or more technically feasible cranes are required for the productivity analysis.

Traditional tower crane operation poses several challenges, namely 1) the wind affects the running of the boom during lifting, 2) torsion forces occur in the central tower, and 3) assembling, dismantling and transporting the crane from one yard to another can be complex, which decrease the productivity of lifting operations. Taking these deficiencies into consideration, the productivity analysis considers a tower crane equipped with two jibs (see Figure 3.49). As cranes are the most expensive equipment in the construction process, the productivity analysis and improvement of crane operations become important factors in the construction industry. This thesis provides a methodology to calculate the crane swing productivity of traditional (single-jib) tower cranes and double-jib tower cranes (see Figure 3.49), which swings with the assistance of mounted propellers.



Figure 3.49: Double-jib crane operation

To derive the mathematical apparatus needed to obtain mean estimations of productivity, the crane is conveniently located at the origin of the Cartesian coordinate's frame, the X axis of which is defined as the line connecting the crane to the pick point (see Figure 3.50). The rotation angle needed to take the load from the pick point to its destination is referred to as α and is subjected to the constraint $0 < \alpha \leq \pi$ degree.

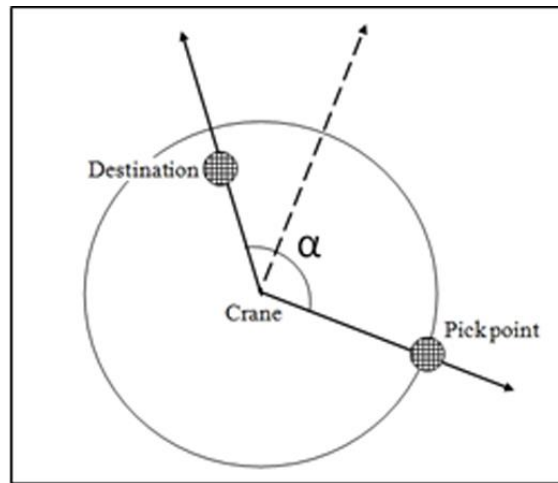


Figure 3.50: Geometrical parameters used for the estimation of mean productivity

Assuming the pick point is fixed, the full cycle of a single-jib crane (pick point to destination to pick point) requires both a forward and a backward rotation totaling (2α) angle units. For a double-jib crane, two different scenarios should be considered (Figure 3.51):

1. When $\alpha < (\pi/2)$, the full rotation cycle is described by (2α) in the same way as its single-jib counterpart.
2. However, for rotations larger than $(\pi/2)$, the total rotation is constant and equals π since in this case both arms are used in sequence to lift loads.

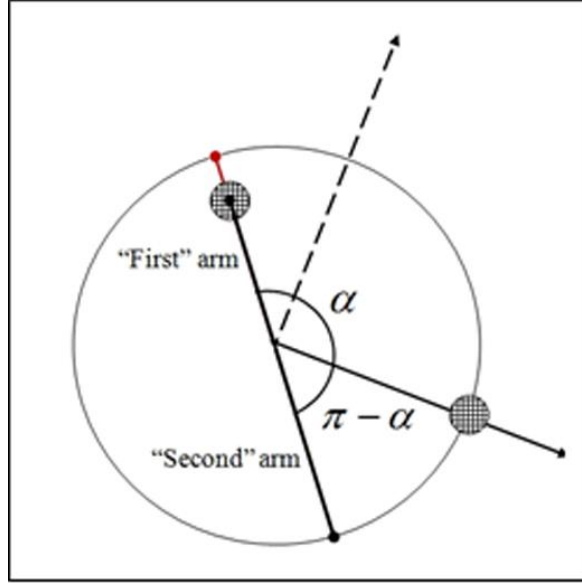


Figure 3.51: Total rotation angle for a double-jib crane when $\alpha > \pi/2$

To analyze the crane's productivity, the swing angle can be assumed to be a uniformly-distributed random variable, that is, $X \sim U(0, \pi)$, and in this way it becomes possible to quantify the average swing savings that results from using a double-jib crane (Hasan et al. 2013).

1. For a single-jib crane, if the swing angle is α then the cycle angle (i.e., pick point to destination to pick point) is 2α . In this case, the average cycle angle can be computed as the expected value of the random variable, $2X$, satisfying Equation (3.55):

$$\langle 2X \rangle_{\text{single}} = \int_0^{\pi} 2x \frac{dx}{\pi} = \pi \quad (3.55)$$

2. On the other hand, for a double-jib crane, the cycle angle is $2X$ for $0 < X < \pi/2$, whereas for $X > \pi/2$ such an angle is constant and equals π . As a result, the expected cycle angle can be computed satisfying Equation (3.56):

$$\langle 2X \rangle_{\text{double}} = \int_0^{\pi/2} 2x \frac{dx}{\pi} + \int_{\pi/2}^{\pi} \pi \frac{dx}{\pi} = \frac{3\pi}{4} \quad (3.56)$$

Based on these expected values, a double-jib crane is on average 25% more efficient in comparison to its single-jib counterpart. However, the distribution of such savings cannot be uniform since it is essentially achieved only for angles greater than $\pi/2$. The ratio between the cycle angles of the double- and single-jib cranes can be modeled satisfying Equation (3.57):

$$s = \frac{\text{Single jib cycle angle}}{\text{Double jib cycle angle}} = \begin{cases} 1 & 0 \leq X \leq \pi/2 \\ \pi/(2X) & \pi/2 < X \leq \pi \end{cases} \quad (3.57)$$

The above function is represented in Figure 3.52.

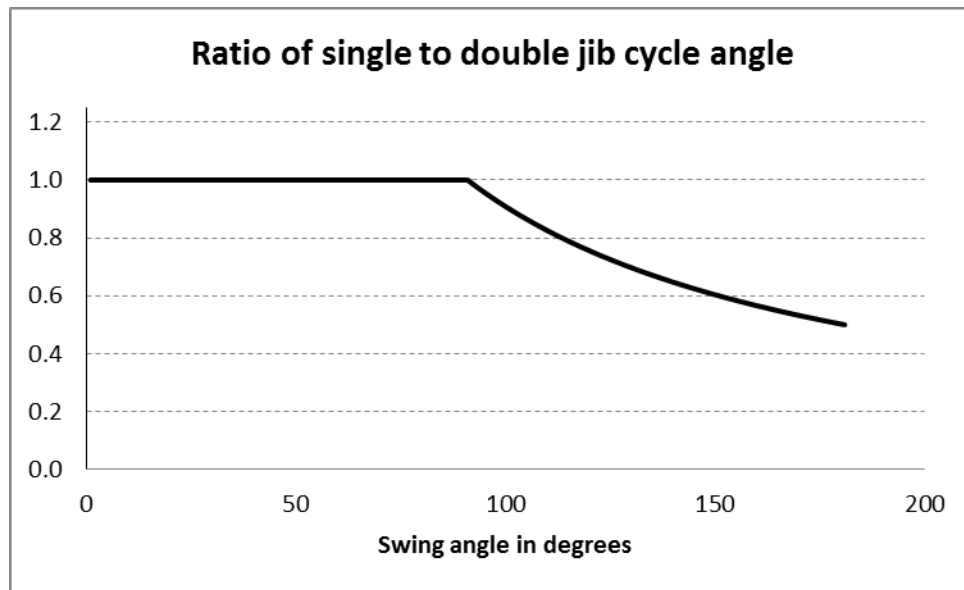


Figure 3.52: Ratio of single-jib to double-jib crane cycle angle (Hasan et al., 2013)

From the above analysis, a recommendation can be made to use a double-jib crane if most of the lifts have swing angles greater than $\pi/2$.

Construction is known to be subject to a variety of uncertainties, and requires a model that incorporates these variables. Let us assume that the number of daily lifts is described by the discrete distribution which provides three different scenarios (see Figure 3.53):

1. the worst-case scenario, in which only n_1 lifts were performed;
2. the most likely case, where the operator manages n_2 lifts; and
3. the best-case scenario, in which n_3 lifts were completed.

Associated with each of the above cases are the probabilities p_1, p_2 and p_3 .

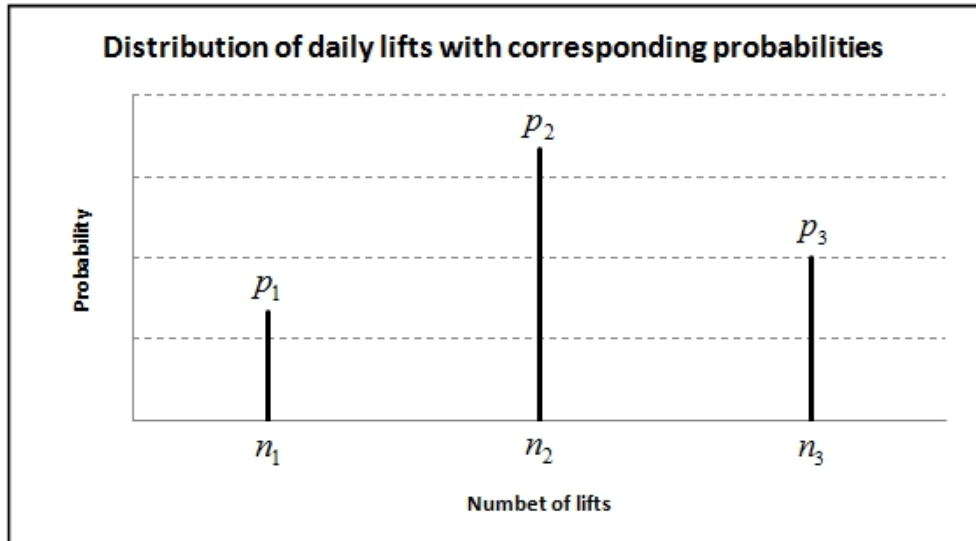


Figure 3.53: Three different scenarios of daily lifts (Hasan et al., 2013)

In addition, it is assumed that the number of lifts is a result of the swing angle, such that the greater the angle, the smaller the number of lifts. Although this is a simplification of crane operations, it has the advantage of providing a framework that takes uncertainty into account. As a result, the following piecewise uniform distributions will be considered for each of the cases enumerated above. According to Figure 3.54, the worst-case scenario (corresponding to n_1 lifts) is

described by the distribution of the swing angle depicted in Figure 3.54a. In this case the probability $q_{1,3}$ of wide swinging (here assumed to be between 120° and 180°) is greater than those corresponding to smaller angles. The swing angles of the most likely lifting scenario were chosen to be uniformly distributed according to Figure 3.54b, with the probabilities written as $q_{2,1} = q_{2,2} = q_{2,3}$. Here the indices are retained for the sake of generality and uniformity of the notation. As for the best-case scenario, it is characterized by a large probability of small swing angles (see Figure 3.54c), thus making the lifting operation faster and more productive.

At this point, using the distribution of swing angles corresponding to the worst-, most likely, and best-case scenarios, the expected value of the cycle angle can be derived, from which one can obtain the productivity ratio between single- and double-jib cranes.

1. For a single-jib crane, the expected daily cycle angle (pick point to destination to pick point) can be represented as a dot product of two vectors, satisfying Equation (3.58) (Hasan et al., 2013):

$$\langle 2X \rangle_{\text{single, daily}} = \left(\begin{bmatrix} q_{11} & q_{12} & q_{13} \\ q_{21} & q_{22} & q_{23} \\ q_{31} & q_{32} & q_{33} \end{bmatrix} \begin{bmatrix} \alpha_1 \\ \alpha_1 + \alpha_2 \\ \alpha_2 + \alpha_3 \end{bmatrix} \right) \bullet \begin{bmatrix} n_1 p_1 \\ n_2 p_2 \\ n_3 p_3 \end{bmatrix} \quad (3.58)$$

Where,

q is the probability of swing angles

p is the probability of number of daily lifts

α_1 , α_2 and α_3 are the swing angles where α_3 is the greatest possible swing angle, which in many practical scenarios can be equated to π .

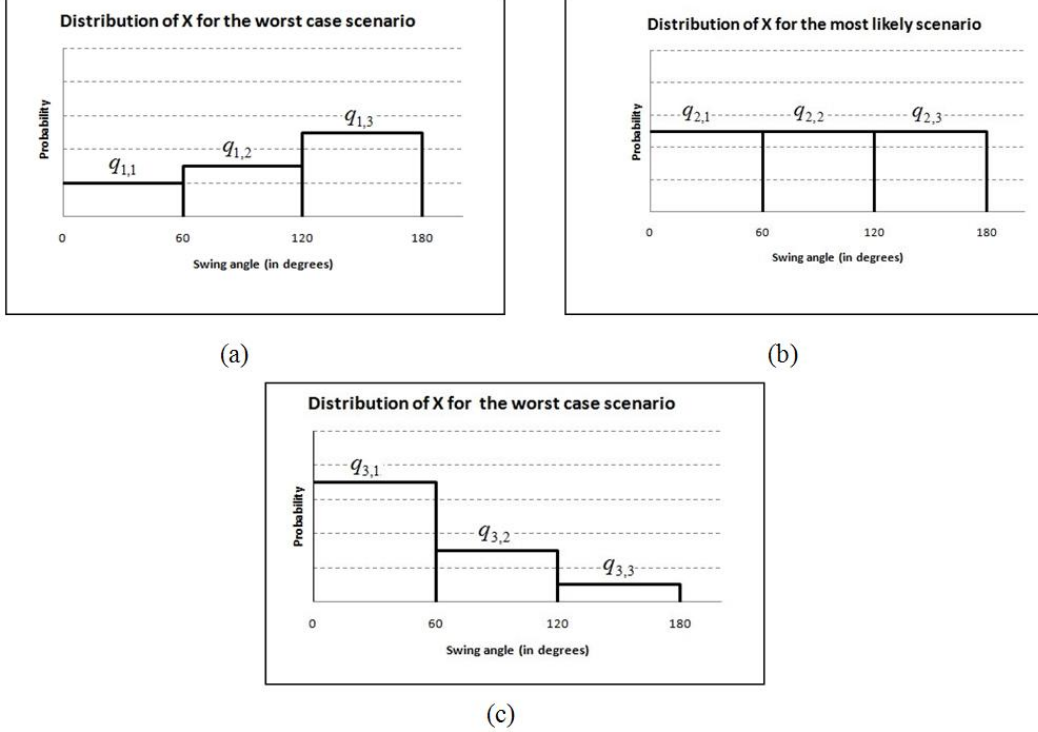


Figure 3.54: Distribution of swing angles for (a) the worst-case, (b) the most likely and (c) the best-case lift scenarios (Hasan et al., 2013)

2. In a similar manner, the expected daily cycle angle for a double-jib crane can be determined based on the distributions given in Figures 3.53 and 3.54 satisfying Equation (3.59) (Hasan et al., 2013). However, in this particular case an assumption can be made that $\alpha_1 + \alpha_2 > \pi/2$, which is well-founded since for angles smaller than $\pi/2$ there is no benefit to using a double-jib crane (see Figure 3.52).

$$\langle 2X \rangle_{\text{double, daily}} = \begin{pmatrix} q_{11} & q_{12} & q_{13} \\ q_{21} & q_{22} & q_{23} \\ q_{31} & q_{32} & q_{33} \end{pmatrix} \begin{pmatrix} \alpha_1 \\ (\pi\alpha_2 - \alpha_1^2 - (\pi/2)^2)/(\alpha_2 - \alpha_1) \\ \pi \end{pmatrix} \bullet \begin{pmatrix} n_1 p_1 \\ n_2 p_2 \\ n_3 p_3 \end{pmatrix} \quad (3.59)$$

To illustrate the usefulness of the above theory, Figure 3.55 shows the productivity ratio (double-jib over single-jib) for varying values of α_1 and α_2 . As for the other parameters, they are set satisfying Equation (3.60) (Hasan et al., 2013):

$$\alpha_3 = \pi, \begin{bmatrix} q_{11} & q_{12} & q_{13} \\ q_{21} & q_{22} & q_{23} \\ q_{31} & q_{32} & q_{33} \end{bmatrix} = \begin{bmatrix} 0.2 & 0.3 & 0.5 \\ 1/3 & 1/3 & 1/3 \\ 0.65 & 0.20 & 0.15 \end{bmatrix} \text{ and } \begin{bmatrix} n_1 p_1 \\ n_2 p_2 \\ n_3 p_3 \end{bmatrix} = \begin{bmatrix} 50 \times 0.25 \\ 80 \times 0.55 \\ 110 \times 0.20 \end{bmatrix} \quad (3.60)$$

Using the input parameters shown above, the contour map as shown in Figure 3.55 was obtained for the productivity.

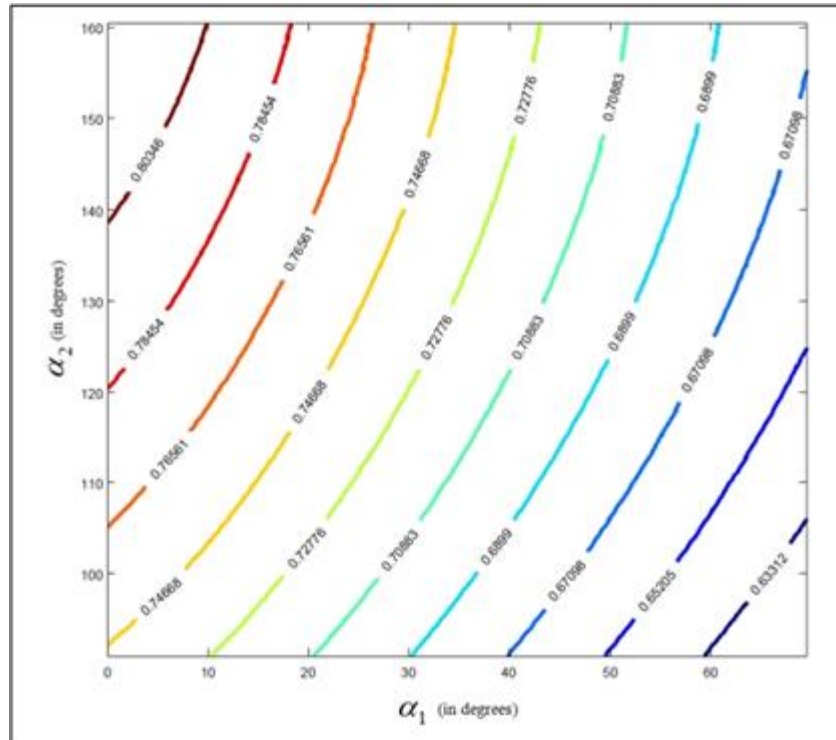


Figure 3.55: Contours for productivity ratios (double-jib over single-jib crane) for varying values of α_1 and α_2 (Hasan et al., 2013)

An interesting application of the contour map depicted in Figure 3.55 is the determination of the angles that will lead to a given goal in terms of productivity. As can be seen, for any given productivity ratio, a range of possible values for

α_1 and α_2 can be easily determined. Such values can, in turn, be used to help locate the position of the crane that will lead to the selected productivity.

Wind also effects the crane operations and due to the high wind conditions in some places cranes need to be shut downed for a significant amount of time which affects the productivity of overall crane operations. Thus, the user needs to calculate the possible stoppage period of the selected crane operations during the crane selection planning process and make his choice accordingly.

3.2.7 Wind Effect Analysis

According to crane manufacturers' information on maximum allowable wind speeds, tower cranes have the advantage of usability in higher wind speeds (on average 9-14 m/s for mobile crane compared to 15-20 m/s for tower crane). However, when practitioners use simulation tools to select the most appropriate cranes for a specific operation, the effect of wind is often ignored even though high wind speed affects the crane's lifting operations and creates safety hazards. The proposed methodology analyzes both crane and project-related factors, considering historical wind speed data in the project location and determining if the selected crane (based on its capacity) would be operational during most of the project days and all the time during those days. Wind speed and direction varies across locations, seasons, and even hours. It is apparent that using daily average (or even maximum) wind speed data from project location does not capture the true scenario. Thus, in this research, hourly historical weather data from the project location has been utilized to sample wind speed and directions

at each hour during construction work. Figure 3.56 illustrates the hourly wind speed in Saskatoon, Canada, for the year 2010.

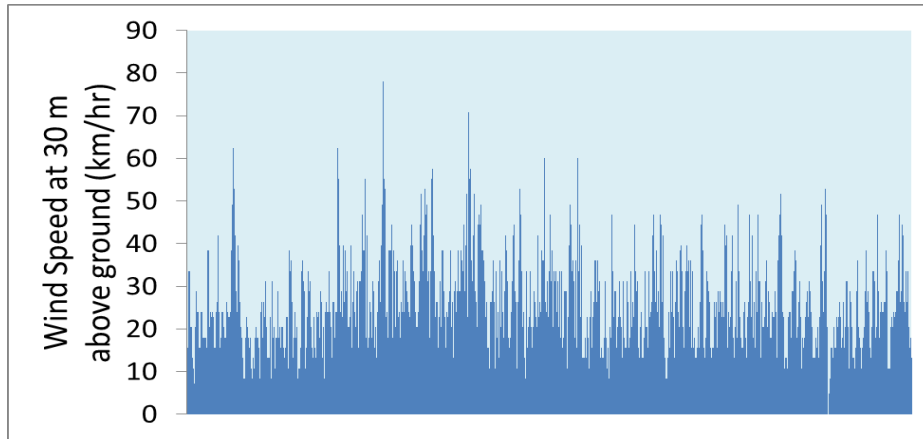


Figure 3.56: Hourly wind speeds in Saskatoon, 2010

The effect of wind on crane operations can be evaluated by plotting the cumulative distribution curve for historical wind speed data and then fitting the crane's maximum allowable wind speed as shown in Figure 3.57. This allows the analyst to determine the percentage of days for which the wind may exceed the maximum allowable speed, i.e., will force the crane to cease operations.

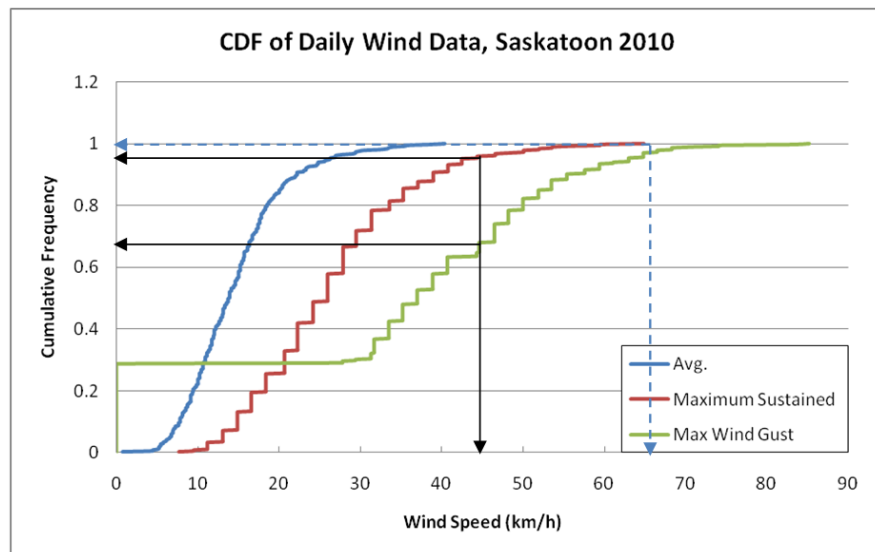


Figure 3.57: Wind cumulative frequency

Usually, crane manufacturers or rental companies provide the maximum wind speed beyond which a specific crane's operations must be shut down. Different jurisdictions may have their own regulations regarding these maximums as well. In this research, the maximum wind speed data is collected through literature reviews, manufacturers' handbooks, agency guidelines, and industry experts' reports. Some guidelines set 32 km/h as the safe wind speed for crane operations (Brookhaven National Laboratory, 2011), while other references suggest 50 km/h and 72 km/h for mobile and tower cranes, respectively (Watson, 2004; Construction Plant-hire Association, 2009) at 10m height from the ground. For this research, maximum allowable wind speeds for mobile and tower cranes are assumed to be 50 km/h and 72 km/h, respectively at 10m above the ground. In a construction project in Saskatoon, if the lifting height is 20m, then the maximum allowable operational wind speed limit need to be reduced by 10% (Construction Plant-hire Association, 2009). Drawing the line at 45 km/h maximum sustained wind speed for the mobile crane operation in Figure 3.57 suggests that the crane operations are to be shut down about 3% of total project duration (in days). The number is significantly greater (more than 30%) if the wind gust is considered. On the other hand, tower cranes' maximum allowable wind speed can be assumed to be 65 km/h at 20m height, and from the Figure 3.57, it is found that the tower cranes can operate safely under both of these conditions. The results are summarized in Table 3.5.

Table 3.5: Wind effects at different crane operations in Saskatoon on 2010

Crane Options	Shutdown Period (in % of days in a year)	
	Considering Max. Sustained Wind	Considering Wind Gust
Crawler Crane	3%	30%
Tower Crane	0%	0%

Once the cranes have been identified satisfying simulation, productivity and wind effects, the final steps are to determine which is most suitable based on the remaining factors, namely carbon emissions, and cost.

3.2.8 Environmental Footprint (Carbon Emission) Analysis

Climate change has emerged as a major challenge for the international community. Carbon footprint quantification, analysis, and reduction are keys to preventing climate change. Construction cranes consume considerable amounts of energy and emit significant volumes of CO₂ on site. Since 2006, the Government of Canada has been introducing regulations to reduce emissions from key sources (Environment Canada, 2010). Cranes were listed in the U.S. Environmental Protection Agency's (EPA) non-road vehicles and equipment category as one of the main sources of emissions (EPA, 2005). Due to the large amount of diesel used on site, the EPA published a Non-road Diesel Program to advance emission control technologies for engines used in non-road equipment (EPA, 2004). However, the NONROAD model data was only intended to predict average emissions for a fleet of vehicles. Similar data is needed to quantify the CO₂ emissions generated by on-site crane engines. One of the primary determinants of CO₂ emissions from mobile sources is the amount of carbon in

the fuel. Carbon content varies, but average carbon content values can be used to estimate CO₂ emissions (EPA, 2005). The Code of Federal Regulations specifies that there are 2,778 grams of carbon content per gallon of gasoline or diesel fuel. Each molecule of CO₂ weighs 3.66 times more than an atom of carbon alone. In an average liquid hydrocarbon-burning engine, it can be assumed that 99 percent of the fuel will oxidize. Thus the CO₂ emission per gallon of diesel consumption is 10,084 gm (2,778g×3.66×0.99). The EPA NONROAD model provides fleet average emission estimates according to Equation (3.54) (EPA, 2004). Due to the machines' duty cycles, the fuel consumption rates vary among individual vehicles. The total amount of CO₂ emissions (*CCE*) by a mobile crane during a year can be calculated satisfying Equation (3.61),

$$CCE = N \times P_{kw} \times LF \times A \times EF \quad (3.61)$$

where *N* is the number of cranes, *P_{kw}* is the average engine power (kW), *LF* is the load factor, *A* is the activity (h/year), and *EF* is the emission factor (g/kW h). During the idle/full throttle/ shut-down periods, the consumption rate changes. One must first observe the differing fuel consumption rates during different periods and then identify how to reduce the CO₂ emissions.

When the mobile crane is swinging, hoisting, luffing, and holding the lift items, it is assumed that the engine is in the full-throttle condition. The duration of full throttle in a day (*LF_f*) can be calculated satisfying Equation (3.62),

$$LF_f = n \times T_f \quad (3.62)$$

where T_f is the total time spent by a crane for a full lifting cycle operation (see Equation 2) and n is the number of crane cycles. Thus, the total amount of CO₂ emissions (CCE) by a mobile crane during full throttling can be calculated satisfying Equation (3.63):

$$CCE_f = N \times P_{kw} \times LF_f \times A \times EF \quad (3.63)$$

Mobile crane operators often idle their engines to operate the air conditioning, or lights, or to keep their engine warm in cold weather. Idling also occurs during the intermittent stage between two lift cycles, or while a crane operator waits to load or unload their lift item. Previous research has established a correlation between idling engine revolutions per minute (rpm), air conditioning (AC), and the amount of fuel consumed during idling (Argonne National Laboratory, 2010). If the total operation time per day is T_O hours, then idling time (LF_i) can be calculated satisfying Equation (3.64):

$$LF_i = T_O - LF_f \text{ hrs/day} \quad (3.64)$$

The total amount of CCE by a mobile crane during idling can be calculated satisfying Equation (3.65):

$$CCE_i = N \times EF_i \times LF_i \times A \times P_{kw} \quad (3.65)$$

where EF_i is the idling emission factor (the grams of CO₂ emitted per hour when idling).

The CO₂ emissions of a tower crane are relatively lower than those of a mobile crane at the same productivity level. In this section, emphasis is placed on

deriving a quantitative estimation for the calculation of CO₂ for tower cranes during the swing operation. Let Y be the cycle angle for a given lift operation; in such a case the energy associated with this motion is defined satisfying Equations (3.66),

$$E_{\text{cycle}} = P_{kw} \frac{[Y/(2\pi)]}{\nu_j} \quad (3.66)$$

The ratio $[Y/(2\pi)]$ is a representation of the cycle angle as a fraction of a full rotation of the jib. ν_j and P_{kw} refer to the speed of jib (expressed in rotations per second) and the power (expressed in kilowatts) required to perform a single full rotation. Assuming the distribution of swing angles is known, the average yearly energy consumption is obtained satisfying Equations (3.67),

$$E_{\text{day}} = n \times E_{\text{cycle}} \Rightarrow E_{\text{annual}} = d \times E_{\text{day}} = P_{kw} \frac{n \times [\bar{Y}/(2\pi)]}{\nu_j} \times d \quad (3.67)$$

where n and d represent the average number of lifts per day and the number of working days per year, respectively.

Tower cranes traditionally operate on electricity. Since a primary energy source, such as coal, natural gas, or petroleum, is needed to generate electricity, CO₂ emissions are attributable to the tower crane lifting process. The Energy Information Administration (EIA) in the United States has collected data on CO₂ emissions from electricity generation (EPA, 2000). The CO₂ emissions are presented on the basis of total mass (tons), output rate (pounds per kilowatt-hour), and the average output rate, which is the ratio of pounds of CO₂ emitted

per kilowatt-hour to electricity produced from all energy sources, both fossil and non-fossil. The greenhouse gas (GHG) emission factor used to estimate GHG reductions is based on the GHG emission intensity of marginal electricity generation in each province. It is assumed that incremental renewable power generation replaces existing marginal electricity generation. To obtain a national factor, the emissions factor for the marginal fuel in each province was weighted by the provincial share of electricity generation, and then summed. Thus, across Canada, a GHG emission factor of 465.88 t/GWh was used (Environment Canada, 2010). Examples of such GHGs are methane, perfluorocarbons and nitrous oxide. The contribution of a given gas to the greenhouse effect is affected by both its characteristics and its abundance. Equivalent CO₂ (CO₂E) is the concentration of CO₂ that would cause the same level of radiative forcing as a given type and concentration of GHG. The total amount of CO₂ emission (*CCE*) by a tower crane during full operation can be calculated satisfying Equation (3.68):

$$CCE = E \times EF \quad (3.68)$$

where *EF* is the emission factor.

3.2.9 Cost Analysis

A primary focus of most projects is cost, and lifting costs depend on the selected equipment (crane) and related resources. Generally, calculating a crane's cost is complex, since the manager needs to account for a large number of direct variables including: (1) crane rental cost per specific period (hour/week/month); (2) transportation; (3) installation; (4) disassembly; (5) support; (6) maintenance;

and (7) operators' wages. This research introduces a methodology for scoring cranes in order to evaluate their effect in terms of cost on a particular project considering direct variables. In order to set up the calculation procedure, two types of scores are requested from the lift planners or managers: (i) a horizontal scoring obtained by comparing the cranes with respect to each individual variable listed in Table 3.6 and (ii) a vertical scoring in which the impact of the variables is evaluated in terms of their impact on the overall cost to the project.

The scores collected after surveying by the lift planner or manager are first normalized and organized into two matrices, the first referred to as the cost matrix and the second the weighting effect matrix. Templates for these matrices are provided in Equation (3.69).

Table 3.6: Crane cost scores

Cost Factors	Project Type: Industrial Project			
	Crane #1	Crane #2	Crane #i
Rental cost of crane per day	R_1^c	R_2^c	R_i^c
Cost of transportation of crane	T_1^c	T_2^c	T_i^c
Cost of installation of crane	I_1^c	I_2^c	I_i^c
Cost of disassembly of crane	D_1^c	D_2^c	D_i^c
Cost of support system	S_1^c	S_2^c	S_i^c
Cost of Maintenance if needed	M_1^c	M_2^c	M_i^c
Crane operator wages	O_1^c	O_2^c	O_i^c

$$C_{cranes} = \begin{bmatrix} \tilde{R}_1^c & \tilde{R}_2^c & \cdots & \tilde{R}_i^c \\ \tilde{T}_1^c & \tilde{T}_2^c & \cdots & \tilde{T}_i^c \\ \tilde{I}_1^c & \tilde{I}_2^c & \cdots & \tilde{I}_i^c \\ \tilde{D}_1^c & \tilde{D}_2^c & \cdots & \tilde{D}_i^c \\ \tilde{S}_1^c & \tilde{S}_2^c & \cdots & \tilde{S}_i^c \\ \tilde{M}_1^c & \tilde{M}_2^c & \cdots & \tilde{M}_i^c \\ \tilde{O}_1^c & \tilde{O}_2^c & \cdots & \tilde{O}_i^c \end{bmatrix} \quad W_{variable} = [\tilde{W}_R \quad \tilde{W}_T \quad \tilde{W}_I \quad \tilde{W}_D \quad \tilde{W}_S \quad \tilde{W}_M \quad \tilde{W}_O]$$

(3.69)

where W_R , W_T , W_I , W_D , W_S , W_M , and W_O are the impact scores on the overall cost of crane rent, transportation, installation, disassembly, support, maintenance, and operator wages, respectively.

To normalize the scores occurring in the matrices of Equation (3.69), a linear utility function is introduced which maps the discrete scores ranging from 1 to 5 (as used in the survey) onto the continuous interval [0, 1]. To illustrate the normalization procedure, let $\{R_1^c, R_2^c, \dots, R_i^c\}$ be the ‘‘Rental cost’’ values for Cranes 1 to i . To obtain the corresponding normalized cost score, a linear utility function is used which maps the subjective opinion scores onto the range [0,1] according to Equation (3.70).

$$u(R_i^c) = \tilde{R}_i^c = -\frac{R_i^c - R_{\min}^c}{R_{\max}^c - R_{\min}^c} \quad (3.70)$$

where $R_{\min}^c = \min(R_1^c, R_2^c, \dots, R_i^c)$ and $R_{\max}^c = \max(R_1^c, R_2^c, \dots, R_i^c)$. From the above equation, it is clear that the largest score is assigned a relative score equal to 1 whereas the smallest is given 0. Here, it is worth mentioning that if all the cranes are equally ranked by the lift planner or manager, the largest and smallest

values are identical, making Equation (3.70) unusable because the denominator becomes zero. This, however, is not an issue since in such a case the contribution from the variable—say “Rental cost”, for instance—can be ignored because its contribution to the overall cost score is identical for all cranes. Before moving on to investigating other issues, Equation (3.70) should be assessed in terms of the consistency of the scoring. In order to illustrate this issue, let us assume three cranes are being compared with respect to two variables: “Rental cost” and “Transportation”, and that the lift planner has reported the following scores $R = \{3,4,5\}$ and $T = \{1,1,2\}$. Based on the underlying assumption of Equation (3.37), the normalized score corresponding to the value “5” in “Rental cost” will be “1”, whereas for the variable “Transport”, it is the value “2” which will be assigned “1” as a normalized score. Of course, absolute scaling can be obtained if one uses the largest (5) and smallest (1) scores as the maximum and minimum values in Equation (3.70). Although this aspect might be viewed as a limitation, it must be emphasized that such a choice is motivated by the need for an algorithm which can be applied to user-suggested scores as well as to quantitative values. Indeed, when actual monetary values for the variables listed in Table 3.1 are known for each crane, normalized scores must be calculated based on such quantities. Note that, in contrast to the case of user-suggested scores, it is not possible to construct an absolute utility function since absolute minimums and maximums cannot be defined for monetary quantities.

At this point, the overall cost score can readily be obtained (for each crane) by taking the product of the matrices W_{variable} and C_{cranes} , which leads to a one-row

matrix the elements of which are the scores for cranes 1 to i ; the best option is expressed according to Equation (3.71),

$$\text{Bestoption} = \max(W_{\text{variables}} \times C_{\text{cranes}}) \quad (3.71)$$

A decision support matrix is created (see Figure 3.58) to identify the most economic cranes by comparing seven different cost factors. The impact score is the percentage impacts of each category on the project are displayed based on the owner/contractor opinions. The crane scores are relative crane cost scores displayed for each feasible crane based on the experts' opinion. The best option will be the crane with the highest score. It is recommended to select for further analysis two or more cranes with the highest scores among those considered.

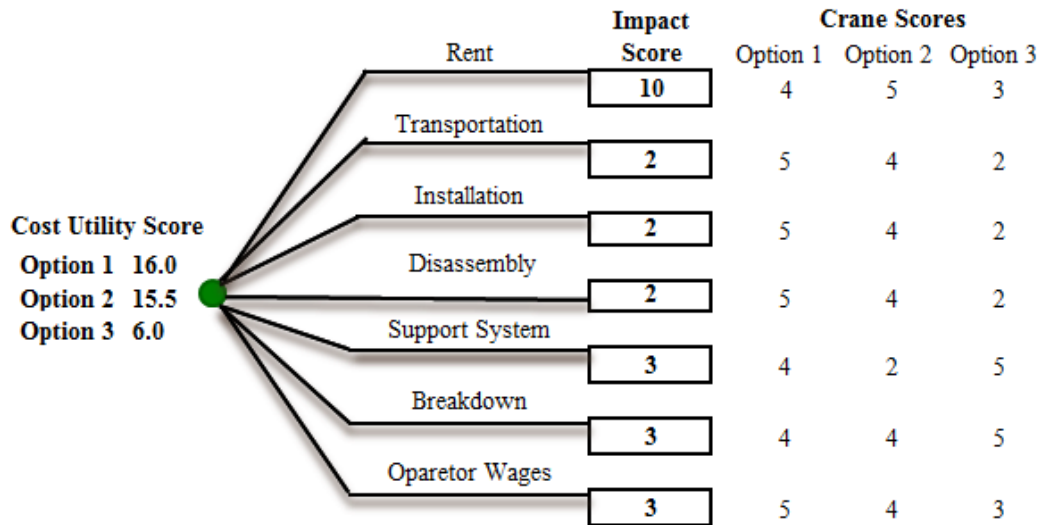


Figure 3.58: Sample for cost utility score assessment

3.2.10 Identifying Most Feasible Cranes

To identify most feasible cranes based on wind, carbon emission, and cost, each crane is first represented by a point in 3D space (referred to in mathematical terms as R^3) with the following coordinates: (W_i, C_i, S_i)

where W_i is the wind parameter, C_i is the CO₂ emission factor, and S_i is the cost score. W_i ranges from 0 to 100% and represents the expected crane utilization under the winds of the region, C_i the average mass (expressed in grams) of CO₂ emission, and S_i is the cost utility score. Accordingly, the most appropriate crane is determined as the closest to a “perfect” prototype which, in the context of this research, is represented by a point the coordinates of which are described according to the Equation (3.72).

$$\text{Perfectcranecoordinates} : (100\%, \min(C_i), \max(S_i)) \quad (3.72)$$

Although the above definition is mathematically sound, in practice it was found that making each coordinate unit-less by normalization increases the discrimination power of the proposed technique. As a result, the “perfect” crane is described according to Equation (3.73):

$$\text{Perfectcranecoordinates} : \left(100\%, \frac{\min(C_i)}{\max(C_i)}, \frac{\max(S_i)}{\max(S_i)} = 1.00 \right) \quad (3.73)$$

The most appropriate crane is identified using an overall utility score, calculated as a Euclidean distance between the point representing the selected crane and the perfect crane defined in Equation (3.72). Such a distance is determined according to Equation (3.74).

$$\text{Best crane} : \min \left(\sqrt{\left(\frac{W_i}{100} - 1 \right)^2 + \left(\frac{C_i - \min(C_i)}{\max(C_i)} \right)^2 + \left(\frac{S_i}{\max(S_i)} - 1 \right)^2} \right) \quad (3.74)$$

where $i = 1, 2, \dots$, all selected lifting options.

The proposed methodology assists in selection of a cost-effective, energy-efficient crane while satisfying other selection criteria, considering both tower and mobile cranes.

3.2.11 Integration with Building Information Model (BIM)

BIM allows better information sharing among project stakeholders and thus can improve safety, productivity, cost, scheduling, and resource management for projects. BIM can be advantageous for visualizing, verifying, and validating lifting activities in large-scale construction projects. Any large-scale construction project involves various inter-related activities where efficient resource sharing and utilization governs the success of the project. As such, BIM, if implemented effectively, should contain all relevant information within a single model. There are a number of external factors (such as wind and snow) which affect the schedule of a project; however, most existing models do not contain such information. Currently, BIM focuses mainly on: (1) laws and regulations, (2) material information and specifications, (3) procurement information, (4) facility information, (5) construction information, (6) simulation results, (7) 2D/3D drawings, and (8) visualization/animation models. This research proposes to integrate weather information into BIM, given the effect of weather on the construction schedule (see Figure 3.59).

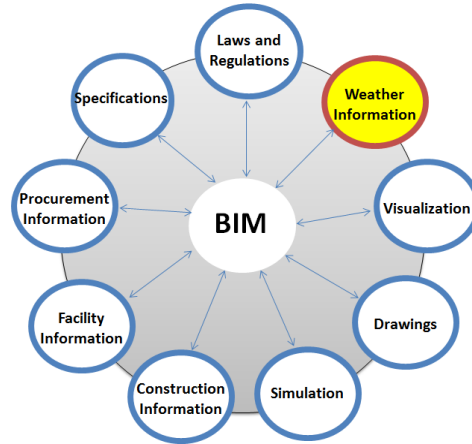


Figure 3.59: Proposed Building Information Model (BIM)

In specific, this research develops a methodology by which to incorporate historical wind speed data into lift analysis and simulation, from which crane support reactions are calculated and stability is checked during each lifting operation. Figure 3.60 illustrates the logical flowchart of the proposed integration, which incorporates wind speed simulation and crane support reaction calculations within the existing BIM. The proposed integrated model performs safety checks, simulates the lifting operations, and modifies the project schedule accordingly. The first step involves sampling hourly wind speed and direction based on historical weather data from the project location. This sampled hourly wind data is used alongside lift activity duration data to perform the simulation. The simulation model, developed using the Simphony.NET3.5 general-purpose template, checks whether or not hourly wind speed is less than the allowable limit and either continues or suspends lift operations for the hour accordingly. The hourly wind data is also used to calculate the crane support reactions, while the output from the simulation model is used to update the

project lifting schedule. The proposed system also develops a 3D visualization model based on the simulation output, which is beneficial for error detections.

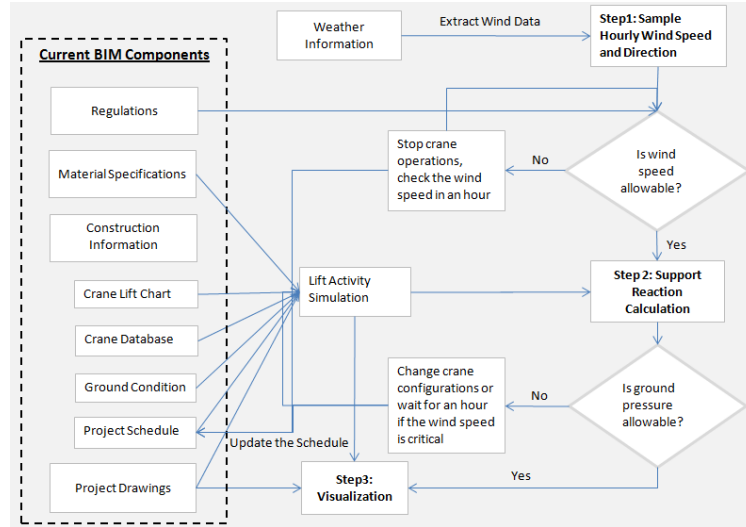


Figure 3.60: Proposed BIM logical diagram (Hasan et al., 2012a)

Figures 3.61 and 3.62 present the visualization of crane operations with wind speed, direction, and support reactions for the crawler crane and tower crane, respectively. Instability accidents due to tipping of mobile cranes have generally resulted from faulty decisions to perform lifts which either exceed the lifting capacity of the crane or swing in an area that is not permitted by the crane load chart. The proposed BIM warns (in red) if the lifting operations are unsafe due to high wind speed (e.g. exceeds the allowable limit) or if any of the support reactions become negative (e.g. tipping failure may occur).



Figure 3.61: BIM-supported visualization model for crawler crane operations

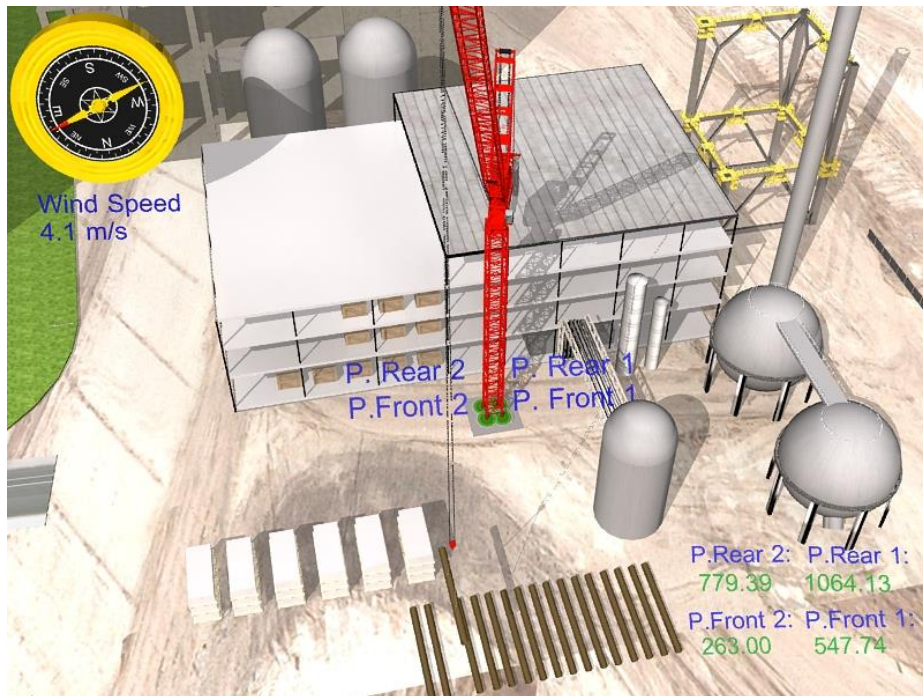


Figure 3.62: BIM-supported visualization model for tower crane operations

3.3 Summary

This chapter has presented a methodology to select most feasible crane (both mobile and tower) in an innovative way considering stability, wind effects, productivity, carbon emissions and cost. The significance of the developed decision support system is that it focuses on improving crane operation safety. This chapter has also presented a new approach to integrate weather information (currently only wind data) in BIM to control the crane operations. Integrating crane stability analysis using the wind data in BIM could open a new dimension to BIM thinking. Wind speed and direction and support reaction information in the visualization model can assist lift engineers to schedule crane operations more efficiently.

Chapter 4: Case Studies

4.1 Introduction

Three cases are used in this chapter to demonstrate the effectiveness of the proposed methodology to improve crane operations. The first case study demonstrates the crane selection and support design for mobile crane operations. The second case presents the tower crane utilization and operations improvements using simulation and optimization. The last case study compares both mobile crane and tower crane in an industrial project in Saskatoon.

4.2 Case 1: Pembina Lodge Project, Westlock, Alberta

The case study involves the construction of a four-storey, 68-unit building for older adults, called Pembina Lodge, located at 10247-104 street, Westlock, Alberta, Canada (see Figure 4.1). The earthwork of the project started on July, 2011. 30 modules were required to construct the top three floors, and the main floor was constructed on-site. The module dimensions were 22 ft (6.7m) X 56 ft (17m) X 11 ft (3.4m) and the weight was 24.95 tons.

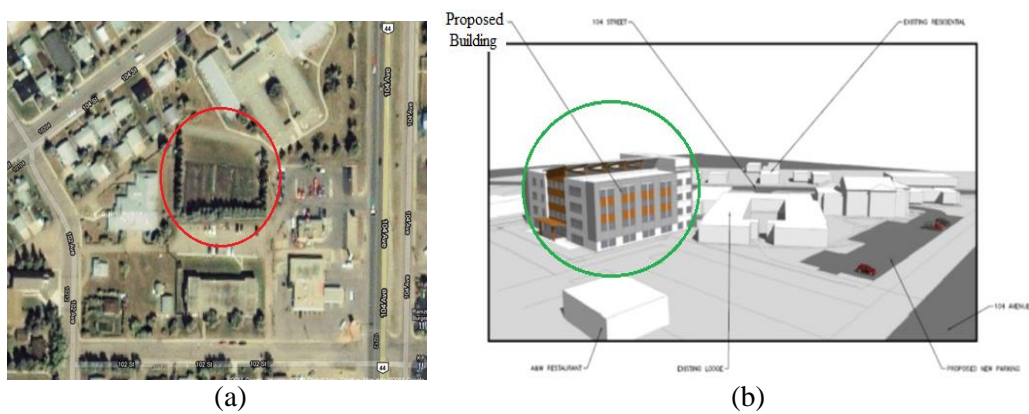


Figure 4.1: Pembina Lodge project, (a) site map from Google Maps, (b) proposed building

The site had some constraints, most notably mature trees and overhead power lines, which influenced the crane’s location for module installation. The mature trees and the power lines served to limit crane accessibility; Routes 1 and 3 are the only options on the site by which the cranes can gain access from the existing roads, as shown in Figure 4.2.

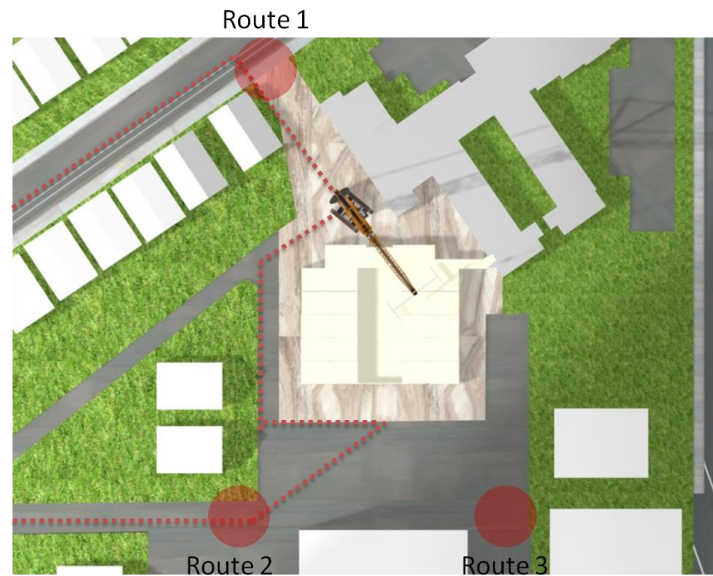


Figure 4.2: Site layout with feasible entrances

According to the proposed methodology, the possible cranes were selected, and three possible paths were identified from the crane operations simulations. Table 4.1 summarizes the three different scenarios with different crane types.

Table 4.1: Scenarios with crane information

	Crane Type	Required Capacity	Working Radius	Clearance errors
Scenario 1	Liebherr LTM 1800 mobile crane	32 Ton	46 m	None
Scenario 2	Liebherr LR 1300 crawler crane	30 Ton	28.3 m	None
Scenario 3	Liebherr LR 1160 crawler crane	28 Ton	19.6 m	None

Scenario 1, described in Figure 4.3, involved a required radius of 39 m with a 32-ton capacity requirement. The Liebherr LIM 1800 all-terrain crane was

selected to satisfy the requirements. This scenario included two possible crane locations, one at the front side of the building, and the other at the back. In order to maximize crane and truck accessibility, the back location was selected, from which the crane could install all modules. Based on this analysis, 3D visualization in 3DS was built and simulated to identify conflicts and clearances between crane configurations and the building, or between crane configurations and modules, during lifting operations. The module installation sequences were also simulated using 3D visualization. There were no conflicts found in the 3D visualization.

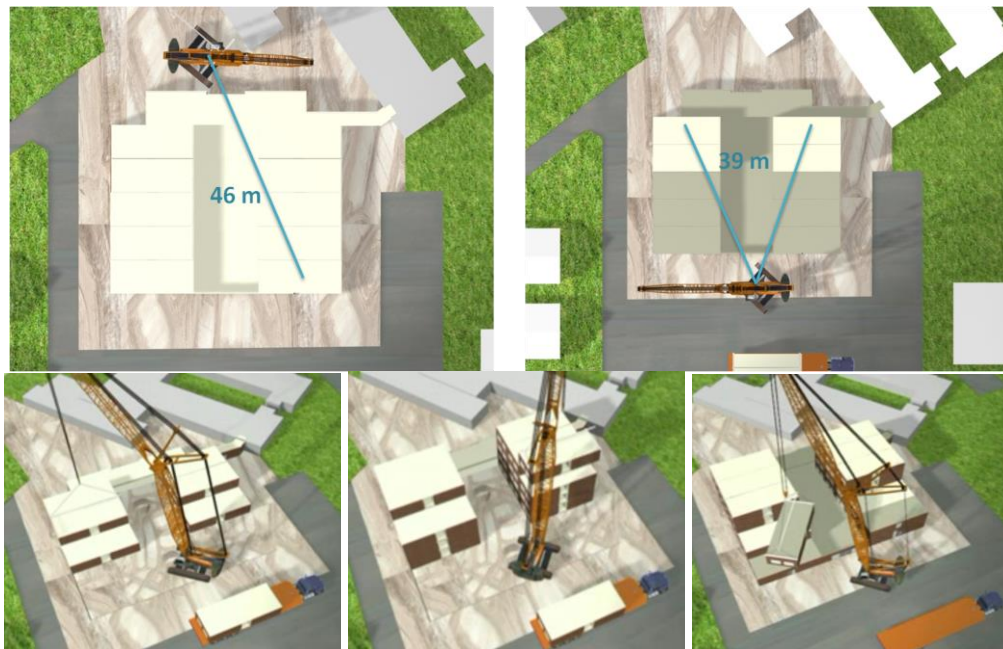


Figure 4.3: Simulation of Liebherr LTM 1800

Scenario 2, illustrated in Figure 4.4, involved a required radius of 28.3 m and a capacity of 30 tons. The Liebherr LR 1300 crawler crane was selected for this scenario. The crane operations for this crane were as follows: (1) install the front two building units from the right side of the building to the left side, (2) move

the crane to the back side of the building, and (3) install the remaining units from the back side of the building. Based on these scenarios, 3D visualization in 3DS was built and simulated to identify clearances and crane operation sequences in order to install the modules. No conflicts, including clearance difficulties, were found in the model by visual observation.

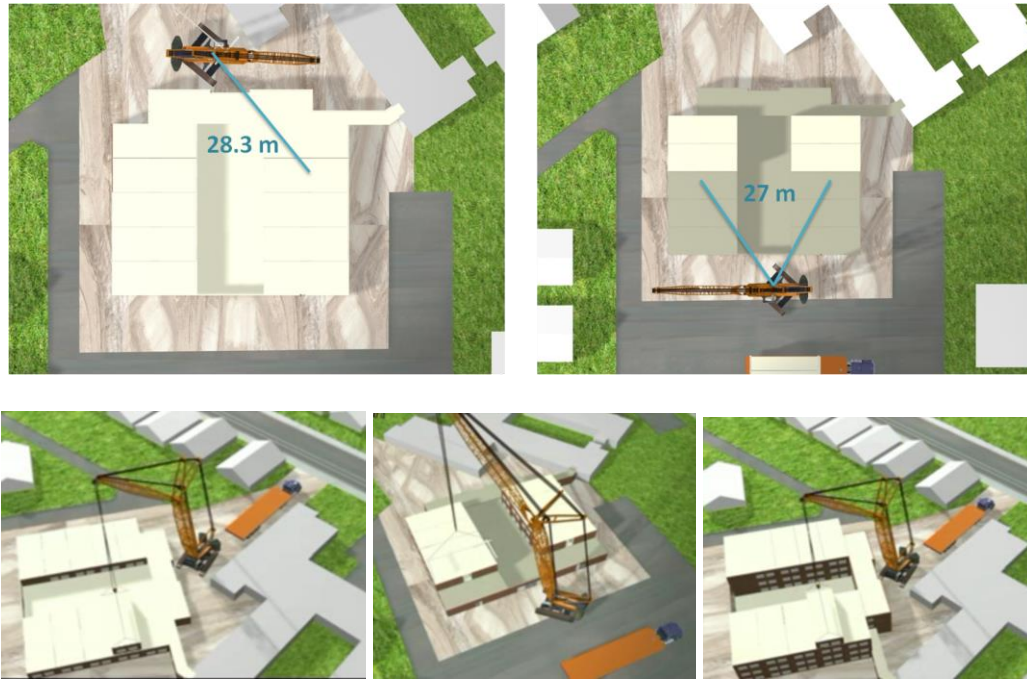


Figure 4.4: Simulation of Liebherr LR 1300

Scenario 3, as shown in Figure 4.5, involved a required radius of 19.6 m and capacity of 28 tons. According to the crane selection calculation, in order to satisfy requirements, the Liebherr LR 1160 crawler crane was selected. The sequence of crane operations for this crane was as follows: (1) lift the module, (2) move the crane to the proper location between two towers of the building, (3) install the module onto the correct location and (4) move the crane back to the lifting location. The core point of the crane operation in this scenario was that the crane was moving forward and backward between two towers of the building

to reach optimal locations for module installation. This operation could result in spatial collisions between crane configurations and the building. Therefore, clearance identification was the most critical analysis. The 3D visualization identified clearances, feasible errors, and module installation sequences before the plans were implemented in practice. No conflicts were found in the model by visual observation..

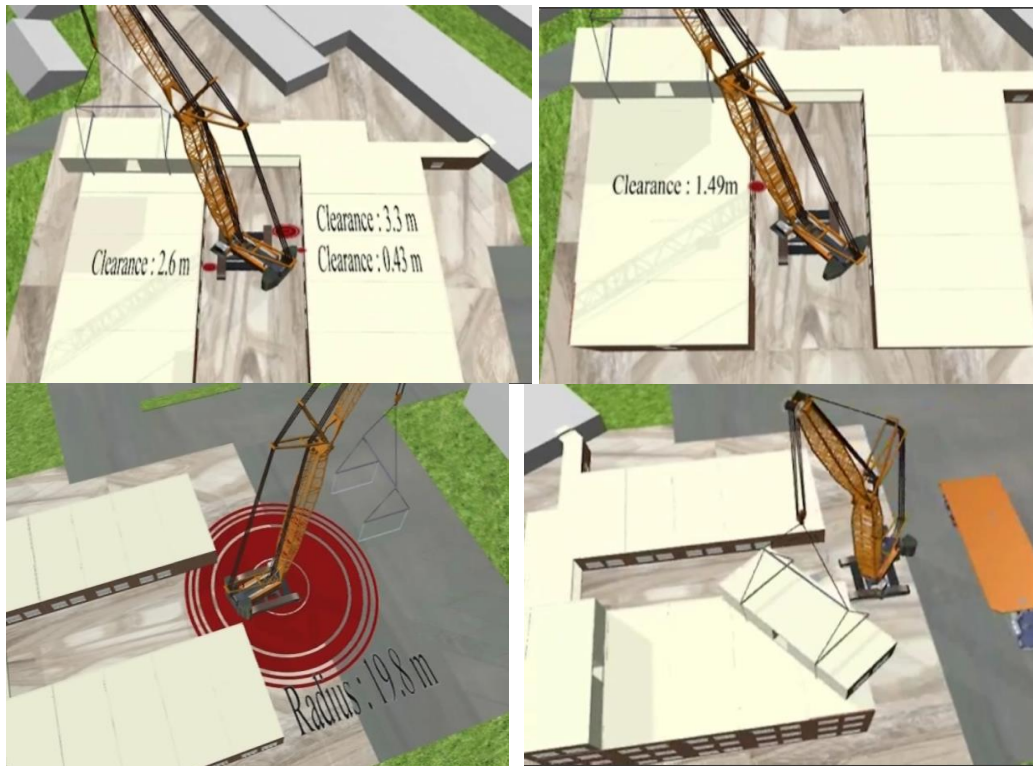


Figure 4.5: Simulation of Liebherr LR1160

Based on these three scenarios, the company selected Scenario 3 due to cost and time savings during crane operations. The crane stability was checked using the developed crane stability analysis system shown in Figure 4.6. According to the visualization of Scenario 3, the reaction influence chart for crane operations was generated as shown in Figure 4.7. Using the influence chart, it was determined

that the 360° swing operation of the Liebherr LR1160 was safe, and that the maximum ground pressure to lift a 25-ton module is 217 kPa when the crane swings 150° from the front (see Figure 4.8).

Figure 4.6: Crane stability analyses

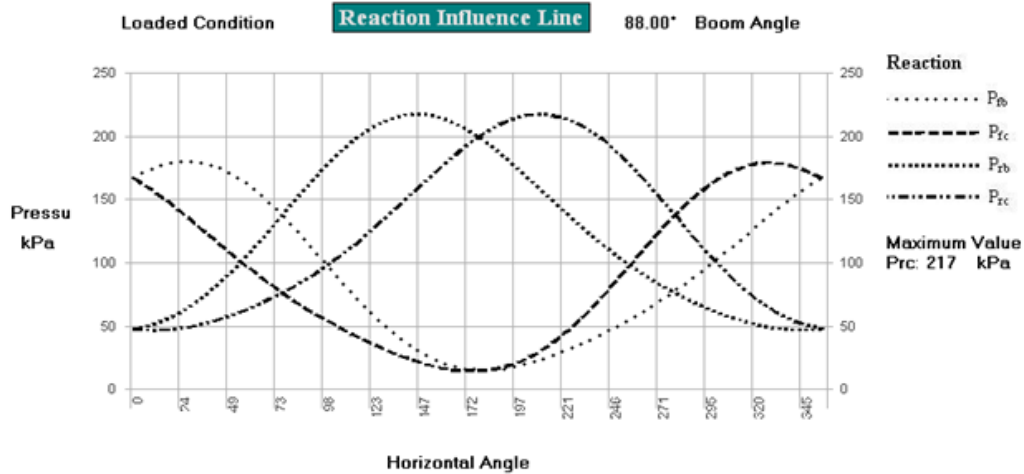


Figure 4.7: Reaction influence chart for Scenario 3

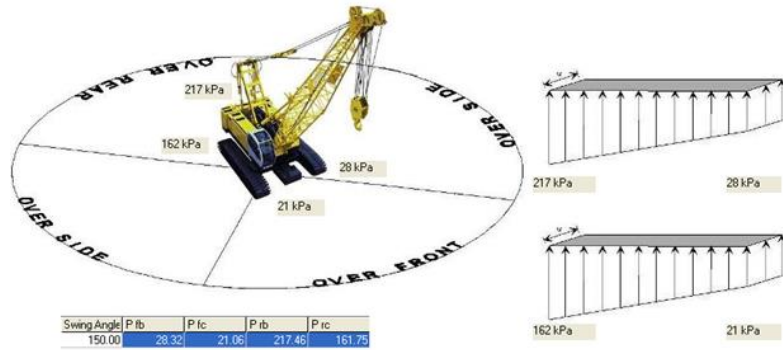


Figure 4.8: Crawler track pressure diagram at 150° swing for Scenario 3

Stability design results are summarized in Figure 4.9.

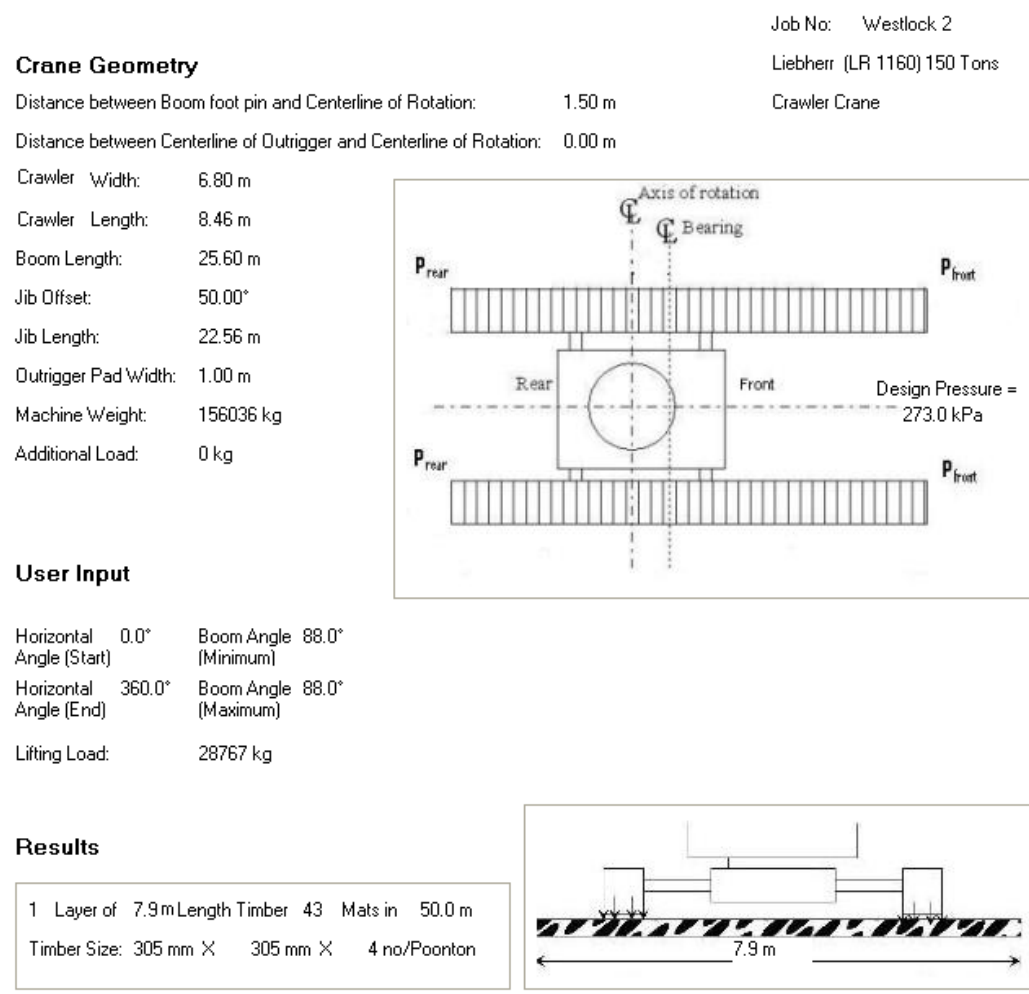


Figure 4.9: Crane support design summary

A lifting operation sequence animation model was created using 3D Studio Max (3DS). The model provided the sequence for module installation, as shown in Figure 4.10. The visualization model checked all the clearances for successful crane operations using Liebherr LR1160. The model also assisted the construction team with proper planning of crane movement, truck arrival, and module installation.



Figure 4.10: Proposed lifting visualization model

All the lifts were critical since the clearances between the crane tail and the proposed building were less than half of a metre, as shown in Figure 4.11. The visualization model was shared with the crane operator and all members of the construction team. With the assistance of the developed visualization model the crane operator was able to perform all critical lifts successfully. Compared to the visualization, the actual lifting operations followed a similar sequence, and similar clearances between the crane and the constructed main floor were encountered (see Figure 4.11). Figure 4.12 illustrates the actual lifting sequences using the Liebherr LR1160 crawler crane. The value of the visualization model was in improving construction (lifting) operation efficiency while maintaining

worker safety. The difference between the visualization and the actual case was the module installation. Unlike in actual construction, 3D visualization did not consider human activities during module installation, which served to speed the module installation process, which was completed in only two working days.

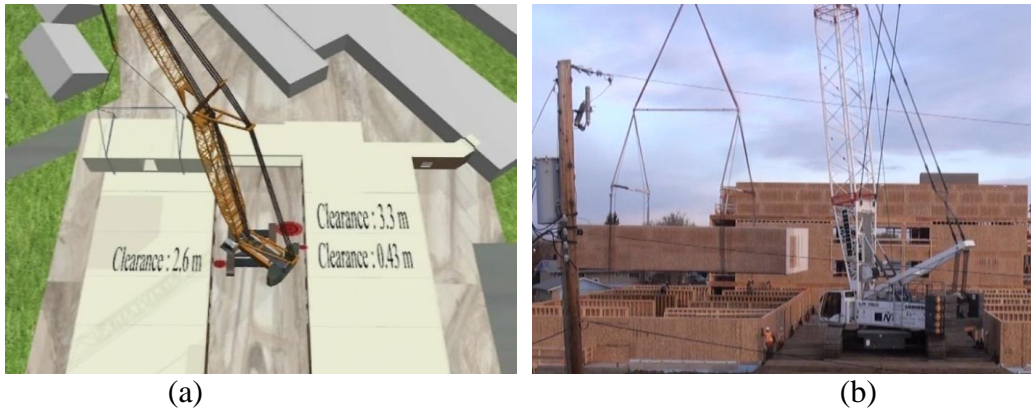


Figure 4.11: Crane clearances: (a) visualization model, (b) construction site



Figure 4.12: Actual lifting sequence photos

4.3 Case 2: 34-Storey Modular Building, Brooklyn, New York

This analysis is based on the installation of 950 structural steel modules for a 34-storey modular building in downtown Brooklyn, New York, USA. Tall modular buildings have been successfully built as high as 24-storeys, but few have been erected in the US, and certainly none at the proposed height of 34 storeys. One of the challenges that has been investigated thus far is the logistics of installing 950 modules and shear wall components, including over 1000 lifts, on one of the busiest street in Brooklyn. The main floor will be constructed on site, and the remaining floors will be lifted into place by a tower crane. The team will be challenged to maintain ambitious minutes-based schedules. The schedule challenges on site include the logistics of sequencing the scaffolding to complete the building from outside while modules are erected and floors are raised. The general contractor decided to use a tower crane, either single- or double-jib, for transporting these modular units from pick location to installation location. The typical modular construction process using a tower crane is shown in Figure 4.13.

The typical floor plan and the optimal position of the crane are shown in Figure 4.14. In order to keep the installation sequence flowing, it will be necessary to have a minimum of two (2) trailers (loaded with ready modules) on site to move the delivered modules to the lifting zone. The following assumptions have been considered in analyzing the project:

- 1) Hoisting and luffing speeds are based on the proposed tower crane features.

- 2) The working day begins at 7:30 a.m. and will finish around 4:30 p.m.
- 3) Critical modules will require 50% additional time for bolting/welding:
 - a. modules next to shear walls;
 - b. modules next to stairs/elevator shafts; and
 - c. final corner modules for every floor.
- 4) Modules will be unhooked at their final location once they are aligned.

Welding/bolting will continue immediately thereafter.



Figure 4.13: 34-storey modular building construction using (a) single-jib tower crane, or (b) double-jib tower crane

Step 1 - Crane Selection: Based on expert analysis, without considering a double-jib crane, the most appropriate crane to be used on site is a 32-ton-capacity tower crane with a 164-ft luffing jib. The operation of the proposed 32-ton-capacity tower crane is shown in Figure 6.15. In this case, management wanted to compare the lifting productivity and the environmental impact of the selected crane with a double-jib crane with the same capacity.

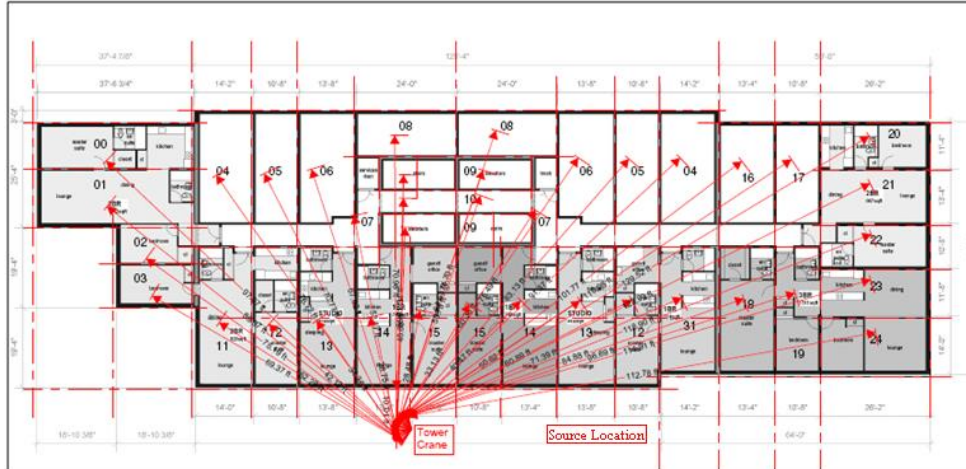


Figure 4.14: Typical floor plan and crane location



Figure 4.15: Luffing-jib crane operation on site

Step 2 – Productivity Analysis: Based on the source location (module pick point), module placement position, and the crane position (Figure 4.14), the angle of each module from the source is calculated. The total rotation of the jib from pick point to placement to pick point is calculated for both types of cranes, as shown in Table 4.2. Assuming the same swing speed for both types of cranes, the total time for the swing of a jib to complete the different module lifting operations is calculated and presented in Table 4.2.

Table 4.2: Total rotation and time for swing to complete various module lifting operations

Module No.	Angle from Source (deg)	Single-Jib Crane		Double-Jib Crane	
		Total Rotation (deg)	Time (min)	Total Rotation (deg)	Time (min)
1	135	270	1.50	180	1.00
2	139	278	1.54	180	1.00
3	140	280	1.56	180	1.00
4	147	294	1.63	180	1.00
5	123	246	1.37	180	1.00
6	142	284	1.58	180	1.00
7	114	228	1.27	180	1.00
8	134	268	1.49	180	1.00
9	105	210	1.17	180	1.00
10	120	240	1.33	180	1.00
11	81	162	0.90	162	0.90
12	79	158	0.88	158	0.88
13	78	156	0.87	156	0.87
14	98	196	1.09	180	1.00
15	77	154	0.86	154	0.86
16	60	120	0.67	120	0.67
17	47	94	0.52	94	0.52
18	57	114	0.63	114	0.63
19	35	70	0.39	70	0.39
20	50	100	0.56	100	0.56
21	29	58	0.32	58	0.32
22	44	88	0.49	88	0.49
23	26	52	0.29	52	0.29
24	38	76	0.42	76	0.42
25	21	42	0.23	42	0.23
26	35	70	0.39	70	0.39
27	19	38	0.21	38	0.21
28	33	66	0.37	66	0.37
29	28	56	0.31	56	0.31
30	23	46	0.26	46	0.26
31	18	36	0.20	36	0.20
32	12	24	0.13	24	0.13
		Total :	25.41		20.89

The total time to place the 32 modules in each floor will be approximately 25.41 minutes for the luffing-jib crane and approximately 20.89 minutes for the

double-jib crane (see Table 4.2). Thus the double-jib crane can complete the swing activity 17.8% faster than the luffing-jib crane.

Optimizing tower crane activities will increase the number of modules installed per day. Other non-lifting activities can be adjusted to accommodate the scheduled crane operations by changing the resources in the simulation model. A visualization model for the activities is created based on scaled activity times. To minimize the duration of the hook-up activity, a platform is constructed up to the module height near the trailer arrival zone. The crew for the hooking process will wait on the platform, and as soon as the trailer arrives, they can start the hook-up activity, as shown in Figure 4.16.



Figure 4.16: Hook-up activity using a platform

The scaffolding operation for this type of modular construction is critical. Visualization of the scaffolding activity identifies any potential conflicts and minimizes the duration. Scaffolding is required in each module for bolting-welding activities. However, each module supplied with the scaffolding set-up will be costly. Thus, it has been decided that each day the first two modules will be supplied with scaffolding setup while, for the rest of the modules, the scaffoldings will be transferred using the tower crane, as shown in Figure 4.17.

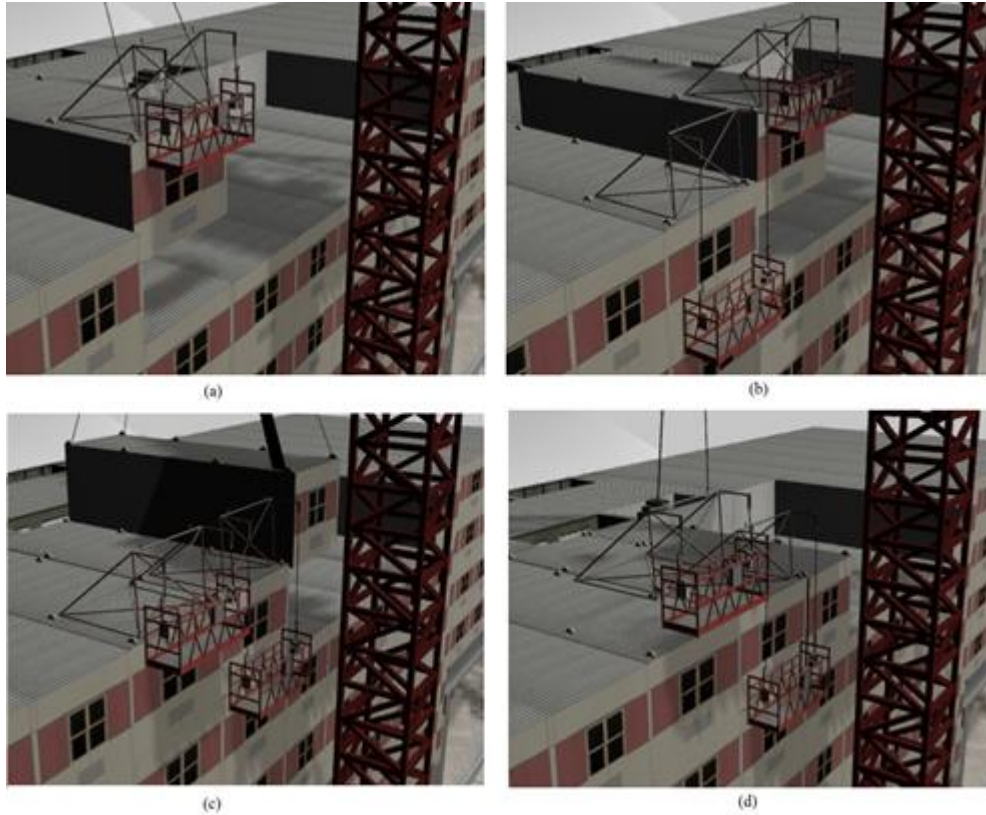


Figure 4.17: Scaffold transfer from one module to another

Step 3 - CO₂ Emissions Analysis: CO₂ emissions per year for the luffing-jib tower crane and a double-jib crane of the same capacity can be calculated using Equations 3.59 to 3.61, as presented earlier in this thesis. Assuming the power consumption and the swing rate for the proposed luffing-jib crane are 20 kW and 0.6 rpm, respectively, and for the double-jib crane with propellers 10 kW and 1 rpm, respectively, the energy consumption and CO₂ emissions per year are calculated as presented in Table 4.3.

Table 4.3: Energy consumption and CO₂ emission comparison of luffing-jib and double-jib crane

Crane Type	Crane Capacity for Swing	Swing Speed	Energy Consumption per year (<i>E</i>)	Emission Factor (<i>EF</i>) in Canada	CO ₂ Emissions per year (<i>C</i>)
Luffing-Jib Crane	20 kW	0.6 rpm	10140 kWh/year	465.88 gm/kWh	4724 kg/year
Double-Jib Crane	10 kW	1.0 rpm	2280 kWh/year	465.88 gm/kWh	1062 kg/year

The results show that a double-jib crane emits 77.5% less CO₂ than the luffing-jib tower crane for the swing operation only.

Step 4 - Simulation:

A simulation model is developed using Simphony.NET3.5 (Hajjar and AbouRizk, 1999), as illustrated in Figure 4.18. In this model, all activity durations are analyzed within a triangular distribution, and 500 minutes of working time per day are considered. In specific, since workers are not required to work overtime, a total of 480 minutes (8 hours) of working time plus an hour lunch break is considered for each crew. The objective of the simulation model is to provide minute-by-minute schedules for crane operations. However, some unpredictable factors such as wind may affect the crane operations and, thereby, scheduling. The effect of wind on crane operations for a particular project, of course, depends on the crane type and project location.

Mobile crane operations are more vulnerable to high wind-related failure than those of tower cranes (Shapira and Lyiachin, 2009). In the case study, both selected cranes are tower cranes, which offer the advantage of usability in higher wind speeds; the effect of wind is thus omitted from this simulation model.

However, wind gusts—instantaneous, powerful wind speeds usually lasting less than 20 seconds (USA National Weather Services, 2011)—can affect tower crane operations. For instances of wind gusts, the project manager or crane operator may need to make the decision to stop crane operations until it is safe to continue.

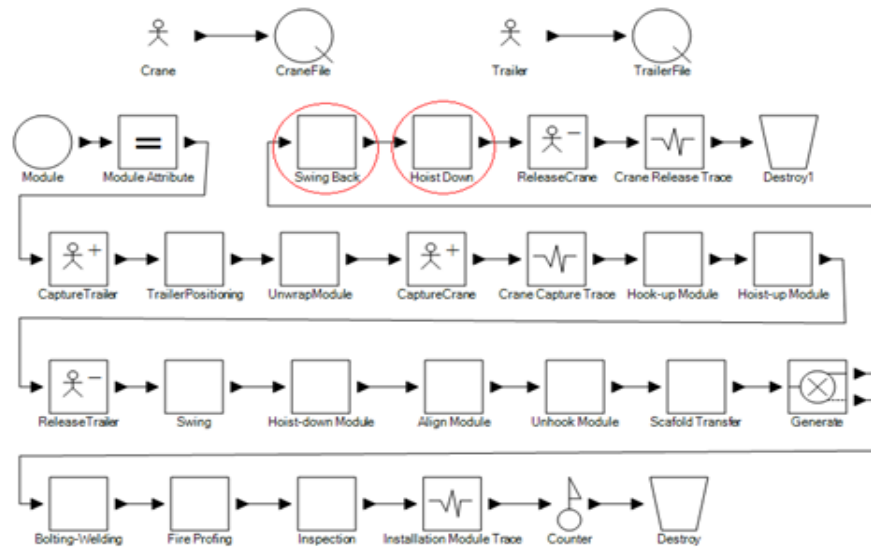


Figure 4.18: Simulation model from Symphony.NET3.5

The proposed schedule is also affected by traffic conditions, which may increase the time required to transport the module unit to the construction site. To keep the installation sequence flowing, a minimum of two trailers (loaded with ready modules) are required on site to move the delivered modules to the lifting zone. Ultimately, the efficiency of most crane activities varies based on the complexity of the work and the crew’s performance and productivity. The swing module activity depends on the radial distance between the pick point of the module and the placing point and the crane’s swinging speed. Similarly, hoist-up and hoist-down activities depend on the hoisting speed of the crane with and without the

load, as well as the floor height. For a 34-storey building, the lifting height varies from 10 m to 110 m. Thus, hoisting the module to the 34th floor (activity # 4) can take up to seven minutes. Given that accuracy is an issue, the probability distribution which describes the ascending hoisting is updated for each floor. Figure 4.19 illustrates different activities, along with the crane operations involved in installing the modules.



Figure 4.19: Different crane work processes

Table 4.4 summarizes the possible durations for different types of activities associated with module installation at Floor 2 using a single-jib crane. One of the main advantages of using a double-jib crane is that the second jib is always ready to take on another load. Thus, use of a double-jib crane reduces the swing-

back time of the jib and hoist-down time to take another load, and this time savings is considered in the simulation model (see Figure 4.18).

Table 4.4: Possible duration for different types of activities using a single-jib crane at Floor 2

Activity	Activity Description	Duration (min)		
		Pessimistic	Most likely	Optimistic
1	Trailer Positioning	2	1	0
2	Unwrap module	10	8	6
3	Hook-up module	5	4	3
4	Hoist up module	1	0.9	0.75
5	Swing module	1	0.75	0.5
6	Hoist down module	1	1	1
7	Align module	12	10	8
8	Unhook module	2	1	1
9	Scaffold transfer	6	5	4
10	Swing back to loading zone	0.75	0.5	0.4
11	Hoist down main line	0.5	0.4	0.3
12	Bolt/Weld module to structure	15	12	10
13	Fireproofing partition walls	15	12	10
14	Inspect installation	6	5	4

Using a single-jib tower crane while satisfying all the required criteria, 20 modules can be installed per day at Floor 2. For Floor 33, using this crane operation sequence, 15 modules can be installed per day. Using a double-jib crane, 22 modules can be installed per day at Floor 2, and 17 modules can be installed per day at Floor 33. Figure 4.20 illustrates the module installation per day on each floor using both crane types.

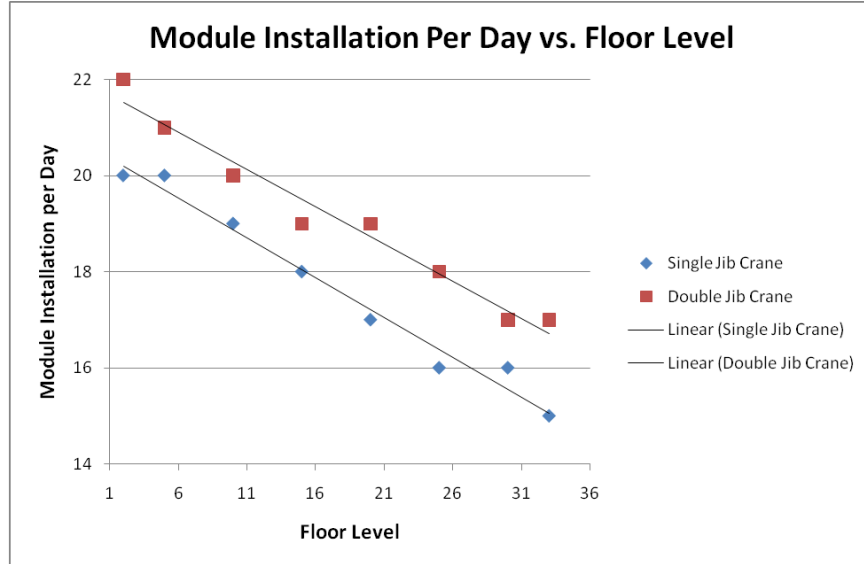


Figure 4.20: Number of module installations per day at each floor level for both tower cranes

Although simulation models are routinely used in a variety of applications in science and engineering, it is instructive to calculate the average time corresponding to the case described in Table 4.5. For such a case, X_i is the random variable representing the time for activity i . As a result, the random variable X gives the total time for the 14 steps, and can be expressed using Equation (4.1).

$$X = \sum_{k=1}^{14} X_k \quad (4.1)$$

Since the random variables occurring on the right-hand side correspond to independent activities, the total average time can be calculated satisfying Equation (4.2).

$$\langle X \rangle = \sum_{k=1}^{14} \langle X_k \rangle \quad (4.2)$$

Now, given that a triangular distribution profile is assumed for each task (Hasan et al. 2011), the total mean time can easily be calculated using Equation (4.3).

$$\langle X \rangle = \sum_{i=1}^{14} \frac{a_i + b_i + c_i}{3} \quad (4.3)$$

Where a_i, b_i and c_i represent the worst-case the most likely, and the best-case times, respectively. Using the above relationship, the expected time to install the first module in a day at the second floor, $\langle X \rangle = 62.58$ minutes, is obtained immediately. As for the remaining modules, the installation time will decrease since some tasks are performed in parallel (see Figure 4.18). In fact, since the installation is crane-controlled, the expected installation time for subsequent modules is calculated using the operation cycle of the crane: swing back, hoist down the main line, hook up, hoist up, swing forward, hoist down, align, unhook, and scaffold transfer. The use of the probability density functions describing such a sequence of activities (see Table 4.4) in connection with Equation (4.3) yields the following mean installation time: $\langle X \rangle = 23.91$ minutes. It is this time that is used to set up a schedule for Module #3 and following. Modules #1 and #2 for the given day come with scaffolding set-up; thus there is no need to transfer scaffolding for these modules, which makes the installation time approximately 20 to 21 minutes for Modules #1 and #2. Of course, simulation times may differ slightly, but the differences should fall within the limits of the chosen confidence interval. Indeed, if the sequence of installation times given in Table 4.4 for the second floor using a single-jib crane is considered, the 95% confidence interval for the mean installation time calculated (using the times corresponding to Module #3 and on) can be written as follows:

$$\bar{x} - t_{\alpha/2, n-1} \frac{s}{\sqrt{n}} \leq \mu_X \leq \bar{x} + t_{\alpha/2, n-1} \frac{s}{\sqrt{n}} \Rightarrow 21.90 \leq \mu_X \leq 24.33$$

After validating the simulation model with the mathematical model, a possible daily crane lifting schedule for different floors is prepared which incorporates both types of cranes. Table 4.5 summarizes the start and finish times of a working day, including the installation completion time of each module at the 2nd and 34th floors for both types of crane.

The analysis shows that the double-jib tower crane operation uses resources more efficiently than a single-jib crane. Table 4.6 summarizes the number of crew members required for each activity, the start time and finish time, and the percentage of working time used by each crew for both types of cranes' operations at Floor 2. The loading zone crew's main responsibility is to un-wrap the module when delivered and assist in hooking up the module in the loading zone (pick point). In the building zone, crews are required to assist in un-hooking, aligning, and positioning the module and managing scaffolding hook-up and un-hooking operations. From Table 4.6 it can be seen that loading zone crews are using only 54% of their working hours. These crews can be used for other activities at the loading zone, if required, without any effect on the module installation schedule. On the other hand, building crews use around 70% of their working hours. Thus, if they were to be required to perform any extra activities, it would be more likely to create a delay in the installation process. Moreover, the focus of the developed simulation and visualization model is to optimize the activities which depend on crane operations and provide time and location

schedules for these activities. For each crew, the job and location will be pre-determined as per the schedule. Crews will not seek out work; instead, the jobs will be assigned.

Table 4.5: Typical module installation schedule on a given day at 2nd and 34th floors using single- or double-jib crane

Single-Jib Crane				Double-Jib Crane			
2 nd Floor		34 th Floor		2 nd Floor		34 th Floor	
Module	Time Installed	Module	Time Installed	Module	Time Installed	Module	Time Installed
(Start at 7:40:00 AM)							
1 st	8:40:00 AM	1 st	8:45:00 AM	1 st	8:35:00 AM	1 st	8:40:00 AM
2 nd	9:00:00 AM	2 nd	9:16:00 AM	2 nd	8:54:00 AM	2 nd	9:05:00 AM
3 rd	9:23:00 AM	3 rd	9:47:00 AM	3 rd	9:15:00 AM	3 rd	9:33:00 AM
4 th	9:46:00 AM	4 th	10:18:00 AM	4 th	9:36:00 AM	4 th	10:01:00 AM
5 th	10:09:00 AM	5 th	10:49:00 AM	5 th	9:57:00 AM	5 th	10:29:00 AM
6 th	10:32:00 AM	6 th	11:20:00 AM	6 th	10:18:00 AM	6 th	10:57:00 AM
7 th	10:55:00 AM	7 th	11:51:00 AM	7 th	10:39:00 AM	7 th	11:25:00 AM
8 th	11:18:00 AM	-	Lunch Break	8 th	11:00:00 AM	8 th	12:53:00 AM
9 th	11:41:00 AM	8 th	1:22:00 PM	9 th	11:21:00 AM	-	Lunch Break
10 th	12:05:00 PM	9 th	1:53:00 PM	10 th	11:42:00 AM	9 th	1:21:00 PM
-	Lunch Break	10 th	2:24:00 PM	11 th	12:03:00 PM	10 th	1:49:00 PM
11 th	1:28:00 PM	11 th	2:55:00 PM	-	Lunch Break	11 th	2:17:00 PM
12 th	1:51:00 PM	12 th	3:26:00 PM	12 th	1:24:00 PM	12 th	2:45:00 PM
13 th	2:14:00 PM	13 th	3:57:00 PM	13 th	1:45:00 PM	13 th	3:13:00 PM
14 th	2:37:00 PM	14 th	4:28:00 PM	14 th	2:06:00 PM	14 th	3:31:00 PM
15 th	3:00:00 PM	15 th	4:59:00 PM	15 th	2:27:00 PM	15 th	3:59:00 PM
16 th	3:23:00 PM			16 th	2:48:00 PM	16 th	4:27:00 PM
17 th	3:46:00 PM			17 th	3:09:00 PM	17 th	4:55:00 PM
18 th	4:09:00 PM			18 th	3:30:00 PM		
19 th	4:32:00 PM			19 th	3:51:00 PM		
20 th	4:55:00 PM			20 th	4:12:00 PM		
				21 st	4:33:00 PM		
				22 nd	4:55:00 PM		

Table 4.6: Utilization of different type of resources at Floor 2

Crew Type	No.	Start	Finish	Available Time (min)	Active (min)	Idle (min)	% of Utilization
Single-Jib Crane							
Loading Zone	4	7:40:00 AM	4:40:00 PM	480	260	220	54%
Crane Operator	1	7:45:00 AM	4:45:00 PM	480	457	23	95%
On Building	6	7:50:00 AM	4:50:00 PM	480	320	160	67%
Bolt and Welding	4	7:55:00 AM	4:55:00 PM	480	300	180	63%
Fireproofing and Inspection	4	8:00:00 AM	5:00:00 PM	480	400	80	83%
Double-Jib Crane							
Loading Zone	4	7:40:00 AM	4:40:00 PM	480	286	194	60%
Crane Operator	1	7:45:00 AM	4:45:00 PM	480	472	8	98%
On Building	6	7:50:00 AM	4:50:00 PM	480	352	128	73%
Bolt and Welding	4	7:55:00 AM	4:55:00 PM	480	330	150	69%
Fireproofing and Inspection	4	8:00:00 AM	5:00:00 PM	480	440	40	92%

From the above four steps it can be seen that the selected double-jib crane is more feasible, productive, and environmental-friendly crane than the selected luffing-jib crane. However, installation of the double-jib crane on a downtown street of a busy city creates major challenges and increases the cost of installation. Thus, it is recommended that the project manager perform a cost-benefit analysis before finalizing the crane selection. Again, the final selection of the crane also depends upon the management policy, crane ownership, and availability of technical support.

4.4 Case 3: Industrial Project, Saskatoon, SK

The proposed crane selection methodology has been tested in an industrial project in Saskatoon, Canada where three different industrial buildings need to be constructed. The heaviest load, an Electrical Switch-room Module, weighs 102 tons. The project duration is approximately one year. The project team needs to select the most efficient crane for Building #1 (see Figure 4.21) that satisfies the lift requirements of configuration flexibility and mobility.

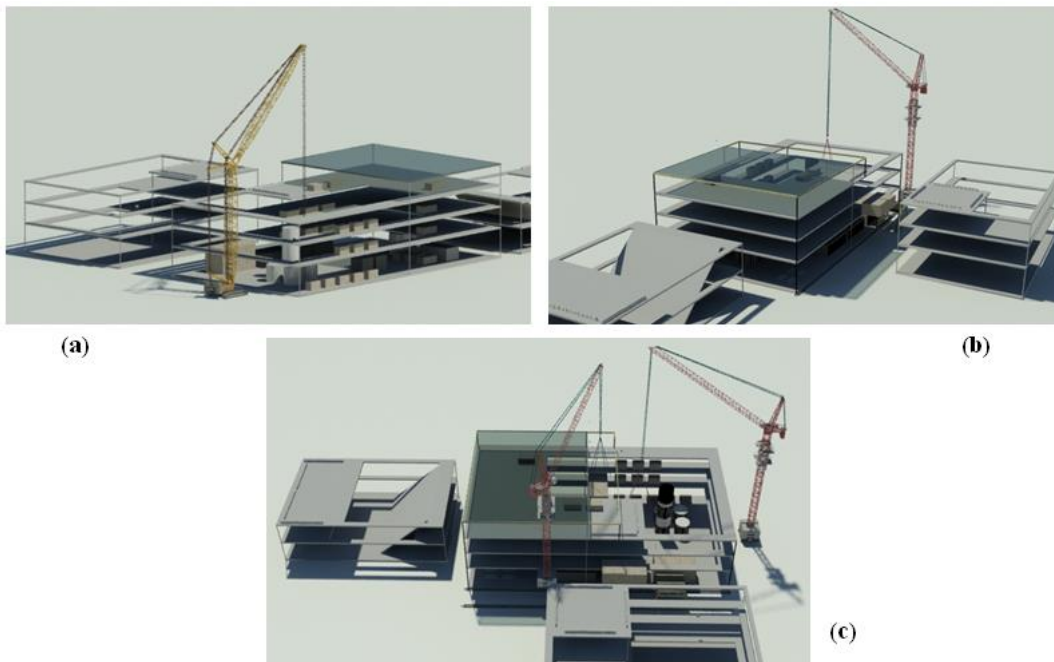


Figure 4.21: Three different simulation options: (a) one 440-ton crawler crane, (b) one 128-ton tower crane on rail, and (c) two 128-ton tower cranes

Step 1 - Crane Selection: Using the crane selection automated system as described in Section 3.2.2, three cranes were selected: a 440-ton capacity crawler crane with a maximum reach of 142 m, a 300-ton capacity crawler crane with a

maximum reach of 100 m, and a 128-ton capacity tower crane with a maximum reach of 78 m.

Step 2 - Simulation: It is assumed that the building erection sequence allows the crane to access lifting equipment and maintain proper boom clearances. The mobile crane must maintain a distance of 6 m between the west edge of the building and the crane's center of rotation. The 440-ton-capacity crawler crane can lift all the loads while satisfying all the constraints described in Stage 2 of the proposed methodology. However, the 300-ton-capacity crawler crane fails to lift some of the critical loads. The crane capacity at the radius and boom angle required to lift the critical load, with a 15% reduction for safety, is less than the total weight with the attachment (approximately 20 tons), and therefore this particular crane was removed from further analysis. The 128-ton-capacity tower crane can lift all the loads when it is on the rail, which is located within 6 m of the building edge. Two 128-ton-capacity tower cranes are required to complete the same operation from fixed crane positions. The simulation results thus provide three options: (1) a 440-ton-capacity crawler crane on a mat (see Figure 4.21a); (2) a 128-ton-capacity tower crane on a rail (see Figure 4.21b); and (3) two 128-ton-capacity tower cranes at fixed locations (see Figure 4.21c).

Step 3 - Wind Effect Analysis: As outlined in the methodology section, the daily wind speed data for the case study location, Saskatoon, has been collected (Tutiempo, 2011). The cumulative frequency of the collected data was then plotted (Figure 3.57). The figure shows the daily average, maximum sustained, and wind gust speeds recorded in Saskatoon in 2010. The maximum allowable

wind speed limits for the selected cranes are superimposed in the plot. The effect of wind on the crane operations have been summarized in Table 3.5.

Step 4: CO₂ Emission Analysis

Cranes consume a significant amount of fuel and power, which transform into CO₂ emissions. Crane selection has great potential to provide environmental benefits without sacrificing productivity. For this study, emission factors (EFs) were generated from the NONROAD2005 model for the 2006 calendar year (EPA, 2006). In order to identify a technique to reduce mobile crane CO₂ emissions, fuel consumption rates for different periods are required. It is assumed that the crane operates 10 hours per day, including 1 hour for start-up, 5 hours operating at full throttle, and 4 hours idling. The selected 440-ton crawler crane has a diesel OM 501 LA engine which uses 260 kW of power and idles at 560 rpm (Argonne National Laboratory, 2010). Table 4.7 summarizes the CO₂ emissions for the crawler crane at full throttle and while idling.

Table 4.7: CO₂ emission calculation for a 440-ton crawler crane at full throttle and while idling

Type of mobile crane	n _c	Power kW	LF Hrs/day	A Das/yr	EF	CCE tons/yr
440-ton crawler crane	1	full throttle	5	260	721.4 g/kW-hr	268.7
		Start & idle	5	260	5344.52 g/h	7.66

The selected 128-ton tower crane is one of the largest luffing jib cranes available. It is assumed that during the 5 hours at full throttle, 25% of the time is spent swinging and 75% hoisting. The energy needed for full throttle for the

tower crane is 587.5 kWh. During the 5 hours comprising start-up and idle time, the energy needed for air conditioning, heating, and lighting is 25 kWh. Thus, the cross-Canada greenhouse gas (GHG) emission factor, 465.88g/kWh, multiplied by the total kWh is the total CO₂ emissions for each tower crane's cycle. Table 4.9 summarizes the CO₂ emission for the selected tower crane at full throttle and idling state.

With two tower cranes operating in tandem, each crane's full throttle time is lowered by 50% and the idle time increased by around 50%. Table 4.8 summarizes the CO₂ emissions for the selected tower cranes at full throttle and idling, assuming that during the 2.5-hour full throttle time, 25% is spent swinging and 75% hoisting. The energy needed for full throttle for the tower crane is 293.75 kWh. During the 7.5-hour idle time, the energy required for air conditioning, heating, and lighting is 37.5 kWh.

Table 4.8: Calculation for tower crane's CO₂ emissions

Type of tower crane	n_c		Power \times LF (kW- hrs/day)	A (Das/yr)	EF (g/kW- hr)	CCE (tons/yr)
128 ton Tower Crane	1	Full throttle	587.5	260	465.88	78.42
		Idle	20	260	465.88	2.67
128 ton Tower Crane	2	Full throttle	293.75	260	465.88	78.42
		Idle	37.5	260	465.88	10.01

Step 5 - Cost Analysis: Based on consultations with various construction companies and lift engineers, crane cost scores were estimated for each sub-category and the impact scores of the cost sub-categories on the overall lifting cost were identified (see Figure 3.58). The overall cost utility score of these three

options is calculated satisfying Equations (3.69) and (3.70), as presented in Figure 3.56.

The best option considering cost can be calculated satisfying Equation (3.71). The selected crawler crane option is expected to be more cost-effective than the other two options. The two 128-ton tower cranes option has a low score, meaning it is an expensive option; however, having two cranes instead of one will increase the productivity of construction, which can reduce the overall cost of the project.

Step 6 – Results Comparison: Table 4.9 summarizes the wind, CO₂, and cost analyses for the three feasible options provided in Step 2. The mobile crane operations are to be shut down for around 3% of the total project duration (in days) based on maximum sustained wind speed, and more than 30% when taking into account maximum wind gusts. Wind gusts can affect a few hours of operation during a working day. Thus, both sustained high wind speeds and wind gusts will extend by at least 15% the project duration (in days) of crawler crane operations, whereas the tower crane can operate safely under both of these wind conditions. Furthermore, the selected tower crane emits less CO₂ than the selected mobile crane. The cost is represented by calculating a unit-less measure called “cost utility score” using Equations (3.69) to (3.71). Using Equation (3.74), the Euclidean distances for all the options can be calculated and the most appropriate crane identified. Using this approach, Option 2—one-128-ton tower crane on rail—was identified. However, the final selection of the crane depends

on management’s policies, crane ownership, and availability of technical support.

Table 4.9: Summary of different analyses

Simulation Options	Wind Operational per Year	CO ₂ Emission (tons/yr)	Cost Score	Euclidean distance
Option 1 (440-ton crawler crane)	85%	276.36	16.0	0.72
Option 2 (128-ton tower crane on rail)	100%	81.09	15.5	0.03
Option 3 (Two 128-ton tower cranes)	100%	88.43	6.0	0.63

Chapter 5: Conclusions

5.1 Research Summary

This research has been motivated by the large number of cranes used in the construction industry and the consequent need to improve crane operations. This thesis has described a crane selection methodology which considers some important factors including stability and wind effect. The primary focus of the crane selection methodology has been to select the most feasible crane in terms of performance, environmental footprint, and cost. This thesis has aimed to develop an algorithm to assist practitioners in planning detailed schedules for crane operations integrated with visualization. This thesis has presented a new approach to integrate crane support reactions, along with wind speed and direction, into building information modeling (BIM). Integrating crane stability analysis with BIM will bring a new dimension to BIM thinking. Including wind speed and direction and support reaction information in the visualization model will assist lift engineers to schedule crane operations more efficiently. The proposed methodology identifies instances of instability, which will assist in preventing crane accidents caused by poor design practices.

To these ends, the proposed methodology described in this research can assist with the proper planning of operations for both mobile cranes and tower cranes, as well as in utilizing resources efficiently. The developed methodology has been incorporated into the “D-Crane” and “Crane 2007” databases, which are

designed to house information about construction cranes, including the geometrics, weight, and lifting capacity of commercially-available cranes. The stability analysis and vessel lift optimization system were developed using Microsoft Visual Basic™ in order to control the data-integrity as well as to provide a user-friendly interface.

5.2 Research Contributions

The current practice in crane operations is inconsistent, costly, and time-consuming. Researching more effective ways to perform crane selection and design will establish best practices within the construction industry. Automating and optimizing heavy lift crane configurations can enhance the planning process and cost efficiency. The methodology presented in this thesis can potentially benefit many aspects of current construction practice. A partial list of the contributions of this research is summarized below:

- *Mobile Crane Support Reaction:* In current practice, design of the mobile crane support system has been carried out manually based on a number of rules of thumb without calculating the proper reaction of the outrigger or crawler track. This research has described the development of an automated system for the analysis of crane support reaction. The developed automated system provides its users with additional graphics in the form of 2D reaction influence charts supporting the visualization of the forces being exerted upon the outriggers or crawler tracks for the planned lift.

- *Tower Crane Location Optimization:* Several researchers have developed approaches to assist practitioners in optimizing site layout. In these approaches some constraints such as safety, time and costs are taken into account to determine the best possible crane locations. However, none of the approaches considered the effect of crane support reactions due to the reach from crane base to pick points or set points and weight of the lifted load. Thus, using these developed approaches to select the best possible crane and location cannot necessarily result in an optimum crane selection. This research presents a methodology to optimize crane and source locations through evaluating moments created on the crane base. The key contribution of the proposed methodology is that it optimizes the load moments for all lifted loads which can assist in selecting the best possible crane and thus results in optimum crane location.
- *Crane Swing Information:* The proposed methodology produces a reaction influence chart which shows the relationship between a crane support reactions and the crane swing angles and vertical boom angles to the ground. The reaction influence chart provides 2D visualizations which can help contractors or crane operators to control the direction of crane swing and changing boom positions for a particular crane operation. These visualizations are much more understandable than the crane load charts provided by manufacturers.
- *Wind Effect Information:* Traditionally, mobile cranes have been used for heavy industrial construction projects; however, to prevent safety

hazards, mobile crane operation is stopped during high-wind conditions, affecting the schedule and budget. Alternatively, tower cranes can withstand higher wind speeds, and thus are less prone to schedule delays and budget increases during these conditions. Considering both crane types (mobile and tower), this thesis presents a methodology for selecting cranes on industrial construction sites based on lifting configuration, operating efficiency considering wind effects on the selection process. The proposed methodology evaluates the wind's effect on the crane operation by calculating the support reaction and provides the information about possible stoppage of the selected crane operations due to strong wind.

- *Carbon Emission of Crane Operations*: This thesis presents a methodology to quantify and assess the environmental footprint (CO₂ emissions) associated with the crane operations. Analyzing the CO₂ emissions of crane operations can assist practitioners to select environmental-friendly cranes, thereby reducing unnecessary CO₂ emissions and energy consumption.
- *Cost Effective Crane Selection*: The proposed crane cost scoring method can assist lift engineers to identify the economical cranes for the duration of the project. Again, currently cranes on construction sites are relocated many times in order to accommodate the delivery schedule and the delays in the arrival of modules on site. These relocations contribute to project delays and cost over-runs. Through simulation, optimized heavy-

lift crane configurations can enhance the planning process and cost efficiency.

- *Worker safety*: An additional benefit of crane operations improvement is its focus on worker safety. Proper planning of crane operations and provision of the outputted information to all personnel involved in the project can eliminate the potential hazards of crane utilization. The visualization model of the lifting process can be shared with the crane operator, the lifting crews, and engineers, which will assist in addressing any potential conflicts between objects and the cranes, thus creating safer worksites.
- *Better practices within the industry*: The current practice in crane operations is inconsistent, costly, and time-consuming. Researching more effective ways to select and plan crane operations can serve to establish best practices within the construction industry. This research offers an approach by which to standardize operations for large projects involving multiple heavy lifts, such as modular construction or Oil-Sands projects.

5.3 Research Assumptions and Limitations

The methodology described in this research retrieves the crane's geometric information from either the "D-Crane" database or the "Crane 2007" database, depending upon the user's requirements. If any required data is missing in either of these databases, the user must provide the correct values for each of the missing data. One of the limitations of this research is that it requires some geometric information, such as the center of gravity for each crane component,

which is not ordinarily given in the literature from the manufacturer. However, if manufacturers recognize that there are increasing demands for these data, they may begin to include them in their crane manuals in the future.

The calculations of forces carried out in this methodology are all based on static analysis and equilibrium; the dynamic effect due to movement during the lifting process has not been taken into consideration. The calculations of angles have assumed constant lengths for all members. This research also assumes that the ground area of a construction site is flat and can safely support cranes. The methodology assumes a sufficient soil-bearing capacity of the ground area where the crane will operate based on the geotechnical soil report. Another limitation of this research is that the methodology to calculate support reactions for the wind speed is approximate and static.

5.4 Recommendations for Future Work

While this proposed research has explored the prospect of improving crane operations through an integrated model of selection, optimization, and automation, there are some areas that may require further research. These include:

- Development of a methodology for dynamics analysis of crane stability and comparison with static analysis;
- Optimization of the crane path for mobile crane operations;
- Development of an information model for crane operations using IFC (Industry Foundation Classes) to integrate all the developed systems

described in this thesis (i.e., crane selection system, vessel lift optimization system, crane support reaction system, wind analysis spreadsheet, 3D model) to one single system;

- Development of innovative device design systems for construction heavy lift operations and integrate with the developed crane selection automation system.

REFERENCES

- Abudayyeh, O. and Al-Battaineh, H. T. (2003). "As-Built Information Model for Bridge Maintenance." *Journal of Computing in Civil Engineering*, ASCE, 17(2), 105-112.
- Akinci, B., Tantisevi, K., and Ergen, E. (2003). "Assessment of the capabilities of a commercial 4D CAD system to visualize equipment space requirements on construction sites." *Proceedings, Construction Research Congress: Winds of Changes: Integration and Innovation in Construction*, ASCE, Honolulu, HI, Mar. 19-21, 1-7.
- AlBahnassi, H. and Hammad, A. (2012). "Near real-time motion planning and simulation of cranes in construction: Framework and system architecture." *Journal of Computing in Civil Engineering*, 26(1), 54-63.
- Al-Hussein, M., Niaz, M. A., Yu, H. T., and Kim, H. (2006). "Integrating 3D visualization and simulation for tower crane operations on construction sites." *Automation in Construction*, 15(5), 554-562.
- Al-Hussein, M., Alkass, S., and Moselhi, O. (2005). "Optimization algorithm for selection and on-site location of mobile cranes." *Journal of Construction Engineering and Management*, ASCE, 131(5), 579-590.
- Al-Hussein M., Alkass S., and Moselhi O. (2001). "An algorithm for mobile crane selection and location on construction sites." *Construction Innovation Journal*, 1(2), 92-105.

- Al-Hussein, M., Alkass, S., and Moselhi, O. (2000). "D-CRANE: Database system for utilization of cranes." *Canadian Journal of Civil Engineering*, 27, 1130-1138.
- Ali, M. S. A. D., Babu, N. R., and Varghese, K. (2005). "Collision free path planning of cooperative crane manipulators using genetic algorithm." *Journal of Computing in Civil Engineering*, ASCE, 19(2), 182-193.
- Alkass, S, Alhussein, M and Moselhi, O (1997). "Computerized crane selection for construction projects." *13th Annual ARCOM Conference*, 15-17 September 1997, King's College, Cambridge. Association of Researchers in Construction Management, Vol. 2, 427-36.
- Appleton, B. J. A., Patra, J., Mohamed, Y., and AbouRizk, S. (2002). "Special purpose simulation modeling of tower cranes." *Proceedings, Winter Simulation Conference*, San Diego, CA, Dec. 8-11.
- Argonne National Laboratory (2010). "How much could you save by idling less?" <<http://www.transportation.anl.gov/pdfs/TA/361.pdf>> (June, 2013)
- Beavers, J. E., Moore, J. R., Rinehart, R., and Schriver, W. R. (2006). "Crane-related fatalities in the construction industry." *Journal of Construction Engineering and Management*, ASCE, 132(9), 901-910.
- Behm, M. (2005). "Linking construction fatalities to the design for construction safety concept." *Safety Science*, vol 43, issue 8, pp 589-611.
- Bernold, L. E., Lorenc, S. J., and Luces, E. (1997). "Intelligent technology for truck crane accident prevention." *Journal of Construction Engineering and Management*, ASCE, 123(3), 276-284.

- Brookhaven National Laboratory. "Weather Factors."
 <<https://sbms.bnl.gov/sbmsearch/subjarea/129/3b05e011.pdf>> (Apr., 2011).
- Bynum, P., Issa, R. R. A., and Olbina, S. (2012). "Building Information Modeling in Support of Sustainable Design and construction." *Journal of Construction Engineering and Management*, ASCE, in press.
- Construction Plane-hire Association (2009). "The effect of wind on mobile crane in-service." <www.ritchiestraining.co.uk/downloads.asp?fileID=27> (Apr., 2011).
- Chang, Y., Hung, W., and Kang, S. (2012). "A fast path planning method for single and dual crane erections." *Automation in Construction*, 22, 468-480.
- Chen P. H., Wana C., Tionga R. L. K., Tinga S. K. and Yang Q. (2004). "Augmented IDEF1-based process-oriented information modeling." *Automation in Construction* 13(6), 735-750.
- Chin, C., Nayfeh, A. H., and Abdel-Rahman, E. (2001). "Nonlinear dynamics of a boom crane." *Journal of Vibration and Control*, 7(2), 199-220.
- Chung, Y. K. (1999). "A neuro-based expert system for facility layout construction." *Journal of Intelligent Manufacturing*, 10(5), 359-385.
- Dalalah, D., Al-Oqla, F., and Hayajneh, M. (2010). "Application of the Analytic Hierarchy Process (AHP) in multi-criteria analysis of the selection of cranes." *Jordan Journal of Mechanical and Industrial Engineering*, 4(5), 567-578.

- Danish Wind Industry Association (2011). Wind Speed Variability, Diurnal Variation of Wind. <<http://guidedtour.windpower.org/en/tour/wres/variab.htm>>. Accessed: April, 2011.
- Eastman, C., Teicholz, P., Rafael, S., and Liston, K. (2011). *A Guide to Building Information Modeling for Owners, Managers, Designers, Engineers, and Contractors, Second Edition*. John Wiley & Sons, Inc., Hoboken, NJ.
- Eastman, C., Teicholz, P., Sacks, R., and Liston, K. (2008). “BIM Handbook: A Guide to Building Information Modeling for Owner, Managers, Designers, Engineers, and Contractors.” 1st Ed., Wiley, NY, U.S.A.
- Edwin T. D. (2010). “Interoperability and the Structural Domain” *Structures Congress*, ASCE, 1652-1659
- Environment Canada (2010). “A climate change plan for the purposes of the Kyoto Protocol implementation Act.”
<http://www.climatechange.gc.ca/Content/4/0/4/4044AEA7-3ED0-4897-A73E-D11C62D954FD/KPIA_2010.pdf>
- Environment Canada (2011). “National climate data and information archive.”
<http://climate.weatheroffice.gc.ca/climateData/hourlydata_e.html?timeframe=1&Prov=SASK&StationID=3328&hlyRange=1953-01-01|2011-11-04&Year=2011&Month=11&Day=4> (Nov., 2011).
- Environmental Protection Agency (EPA) (2006). “Calculation sheet-combustible emission-planned action Hidalgo County.”
<http://www.cbp.gov/linkhandler/cgov/border_security/otia/sbi_news/sbi_enviro_docs/nepa/dsea/download_proposed_fonsi/fonsi_appendices/app_b_c.ctt/app_b_c.pdf>

- EPA (2005). "Emission facts: Average carbon dioxide emissions resulting from gasoline and diesel fuel."
<<http://www.epa.gov/OTAQ/climate/420f05001.htm>>
- EPA (2004). "Final regulatory analysis: Control of emissions from nonroad diesel engines." EPA420-R-04-007, Assessment and Standards Division, Office of Transportation and Air Quality, Washington, DC.
- EPA (2000). "Carbon dioxide emissions from the generation of electric power in the United States."
<<http://tonto.eia.doe.gov/ftproot/environment/co2emiss00.pdf>>
- Furusaka, S. and Gray, C. (1984). "A model for the selection of the optimum crane for construction sites." *Journal of Construction Engineering and Economics*, 2(2), 121-144.
- Goedert, J. D. and Meadati, P. (2008). "Integrating Construction Process Documentation into Building Information Modeling." *Journal of Construction Engineering and Management*, ASCE, 134(7), 509-516.
- Gökçe K. U., Gökçe H. U., Katranuschkov P., (2012). "IFC-Based Product Catalogue Formalization for Software interoperability in the Construction Management Domain." *Journal of Computing in Civil Engineering*, ASCE, in press.
- Gray, C. and Little, J. (1985). "A systematic approach to the selection of an appropriate crane for a construction site." *Construction Management and Economics*, 3(2), 121-144.

- Hajjar, D. and AbouRizk, S.M. (1999). "Symphony: An environment for building special purpose construction simulation tools." *Proceedings, Winter Simulation Conference*, Phoenix, AZ, Dec. 5-8, 998-1006.
- Halfawy M. and Froese T. (2005). "Building Integrated Architecture/Engineering/Construction System Using Smart Objects: 'Methodology and Implementation'." *Journal of Computing in Civil and Engineering*, 19(2), 172-181.
- Hanna, A. S. and Lotfallah, W. B. (1999). "A fuzzy logic approach to the selection of cranes." *Automation in Construction*, 8(5), 597-608.
- Han, S. H., Al-Hussein M., Al-Jibouri S., and Yu, H. (2011). "Automated post-simulation visualization of modular building production assembly line." *Automation in Construction*, 21, 229-236.
- Han, S., Hasan., S., Al-Hussein, M., Gökçe, K. U., and Bouferguène, A. (2012). "Simulation of mobile crane operations in 3D Space." *Proceedings, Winter Simulation Conference*, Berlin, Germany, Dec. 9-12.
- Hasan, S., Bouferguène, A., Al-Hussein, M., Gillis, P., and Telyas, A. (2013). "Productivity and CO₂ emissions analysis for tower crane utilization on high rise building projects." *Automation in Construction*, 31, 255-264.
- Hasan, S., Zaman, H., Han, S., Al-Hussein, M., and Su, Y. (2012a). "Integrated Building Information Model to identify possible crane instability caused by strong winds." *Proceedings, Construction Research Congress*, ASCE, West Lafayette, IN, May 21-23.

- Hasan, S., Lei, Z., Bouferguène, A., Li, H. X., and Al-Hussein, M. (2012b). “An algorithm for optimizing tower crane location and operations.” Submitted for publication in the *Journal of Construction Engineering and Management*, ASCE in September, 2012.
- Hasan, S., Al-Hussein, M., Bouferguène, A., Gillis, P., and Telyas, A. (2011). “Hook time simulation and visualization of tower crane operations.” *Proceedings, International Conference on Construction Applications of Virtual Reality*, Weimar, Germany, Nov. 3-4.
- Hasan, S., Al-Hussein, M., Hermann, U. H., and Safouhi, H. (2010a). “Interactive and dynamic integrated module for mobile cranes supporting system design.” *Journal of Construction Engineering and Management*, ASCE, 136(2), 179-186.
- Hasan, S., Al-Hussein, M., and Gillis, P. (2010b). “Advanced simulation of tower crane operation utilizing System Dynamics modeling and Lean principles.” *Proceedings, Winter Simulation Conference*, Baltimore, MD, Dec. 5-8.
- Hasan, S., Al-Hussein, M., Hermann, U. H., and Safouhi, H. (2009a). “Integrated module for mobile crane dynamic instability analysis and supporting system design.” *Proceedings, Construction Research Congress*, ASCE, Seattle, WA, 386-395.
- Hasan, S., Al-Hussein, M., Hermann, U. H., and Safouhi, H. (2009b). “An automated system for mobile crane selection, swing control and ground pressure calculation.” *Proceedings, International Conference on Civil*,

Structural, and Environmental Engineering Computing, Madeira, Portugal,
Sep. 1-4, Paper 292.

Hendrickson, C., Horvath, A., (2000), “Resource use and environmental emissions of U.S. construction sectors”, *Journal of Construction Engineering and Management*, 126(1), 38-44.

Hermann, U. H., Hasan, S., Al-Hussein, M., and Bouferguène, A. (2011). “Innovative system for off-the-ground rotation of long objects using mobile cranes.” *Journal of Construction Engineering and Management*, ASCE, 137(7), 478-485.

Hermann, U., Hendi, A., Olearczyk, J., and Al-Hussein., M. (2010). “An integrated system to select, position, and simulate mobile cranes for complex industrial projects.” *Proceedings, Construction Research Congress*, ASCE, Banff, AB, May 8-10, 267-276.

Hong, W. K., Son, K., Wang, X., Kim, J. T., Lim, C. Y., and Kim, S. (2012) “Optimum Tower Crane Selection and Supporting Design Management”, *Proceedings of 2012 Australasian Conference on Innovative Technologies in Construction*, Wuhan, China, December 6-7

Jeng, S., Yang, C., and Chieng, W. (2010). “Outrigger force measure for mobile crane safety based on linear programming optimization.” *Mechanics Based Design of Structures and Machines*, 38, 145-170.

Jerman, B. (2006). “An enhanced mathematical model for investigating the dynamic loading of a slewing crane.” Published in the proceedings of the

- Institution of Mechanical Engineers, Part C, *Journal of Mechanical Engineering Science*, 220(4), 421-433.
- Kam C. and Fischer M. (2002). "Product Model & 4D CAD-Final Report." *Technical Report Nr. 143*, Center of Integrated Facility Engineering, Stanford University, CA.
- Kamat, V. and Martines, J. (2001). "Visualization simulated construction operations in 3D." *Journal of Computing in Civil Engineering*, 15(4), 329-337.
- Kamat, V. and Martines, J. (2004). "General purpose 3D animation with VITASCOPE." *Proceedings, Winter Simulation Conference*, Washington, DC, Dec. 5-8.
- Kang, J. H., Anderson, S. D., and Clayton, M. J. (2007). "Empirical study on the merit of web-based 4D visualization in collaborative construction planning and scheduling." *Journal of Construction Engineering Management*, 133(6), 447-461.
- Kim, S., Kim, J., Lee, D., and Ryu, S. (2011). "Automatic optimal design algorithm for the foundation of tower cranes." *Automation in Construction*, 20(1), 56-65.
- Kim, H. J. and Anderson K. (2012). "Energy Modeling System using Building Information Modeling (BIM) Open Standards." *Journal of Computing in Civil Engineering*, ASCE, in press.
- Klosinski, J. (2005). "Swing-free stop control of the slewing motion of a mobile crane." *Control Engineering Practice*, 13(4), 451-460.

- Koo, B. and Fischer, M. (2000). "Feasibility study of 4D CAD in commercial construction." *Journal of Engineering and Management*, ASCE, 126(4), 251-260.
- Lee, G., Cho, J., Ham, S., Lee, T., and Lee, G. (2012). "A BIM- and sensor-based tower crane navigation system for blind lifts." *Automation in Construction*, 26, 1-10.
- Lee, U. K., Kang, K. I., Kim, G. H., (2006) "Improving tower crane productivity using wireless technology." *Computer-Aided Civil and Infrastructure Engineering*, 21, 594-604.
- Lei, Z., Behzadipour, S., Al-Hussein, M., and Hermann, U. (2011). "Application of robotic obstacle avoidance in crane lift path planning." *Proceedings, International Symposium on Automation and Robotics in Construction (ISARC)*, Seoul, South Korea, Jun. 29-Jul. 2, S8-6, 292-297.
- Leung, A. W. T. and Tam, D. C. M. (2003). "Scheduling for high-rise building construction using simulation techniques." *Proceedings, CIB W78's International Conference on IT for Construction*, Auckland, New Zealand, Apr. 23-25, Paper w78-2003-186.
- Li, M. and Li, X. (2005), "Investigation of wind characteristics and assessment of wind energy potential for Waterloo region, Canada." *Energy Conversion and Management*, 46, 3014-3033.
- Li, Y. and Liu, C. (2012). "Integrating field data and 3D simulation for tower crane activity monitoring and alarming." *Automation in Construction*, 27, 111-119.

- Lim, C. H., Cho, S. H., Lee, Y. C., and Choi, J. K. (2005). "Basic construction of intelligent expert system for riser design using database system and optimisation tools." *International Journal of Cast Metals Research*, 18(4), 195-201.
- Lin, K. L. and Haas, C. T. (1996). "Multiple heavy lifts optimization." *Journal of Construction Engineering and Management*, ASCE, 22(4), 354-361.
- Liu, X. (2005). "Soil bearing capacity for crawler cranes." MSc thesis, Department of Civil and Environmental Engineering, University of Alberta, Edmonton, AB.
- Maczynski, A. and Wojciech, S. (2003). "Dynamics of a mobile crane and optimisation of the slewing motion of its upper structure." *Nonlinear Dynamics*, 32(3), 259-290.
- Manrique, J. D., Al-Hussein, M., Telyas, A., and Funston, G. (2007). "Constructing a complex precast tilt-up-panel structure utilizing an optimization model, 3D CAD, and animation." *Journal of Construction Engineering and Management*, 133(3), 199-207
- Neeley, D, (2010). "The Speed of Change". 2010SMARTBIM, www.smartbim.com
- Neitzel, R. L., Seixas, N. S., and Ren, K. K. (2001). "A review of crane safety in the construction industry." *Applied Occupational and Environmental Hygiene*, 16(12), 1106-1117.

- Park, H. S., Thomas, S. R., Tucker, R. L., (2005), "Benchmarking of construction productivity", *Journal of Construction Engineering and Management, ASCE*, 131(7), 772-778.
- Reddy, H. R. and Varghese, K. (2002). "Automated path planning for mobile crane lifts." *Computer-Aided Civil and Infrastructure Engineering*, 17, 439-448.
- Rodriguez-Ramos, W. E. and Francis, R. L. (1983). "Single crane location optimization." *Journal of Construction Engineering and Management, ASCE*, 109(4), 387-397.
- Ross, B., McDonald, B., and Saraf, S. E. V. (2007). "Big Blue goes down: The Miller Park crane accident." *Engineering Failure Analysis*, 14, 942-961.
- Russell, A., Staub-French, S., Tran, N., and Wong, W. (2009) "Visualizing high-rise building construction strategies using linear scheduling and 4D CAD." *Automation in Construction*, 18(2), 219-236.
- Sawhney, A. and Mund, A. (2002). "Adaptive probabilistic Neural Network-based crane type selection system." *Journal of Construction Engineering and Management, ASCE*, 128(3), 265-273.
- Safouhi, H., Mouattamid, M., Hermann, U., and Hendi, A. (2011). "An algorithm for the calculation of feasible mobile crane position areas." *Automation in Construction*, 20(4), 360-367.
- Shapira, A., Rosenfeld, Y., and Mizrahi, I. (2008). "Vision system for tower cranes." *Journal of Construction Engineering and Management, ASCE*, 134(5), 320-332.

- Shapira, A. and Lyachin, B. (2009). "Identification and analysis of factors affecting safety of construction sites with tower cranes." *Journal of Construction Engineering and Management*, ASCE, 135(1), 24-33.
- Shapira, A. and Simcha, M. (2009). "Measurement and risk scales of crane related safety factors on construction sites." *Journal of Construction Engineering and Management*, ASCE, 135(10), 979-989.
- Shapira, A., Lucko, G., and Schexnayder, C. J. (2007). "Cranes for building construction projects." *Journal of Construction Engineering and Management*, ASCE, 133(9), 690-700.
- Shapiro, H. I., Shapiro, J. P., and Shapiro, L. K. (1999). *Cranes & Derricks*. McGraw-Hill, New York, NY.
- Shi, J. (1999). "Activity-Based Construction (ABC) modeling and simulation method." *Journal of Construction Engineering and Management*, ASCE, 125(5), 354-360.
- Shi, J. and AbouRizk, S. M. (1997). "Resource-based modeling for construction simulation." *Journal of Construction Engineering and Management*, ASCE, 123(1), 26-33.
- Sivakumar, P., Varghese, K., and Babu, N. (2003). "Automated path planning of cooperative crane lifts using heuristic search." *Journal of Computing in Civil Engineering*, 17(3), 197-207.
- Sochacki, W. (2007). "The dynamic stability of a laboratory model of a truck crane." *Thin-Walled Structures*, 45(10-11), 927-930.

- Sun, G. F. and Kleeberger, M. (2003). "Dynamic responses of hydraulic mobile crane with consideration of the drive system." *Mechanism and Machine Theory*, 38(12), 1489-1508.
- Suraji, A., Duff, A.R., and Peckitt, S. (2001). "Development of causal model of construction accident causation." *Journal of Construction Engineering and Management*, ASCE, 127(4), 337-344.
- Taghaddos, H., AbouRizk, S., Mohamed, Y., and Hermann, U. (2010). "Simulation-based multiple heavy lift planning in industrial construction." *Proceedings, Construction Research Congress*, ASCE, Banff, AB, May 8-10, 349-358.
- Tam, C. M., Tong, T. K. L., and Chan, W. K. W. (2001). "Genetic algorithm for optimizing supply locations around tower crane." *Journal of Construction Engineering and Management*, ASCE, 127(4), 315-321.
- Tamate, S., Suemasa, N., and Katada, T. (2005). "Analyses of instability in mobile cranes due to ground penetration by outriggers." *Journal of Construction Engineering and Management*, ASCE, 131(6), 689-704.
- Tantisevi, K. and Akinci, B. (2009). "Transformation of a 4D product and process model to generate motion of mobile cranes." *Automation in Construction*, 18(4), 458-468.
- Thomas, H. R., Yiakoumis, I., (1987) Factor model of construction productivity, *Journal of Construction Engineering and Management*, Vol. 113 (4), 623-639.

Tutiempo (2011). "Climate Saskatoon."

<<http://www.tutiempo.net/en/Climate/Saskatoon/11-2010/718660.htm>>

(Apr., 2011).

USA National Weather Service (2011). "Wind gust definition." National

Oceanic and Atmospheric Administration.

<<http://www.weather.gov/forecasts/wfo/definitions/defineWindGust.html>

> (Apr., 2011).

Vining, R. and Gregory, J. "Daily wind patterns: Understanding of process."

<<http://www.weru.ksu.edu/symposium/proceedings/vining.pdf>> (Apr.,

2011).

Vivian W.Y. Tama, I. W. H. F. (2010). "Tower crane safety in the construction

industry: A Hong Kong study." *Safety Science*, Elsevier, 49: 208-215.

Watson, T. (2004). "When the wind blows." *Cranes Today*.

<[http://www.cranestodaymagazine.com/story.asp?storyCode=2023201&](http://www.cranestodaymagazine.com/story.asp?storyCode=2023201§ioncode=66)

[sectioncode=66](http://www.cranestodaymagazine.com/story.asp?storyCode=2023201§ioncode=66)> (Mar., 2011).

WeatherStats Canada (2011). Hourly Wind Speed for Saskatoon.

<http://saskatoon.weatherstats.ca/charts/wind_speed-24hrs.html>.

Accessed: April 2011.

Wu, D., Lin, Y., Wang, X., Wang, X., and Gao, S. (2011). "Algorithm of crane

selection for heavy lifts." *Journal of Computing in Civil Engineering*,

25(1), 57-65.

Yan, W., Culp, C., and Graf, R. (2011). "Integrating BIM and gaming for real-time interactive architectural visualization." *Automation in Construction*, 20(4), 446-458.

Zhang, P., Harris, F. C., Olomolaiye, P. O., and Holt, G. D. (1999). "Location optimization for a group of tower cranes." *Journal of Construction Engineering and Management*, ASCE, 125(2), 115-112.